Onsager Heat of Transport at the Liquid-Vapour Interface of Glycerol-Water Solutions

A Thesis completed as requirement for the Degree of Master of Science in Chemistry

Ronald Arthur James
2007

University of Canterbury

Acknowledgments

I would like to thank my superviser Professor Leon Phillips for all the help and guidance over this Master's degree and for the great sailing trips. I would also like to thank Dr Colin Freeman for supervising me during Leon's leave. A big thanks to "Group Leon", which other members include David Bones and Georgina Biggs, for your help, support and friendship over this time.

Thank you Robert MacGregor in the glass blowing workshop, Sandy Ferguson in the electronics workshop, and Russel Gillard, Wayne Mackay and all the others in the mechanical workshop for fixing all my many breakages.

Also a big thanks to all the rest of my good mates in the chemistry department for your support and fun times. To my parents Jesse James and Carmel Kavanagh and my brother Benjamin James, who have been behind every step of the way, I couldn't have done this without you.

Ronald James

Abstract

The Onsager heat of transport, Q^*, has been measured for water vapour above glycerol-water solutions (75 % to 94.5 % glycerol) over a temperature range of -46 to -32 °C. For solutions of concentrations 80 % and above, Q^* varied from 5.41 kJ mol^{-1} ± 0.97 to 17.37 kJ mol^{-1} ± 2.61, consistent with previous results for aniline and *n*-heptanol. The dissociation of glycerol-water complexes was not rate determining, as was the case for sulfuric acid-water solutions, and therefore the glycerol-water system is a better two component system analog for comparison with the CO_2-water system than the sulfuric acid-water system.

Table of Contents

Chapter 1:
Introduction

Onsager's heat of transport is likely to be important whenever there are coupled fluxes of heat and matter. Interest in the heat of transport, Q^*, is not a recent development [1], and its likely significance at a gas-liquid interface was pointed out more than fifty years ago [2], but its value at the liquid-vapour interface was not measured until recently [3]. Early measurements of Q^* were for gases passing through rubber membranes [4, 5], where Q^* took both positive and negative values, with varying magnitudes, depending on the gas used. Coupled diffusive fluxes in liquids has also been studied [6].

With interest in the carbon cycle increasing because carbon dioxide, CO_2, is the most important greenhouse gas, recognition of the likely importance of the heat of transport at the liquid-vapour interface affecting the flux of CO_2 into the ocean surface led to experimental investigations of the irreversible thermodynamics of the gas-liquid interface at Canterbury University.

1.1 CO_2 fluxes with the ocean surface

Accurate measurement of CO_2 fluxes between the atmosphere and the ocean are not easy obtained. This is due to the small size of the fluxes and the varying direction in space and time of these fluxes [7]. At the present time there are two main means of measuring the CO_2 fluxes with the ocean surface, the parameterisation approach and the eddy-correlation method. The parameterisation method obtains the flux from a theoretical parameterization of transfer velocity versus wind speed, while the eddy-correlation method typically uses an infrared laser to measure the CO_2 concentration in addition to a sonic anemometer that measures wind and temperature fluctuations [8].

The parameterisation model is based on equation (1.1):

$$F = K(pCO_{2w} - pCO_{2a}) \qquad (1.1)$$

where F is the flux, K is the gas transfer velocity, pCO_{2w} and pCO_{2a} are the partial pressures of CO_2 in water and air respectively [9]. The partial pressure of CO_2 in air is taken from 10 metres above sea level whilst the partial pressure of CO_2 in the ocean is

taken from a depth of 1 metre. No effort is made to take into account the effect of any air-sea temperature difference, the transfer velocity is assumed to be independent of temperature, and the difference between the solubility of CO_2 in the seawater at a depth of 1 meter and the solubility in the 'cool skin of the ocean' is usually neglected [9]. Various correction factors have been applied to K in equation (1.1) [9] in an effort to reduce the scatter of the measured values. A slight improvement on the direct use of equation (1.1) is represented by the dual-tracer technique [10]. The dual tracer technique gets its name because there are two gases, SF_6 and He, which are used as tracers to calculate the transfer velocity of CO_2. SF_6 and He are used as they are inert, non-toxic gases, with very different transfer velocities. Small quantities of SF_6 and He are simultaneously introduced into a volume of seawater at known concentrations. This seawater is then released into the ocean below the surface. Over a period of days, water samples and measurements are taken to find the concentrations of the tracer gases remaining.

The transfer velocities are calculated by equation 1.2

$$\left(\frac{1}{R}\right)\frac{dR}{dt} = \frac{-(K_{He} - K_{SF_6})}{H} \tag{1.2}$$

where R is the ratio of the tracer concentrations, H is the water depth and K_{He} and K_{SF6} are the transfer velocities of the two gases. The measurements of the concentration ratios are made over a period of 1-2 days. Measurements of the wind speeds are conducted during the experiment in order account for any variances in the resulting transfer velocities. To find the absolute transfer velocities, the Schmidt numbers of the respective gases are used:

$$\frac{K_1}{K_2} = \left(\frac{Sc_2}{Sc_1}\right)^n \tag{1.3}$$

Sc is the Schmidt number of the gas. The value of n is usually 0.5 to $\frac{2}{3}$ but can vary from $\frac{1}{3}$ up to 1 [11],

$$Sc = \frac{\mu}{\rho D_v} \tag{1.4}$$

μ is the kinematic viscosity, ρ is the density and D_v is the diffusivity of the gas in water. Therefore by knowing the transfer velocities and the Schmidt number of the tracer gases and the Schmidt number of CO_2, the transfer velocity of CO_2 can be found [10]. This can then be compared with the relevant wind speeds so that future

readings require only wind speed and CO_2 partial pressure measurements to calculate the gas flux in (1.1).

The eddy correlation technique differs from the dual-tracer technique by measuring the CO_2 flux by using vertical wind velocities and CO_2 density.

$$F(eddy) = \overline{wc} = \overline{w'c'} + \overline{w}\ \overline{c} \qquad (1.5)$$

where w is the vertical wind velocity and c is the CO_2 density. The over-scores indicate mean values over the sampling time of the measurements; the primes indicate deviations of the results from the mean values [12]; w is adjusted by the Webb correction for the effects of heat and water vapour transfer [13].

The CO_2 density measurements are taken by fast response CO_2/H_2O sensors while the wind direction and speed are recorded by a three-dimensional sonic anemometer. These measurements yield absolute fluxes from or into the ocean surface. The time period of the measurement readings can be in the order of days. The measurements are very difficult, the Webb correction is a major fraction of the CO_2 flux, and smaller corrections are applied to account for a number of other effects [14]. Also when measuring on a ship instead of an ocean platform, the motion of the ship must be taken into account for the sonic anemometer to record the true direction of wind flux. The distortion of the wind by the boat/platform, which the instrumentation is mounted, on must also be taken into account.

Both methods have strengths and weaknesses and these are visible in the differences in the results measured. With eddy correlation the fast response CO_2 sensor can take many readings over the course of the experiment, while the dual tracer method can only measure a few readings (Figure 1.1). When eddy correlation was first used over the ocean, the calculated CO_2 flux was up to 2 orders of magnitude larger than the traditional dual tracer method [15] as calibrated against radio-isotope data. Part of the difference is accounted for by the initial measurements being made adjacent to a surf zone. The size of the discrepancy has lessened as eddy correlation has had continued use, but there still remains a significant disagreement between the two methods. For comparison between the two differing methods, the values calculated for k_{660} are used; k_{660} can be calculated from the eddy correlation results; the 660 referring to the Schmidt number of CO_2 .

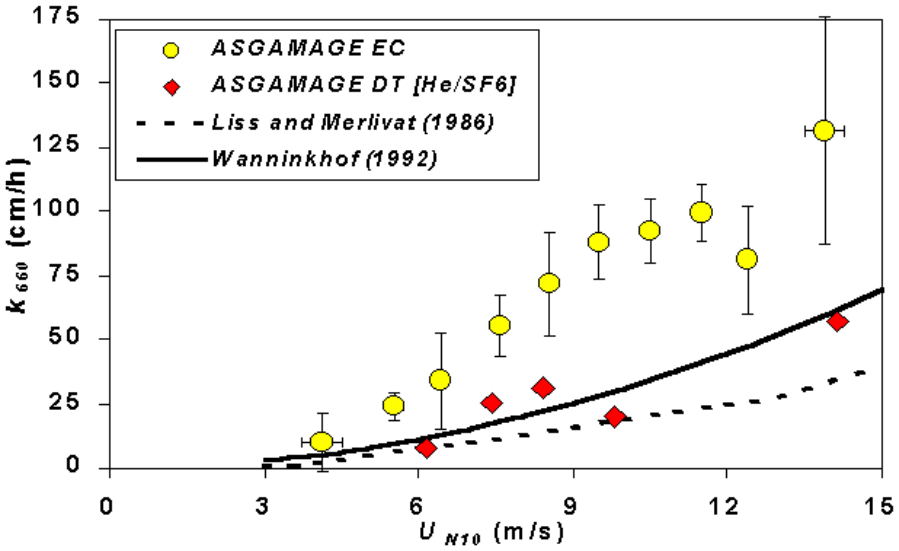

Figure 1.1. Normalized transfer velocity, k_{660}, found by the Challenger crew, using the differential tracer technique (diamonds) and k_{660} according to the crew at MPN, using the eddy correlation technique (circles). Results are plotted for gas transfer versus the wind speed [16]

The recent field experiments in the ASGAMAGE project [16] (Figure 1.1) illustrate the differences in the results, with eddy correlation having a higher k_{660} value by a factor of 2. This difference has still appeared in other experiments such as the GasEx-98 experiment shown below [17].

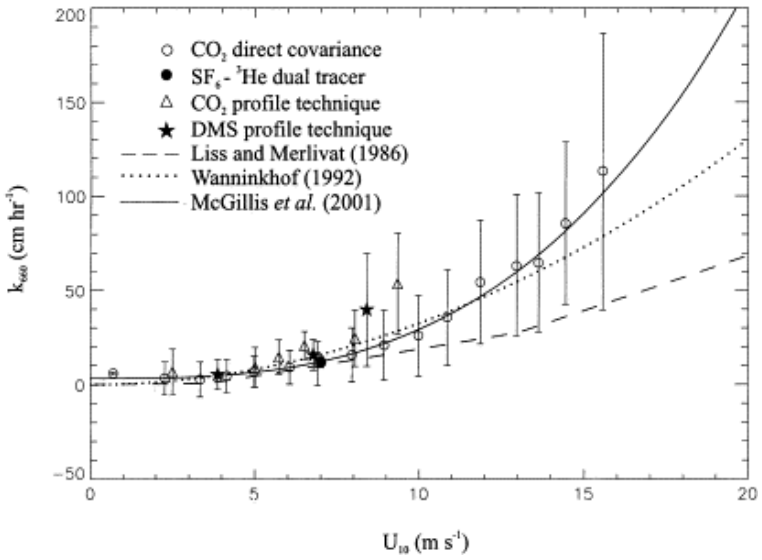

Figure 1.2. Direct covariance air-sea CO_2 transfer velocities and standard deviations corrected to Sc=660 versus 10m wind speed during GasEx-98 [17, 18] The solid line is a cubic fit through the Eddy Correlation data The dotted lines are for the Dual-Tracer technique values using Wanninkhof and Liss and Merlivat equations.

From Figures 1.1 and 1.2 the large standard deviation in the eddy correlation technique can be seen very clearly; however, error limits are not well defined for the parameterization method. There is still some debate over which of the methods of

measurement is more accurate and questions of how to get the two differing methods to agree. Eddy correlation is steadily gaining more support within the research community.

A thermodynamic approach to calculating the transfer velocity has been put forward in the last decade [3, 19, 20]. This new approach involves the use of Onsager's heat of transport, Q^*, to allow for the effect of a temperature gradient at the air-sea interface. Although the parameterisation method has been corrected over the years to take into account differing factors for pH, the cool-skin effect of the ocean, the temperature of the air and chemical enhancement of CO_2 entering the ocean [9, 21], the difference between the water surface temperature and the temperature of the adjacent vapour layer has not been taken into account. This oversight forms the basis of our argument that Q^* should be taken into account.

Early proposals consisted of viewing the flux of CO_2 from the ocean as being limited by rate of diffusion through a thin film at the surface of the liquid [19]. This thin layer, in the order of 10-30 μm, with a mixing time of the order of 0.1 seconds, was expected to remain even in windy conditions, however with the addition of waves the total surface area increases and therefore so does the total flux. The limiting effect of the film only disappears when white caps appear due to the surface breaking at high wind speeds.

Initial definitions of Q^* for the gas- liquid interface were of the form

$$Q^* = Q - C_p T_m \tag{1.6}$$

where C_p is the heat capacity of the gas, T is the temperature of the gas, m signifies adjacent to the liquid interface and Q is the heat of solution or heat of condensation of the gas, depending on which is more appropriate [22]. This was used in (1.7) to calculate the flux using previous measured data [23, 24].

$$Flux = -D_m C_m \left[\left(\frac{Q^*}{RT_m} \right) \frac{T_m'}{T_m} + \frac{C_m'}{C_m} \right] \tag{1.7}$$

where D is the diffusion coefficient, C the concentration and R the ideal gas constant. The prime signifies a gradient with respect to height. Primary calculations showed Q^* to be in the order of 10 kJ mol^{-1} for CO_2 compared to -5.3 and -2.7 for He and SF_6, respectively [3]. This difference between respective Q^* values suggests that the dual tracer method does not accurately convert tracer fluxes to CO_2 fluxes, because the signs of Q^* are opposite and CO_2 acts very differently from the tracer gases at the

liquid interface when there is a significant liquid-vapour temperature difference. The large Q^* value coupled with the temperature in equation (1.7) shows the importance of including the term involving Q^*/RT in the total flux calculations. This was shown using previously measured experimental gas transfer results [23].

This work was criticised by Doney [25-28] who disagreed with equations (1.6-1.7), and calculated that Q^* would be an order of magnitude smaller than the value obtained in previous work by Phillips. With respect to equations (6-7), experimental work in our laboratory has shown that Doney was correct in pointing out that equation (1.6) was wrong (the initial derivation of (1.6) treated the interface as a thin region between two semi-infinite reservoirs). In the correct derivation, which treats the interface as a closed adiabatic system, the term involving the heat capacity is absent and Q^* is correspondingly larger. The correct derivation is given in *section 1.2, Derivation of Onsager's Heat of Transport*. The second point of Doney's argument, concerning the magnitude of Q^*, has been shown to be incorrect by our measurements of Q^* for aniline, *n*-heptanol, water, water vapour over sulfuric acid, and now water vapour over glycerol. This is discussed further in *Section 1.3, Previous Work.*

1.2 Derivation of Onsager's Heat of Transport for the Liquid-Vapour Interface

The foundation of this derivation comes from early papers in the work of heat of transport for gases and liquids passing through membranes [1, 2, 4, 5]. A good definition of the heat of transport comes from Spanner [2], who considers two compartments separated from each other by a membrane (Figure 1.3). This system is isolated from all other surroundings, i.e. there is no loss of heat or matter.

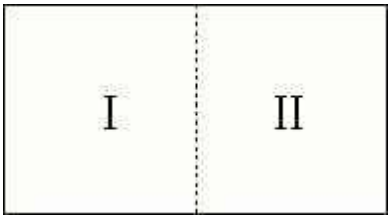

Figure 1.3. Compartments I and II separated by a membrane.

The compartments filled with water differ such that compartment I has slightly higher pressure, P_1 than compartment II at pressure, P_2. The temperatures, T_1 & T_2,

and volumes, V_1 & V_2, across both compartments are uniform. With the separating membrane, higher energy molecules are able to traverse more rapidly from one compartment to the other. Therefore, a higher proportion of high energy molecules pass through the barrier from compartment I to compartment II. These higher energy molecules carry a quantity of heat, which in turn slightly lowers T_1 while raising T_2 as the system moves towards stationary state. If we now manually abstract the heat as to keep T_2 constant, the quantity of heat abstracted per unit of water is the "heat of transfer", Q^*. The reverse of this can also occur where a different membrane acts as a "ditch" which allows the lower energy molecules to pass more easily than the high energy, so in this case the sign of Q^* is reversed.

This definition also works if the two reservoirs are separated by a vapour layer acting as the membrane. Here the evaporation favours the higher energy molecules and Q^* is close to the latent heat of evaporation. In the case of the liquid-vapour interface we can make the assumption that this can be thought of as half of the two reservoirs separated by a vapour layer example, therefore Q^* is calculated from the heat lost in the first reservoir instead of the heat gained in the second reservoir.

Denbigh's work on the heat of transport involved gases in two compartments separated by a rubber membrane [4, 5] but his equations can also be applied to the liquid-vapour system [29].

Consider the steady-state flux equations (1.8) and (1.9)

$$J_1 = L_{11}X_1 + L_{12}X_2 \tag{1.8}$$

$$J_2 = L_{21}X_1 + L_{22}X_2 \tag{1.9}$$

where J_1 is the flux of heat, J_2 is the flux of matter, X_1 is the thermal force and X_2 is the diffusion force. The forces are able to be varied at will; X_2 can be a pressure or concentration, although for our system it is convenient to make it a pressure. The coefficients L_{mn} are fixed by the nature of the system. L_{11} proportional to the thermal conductivity and L_{22} to the diffusion coefficient. L_{12} and L_{21} are coupling constants between the different fluxes. Onsager proved that $L_{mn} = L_{nm}$, which won him the Nobel Prize in Chemistry in 1968. A full proof of this equation can be found in Denbigh [1]. Considering Q^* as the amount of heat transferred per unit flux of water molecules and J_2 as the flux of matter, we can rewrite equation (1.8):

$$J_1 = L_{11}X_1 + Q^*J_2 \tag{1.10}$$

For a derivation of L_{21} we first assume a state where $X_1 = 0$, i.e. with no temperature difference. Substituting into equations (1.8) and (1.9)

$$J_1 = L_{12}X_2 = Q^* J_2 \tag{1.11}$$

$$J_2 = L_{22}X_2 \tag{1.12}$$

Replacing J_2 in equation (1.11)

$$L_{12}X_2 = Q^* L_{22}X_2 \tag{1.13}$$

$$L_{12} = Q^* L_{22} = L_{21} \tag{1.14}$$

Substituting L_{21} back into equation (1.9)

$$J_2 = Q^* L_{22}X_1 + L_{22}X_2 = L_{22}(Q^* X_1 + X_2) \tag{1.15}$$

The values for the forces X_1 and X_2 are taken from Denbigh [1]

$$X_1 = \frac{-1}{T} grad(T) = \frac{-dT}{Tdx} \tag{1.16}$$

$$X_2 = -T.grad\left(\frac{\mu}{T}\right) \tag{1.17}$$

here μ is the chemical potential

$$\mu = RT.Ln(P) \tag{1.18}$$

$$X_2 = -RT\,\frac{dP}{Pdx} \tag{1.19}$$

By substituting the two driving forces into equation (1.15) we have

$$J_2 = -L_{22}\left(Q^*\,\frac{\Delta T}{T\delta} + RT\,\frac{\Delta P}{P\delta}\right) \tag{1.20}$$

Note that dx has been replaced by δ, which is the distance over which the change in temperature occurs. Rearrangement of equation (1.20) gives the gas-flux equation.

$$J_2 = -\frac{L_{22}}{\delta}\left(\frac{Q^*}{RT}\,\frac{\Delta T}{T} + \frac{\Delta P}{P}\right) \tag{1.21}$$

where the L_{22} in (1.21) differs from that in (1.20) by a factor of RT. During the experiment the liquid-vapour system will be allowed to come to a stationary state with $J_2 = 0$, so equation (1.21) can be rearranged to give the steady-state expression.

$$\frac{Q^*}{RT} = -\frac{\Delta P}{P}\,\frac{T}{\Delta T} \tag{1.22}$$

The pressure is the observed vapour pressure above the liquid and the change in pressure is the difference between the original pressure and the pressure when the temperature difference is introduced. The change in temperature is the temperature

difference between the liquid and vapour. Equation (1.22) shows that Q^* can be calculated by varying the temperature and recording the change in pressure, providing the system is in a stationary state.

Equation (1.21) shows the coupling of ΔT and Q^* in the liquid-gas exchange, and that Q^*/RT has to be large for the difference in temperature between the liquid and vapour to be a significant factor when calculating the flux. Initially it was thought that this coupling of heat and pressure could only be effective over a distance of a few mean free paths from the surface, where there is a significant gradient of both forces. In the Knudsen layer the velocity distributions of molecules moving toward the surface and molecules moving away from the surface are different. This partly shows why this coupling takes place at a molecular level [30]. The small distance over which the strongest coupling occurs allows the steady state to become established over the ocean surface, even in windy conditions [7].

Considerations of detailed balance at the gas-liquid interface have led to the conclusion [31] that the heat of transport is a result of the effect of a temperature gradient on the height of a free-energy barrier to evaporation that is located in the capillary-wave zone at the liquid surface. The constancy of Q^* almost certainly indicates that the decrease, with increasing pressure, in the size of the temperature drop across the Knudsen zone is exactly compensated by an increase in the transfer coefficient which gives the fraction of the temperature difference across the Knudsen zone that is conveyed into the capillary-wave zone [32].

1.3 Previous Experimental Studies

A number of measurements of Onsager's heat of transport at a gas-liquid interface have been completed at University of Canterbury in the past five years [30, 33, 34]. The first two systems studied were the aniline and n-heptanol liquid-vapour interfaces. Both gave Q^* values in the order of tens of kilojoules per mole, which is of similar magnitude to the heat of vaporisation of the liquids used.

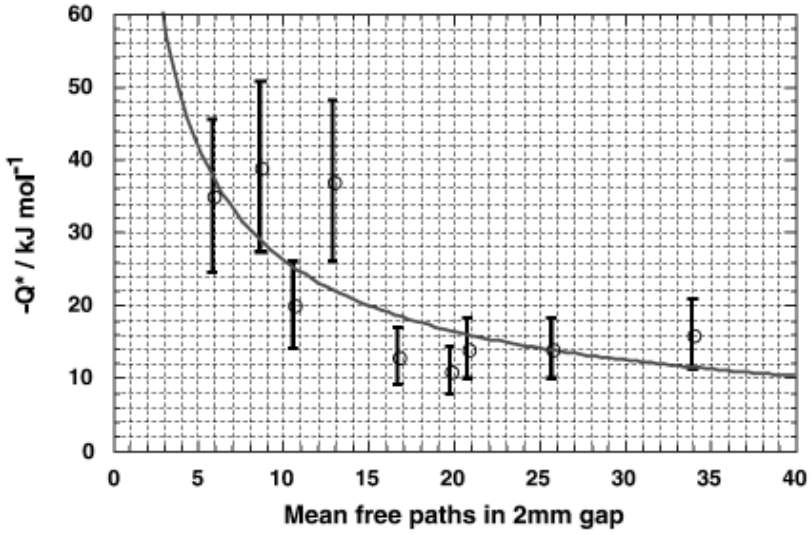

Figure 1.4. Q* vs. δ measured in mean free paths for aniline[30].

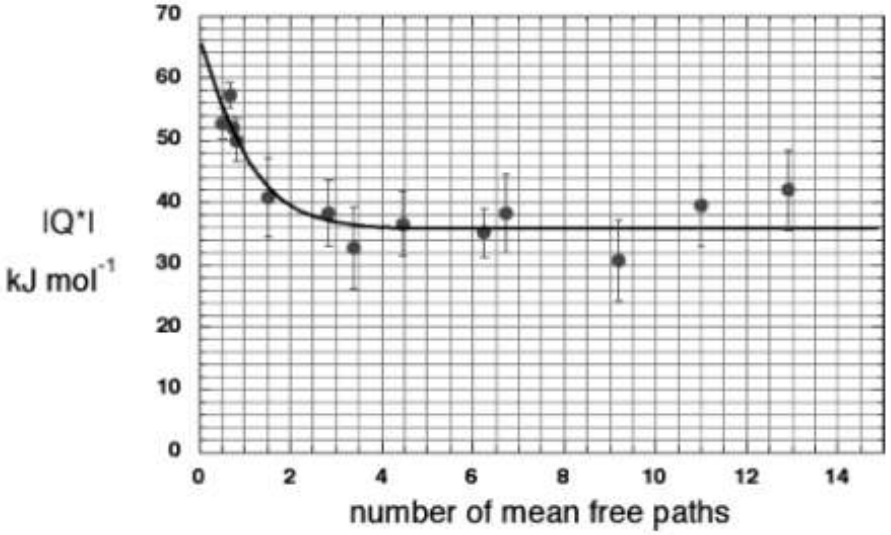

Figure 1.5. Q* vs. δ measured in mean free paths for n-heptanol [33].

In these Figures (1.4-1.5) the curves are drawn only as a representation of what the authors believes to be happening and have no theoretical significance. It can be seen that, with decreasing number of mean free paths, the heat of transport remains constant until within a few mean free paths of the liquid surface, when it seems to rise. We believe this shows the importance of the Knudsen layer to the flux of gas out of the surface. When the distance between the liquid surface and the top plate is more than a few mean free paths, the $|Q^*|$ value does not appear to continue to fall as the number of mean free paths in the vapour gap rises. Recent results for water [35] indicate that the value of Q^* remains constant for vapour gaps up to at least 800 mean

free paths, which implies that Q^* is still likely to be important at atmospheric pressure.

1.3.1 Theory of the Liquid Interface

A partial explanation of the phenomena shown in the two graphs Figures 1.4 and 1.5 involves the temperature profile in the Knudsen layer. The normal water vapour temperature profile from warm surroundings to a cooler liquid is sketched in figure 1.6.

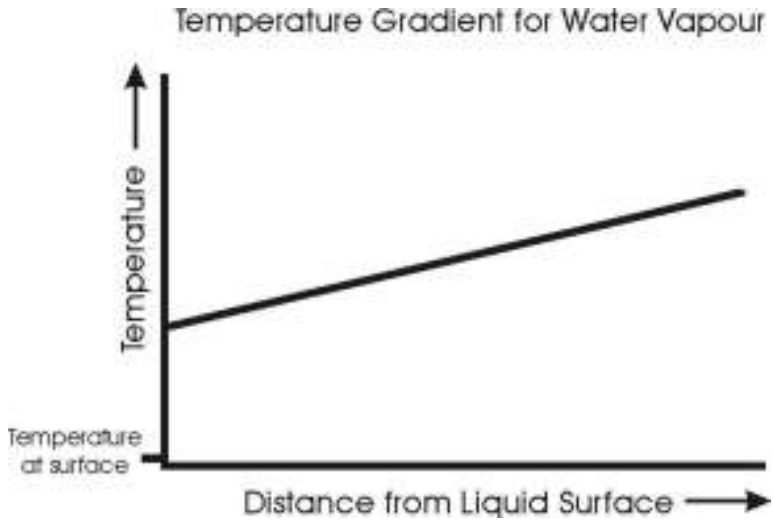

Figure 1.6. Typical temperature gradient graph. (Not drawn to any scale)

This though is not an entirely accurate diagram because the temperature gradient in the Knudsen layer is much steeper at a short distance from the liquid surface. Shown in Figure 1.7 is a combination of two gradients, where the first steeper gradient is only a distance of 1-2 mean free paths from the liquid surface while the second shallower gradient is the same one seen in Figure 1.6 [36].

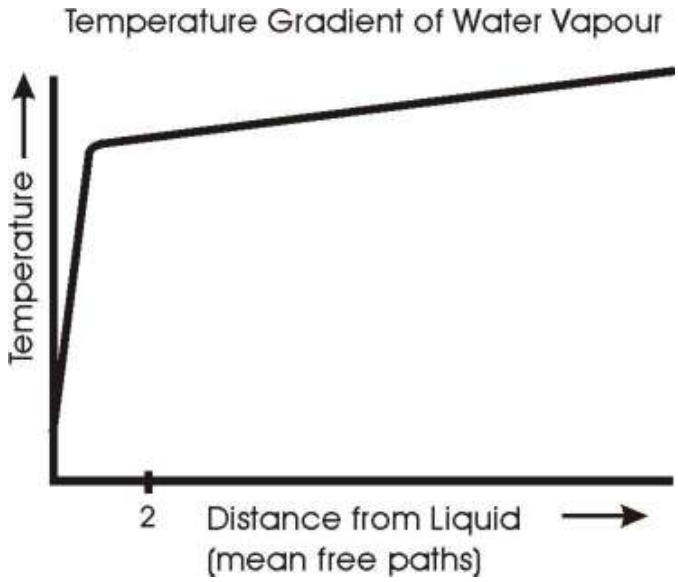

Figure 1.7. An enlarged view of the temperature gradient near the liquid surface. Note that the 2 mean freepath notch on the x axis is only an estimate. This steepness occurs somewhere in the Knudsen Layer, and is the effective temperature gradient for molecules moving parallel to the surface (there is no single temperature for molecules moving at right-angles to the surface).

This difference in temperature gradients arises because there have been only a minimal number of collisions between the molecules leaving the liquid surface and those arriving from the vapour. It is this gradient which determines the flux of matter leaving the liquid layer. This explains the effect of n_λ (number of free mean paths) on $|Q^*|$ shown in Figures 1.4 and 1.5. The steep temperature gradient does not extend completely to the liquid surface temperature; the temperature at the intercept of the curve with the surface is calculated by the theory of gas-kinetic temperature jumps [37].

For this explanation, it is assumed that ΔT is constant for the experimental runs, with a value of α, since ideally only two points are needed to make a straight line to calculate Q^*, (T_0, P_0) and $(T_0+\Delta T, P_0+\Delta P)$. Note that to increase δ in terms of mean free paths, corresponds in practice to increasing the base temperature and hence increasing both the base pressure and the number of mean free paths between the fixed top plate and the liquid surface.

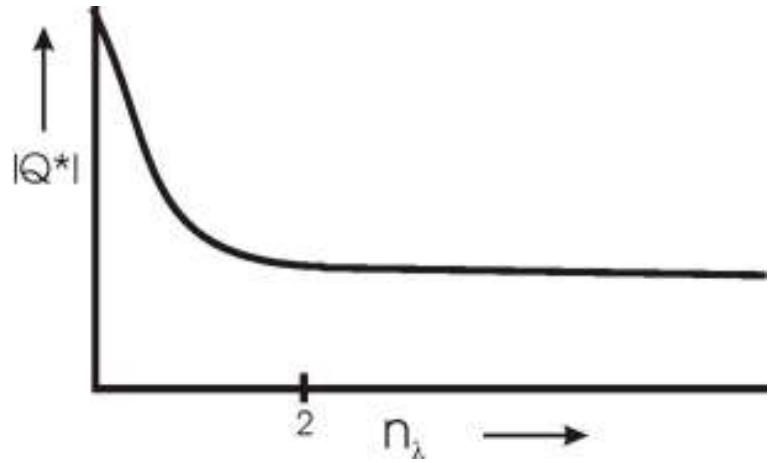

Figure 1.8. Simplified versions of Figures 1.4 and 1.5.

The graph in Figure 1.8 can be split into two parts, before the curve at about 2 mean free paths and after the curve. In the first part of the curve, where $|Q^*|$ rises steeply close to the liquid surface, the distance between the top plate and the liquid surface (which is the distance over which ΔT occurs (δ)) is less than or equal to the distance over which the steep temperature gradient occurs (β). At large numbers of mean free paths, where $|Q^*|$ seems to stabilise, the distance over which ΔT occurs is much larger than β.

For the $|Q^*|$ values calculated when δ is smaller than β, the resulting effective temperature gradient has increased above that which would be seen if δ equalled β. The effective temperature gradient would increase by a factor of δ / β. This increased effective temperature gradient would therefore increase the matter flux out of the surface by a similar magnitude. Referring to Equation 1.22, the change of $|Q^*|$ relies on changes in $T^2\Delta P / P\Delta T$, ΔT is constant therefore Q^* depends on $T^2\Delta P/P$. Therefore the relative change in pressure is greater when $\delta < \beta$ and increases further for smaller values of δ, and so $|Q^*|$ increases for smaller δ values.

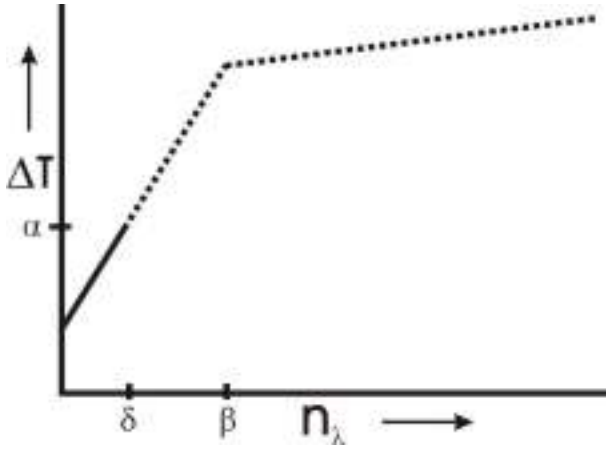

Figure 1.9. ΔT vs. n_λ when δ < β, the dotted line shows theoretical ΔT with increasing δ.

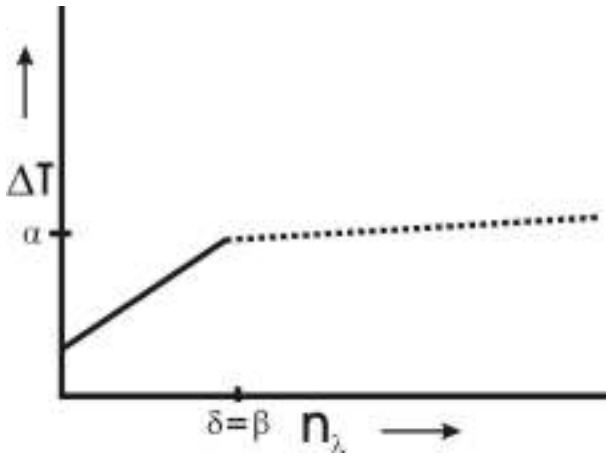

Figure 1.10. ΔT vs. n_λ when δ = β.

This partly explains the decreasing nature of $|Q^*|$ when $\delta \leq \beta$, though more investigation into this is needed. When $\delta = 0$ then $|Q^*|$ is equivalent to the ΔH_{vap}, though this will be explained later.

When $\delta > \beta$, the following system is set up as in Figures 1.11 and 1.12. In the vapour gap, δ, there are now two different gradients instead of the one gradient as shown in Figure 1.11. Therefore the vapour gap can be split into two separate parts as shown in Figure 1.12. As δ increases, less of the total gap is made up of the effective temperature gradient therefore the effective ΔT lowers as there has already been some loss of ΔT through the shallower temperature gradient. This in turn lowers the measured $|Q^*|$ values. This change is not as large as seen when δ tends towards β from $\delta = 0$; a gradual decline is observed.

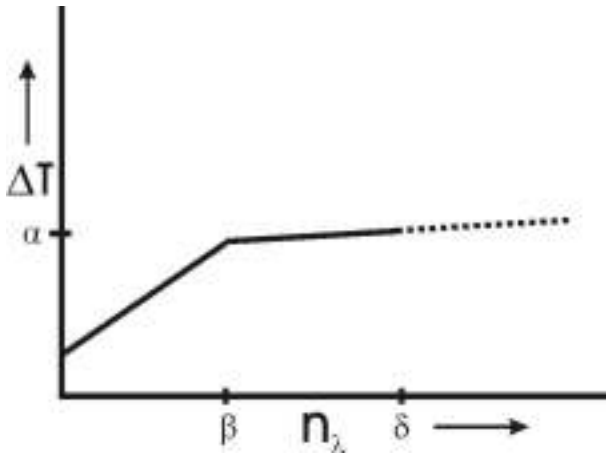

Figure 1.11. ΔT vs. n_λ where δ > β

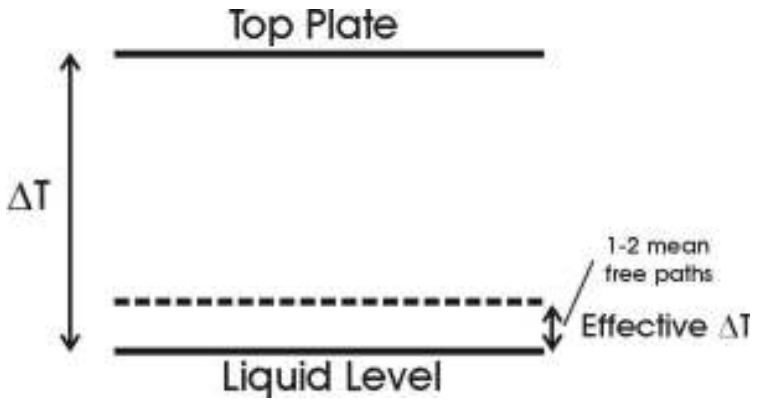

Figure 1.12. Differing view of the gradients observed in the Onsager cell. (Note that δ is larger here than in Figure 1.11)

The values of Q^* have been found in the same order of magnitude of $-\Delta H_{vap}$. This has been proven theoretically by Phillips [31] who showed that

$$-Q^* = \eta \Delta H_{vap} \tag{1.23}$$

where η is a transfer coefficient. η ranges from values of 0.88 to 0.50 depending on δ. At the limiting value of $Q^* = -\Delta H_{vap}$ Equation (1.22) becomes an approximate form of the Clapeyron equation.

A characteristic feature of this profile is the gas-kinetic 'temperature jump' [38], which arises when the thermal accommodation coefficient of molecules colliding with a surface is significantly less than unity. The temperature jump is a discontinuity in the gas-phase temperature profile when it is very close to the surface; the theory of such temperature jumps is well established [39, 40]. When the gap δ over which the temperature gradient is applied is of the order of one mean free path or less, the top plate is largely covered by a layer of adsorbed molecules of the liquid and the accommodation coefficient is close to 1. Under these conditions, the whole of the

applied temperature difference appears across the layer of vapour and a large fraction of the temperature difference can be transferred to the capillary-wave zone. Hence the observed large increase of Q^* when δ is of the order of one mean free path or less, and hence also the linearity of plots of ΔP against ΔT when δ is small. When δ is much greater than one mean free path, plots of ΔP against ΔT show a distinct knee (Figures 1.14, 1.15), such that the initial slope (from which Q^* is determined) is much greater than the slope beyond the knee. This observation is now attributed [35] to a change in the nature of the surface of the top plate when ΔT is of the order of 1ºC, the surface becoming progressively drier and the accommodation coefficient much smaller as ΔT increases. Recently Biggs [41] has shown that the temperature jumps and accommodation coefficients derived from this model can be fitted to BET isotherms, with the assumption that the liquid on the top plate is present in localised islands and the accommodation coefficient is proportional to the fractional coverage of the surface by such islands.

1.3.2 Observed Paradoxical Behaviour with Aniline

During the course of the aniline experiments, the phenomenon of liquid distillation to a warmer surface was observed [42]. This was the result of temperature and vapour pressure gradients at the liquid surfaces. The cooler liquid below experienced a positive temperature gradient (a positive gradient increases with distance from the liquid) while the warmer surface above had a negative temperature gradient. The positive temperature gradient enhanced the cooler liquid's vapour pressure and the negative temperature gradient above the warmer liquid decreased the warmer liquid's vapour pressure. Some liquid on the upper (warmer) plate was present as a result of adsorption (provided the upper-plate temperature was not too high). When the conditions were such that the overall pressure was low enough for the Q^* value to be greater than half the latent heat of vaporisation, the vapour pressure of the cooler liquid could exceed the warmer liquid's vapour pressure, causing the distillation of the cool liquid onto the warmer surface [43].

A related paradox was discovered theoretically by Pao [44] whose solution to the Boltzman equation for a "two-surface problem" showed the possibility of inverted gas-phase temperature profiles during trap-to-trap distillation. Pao's prediction of

inverted temperature profiles differs from what was observed in the aniline experiment.

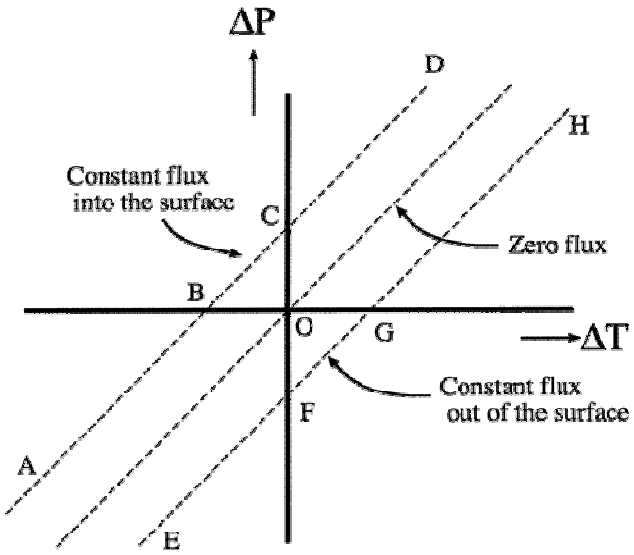

Figure 1.13. ΔT and ΔP are the temperature differences (positive or negative) across the vapour layer at the surface. The dotted lines are the lines of constant flux to or from the surface of the liquid [43].

Figure 1.13 shows the different possibilities at the liquid surface. For the Onsager heat of transport experiments, the aim is measure the stationary state along the middle line where there is no overall flux in and out of the surface. The paradoxical behaviour predicted by Pao is represented by the regions E-F, where the ΔT and ΔP are both negative at the surface of the evaporating liquid, and C-D, where both increments are positive at the surface of the condensing liquid. These two regions should be able to occur in the same system, though experimental results have yet to show this. The F-G region, where ΔT is positive while ΔP is negative for a evaporating surface, has been reported by Fang and Ward [45]. Though the region B-C has not been reported yet, it would be complementary to F-G in a two surface system. Regions A-B and G-H are the regions observed during the aniline cool-to-warm distillation. With all of the corresponding regions in Figure 1.13 accounted for, the conclusion is that there are no new forms of paradoxical behaviour to be discovered [43].

1.3.3 Curvature observed in the n-Heptanol and Aniline Experiments

During the course of the aniline and n-heptanol experiments, it was observed that at the higher temperatures for n-heptanol and at all temperatures for aniline there was curvature in the ΔT *vs.* ΔP graphs as shown in Figures 1.14 and 1.15.

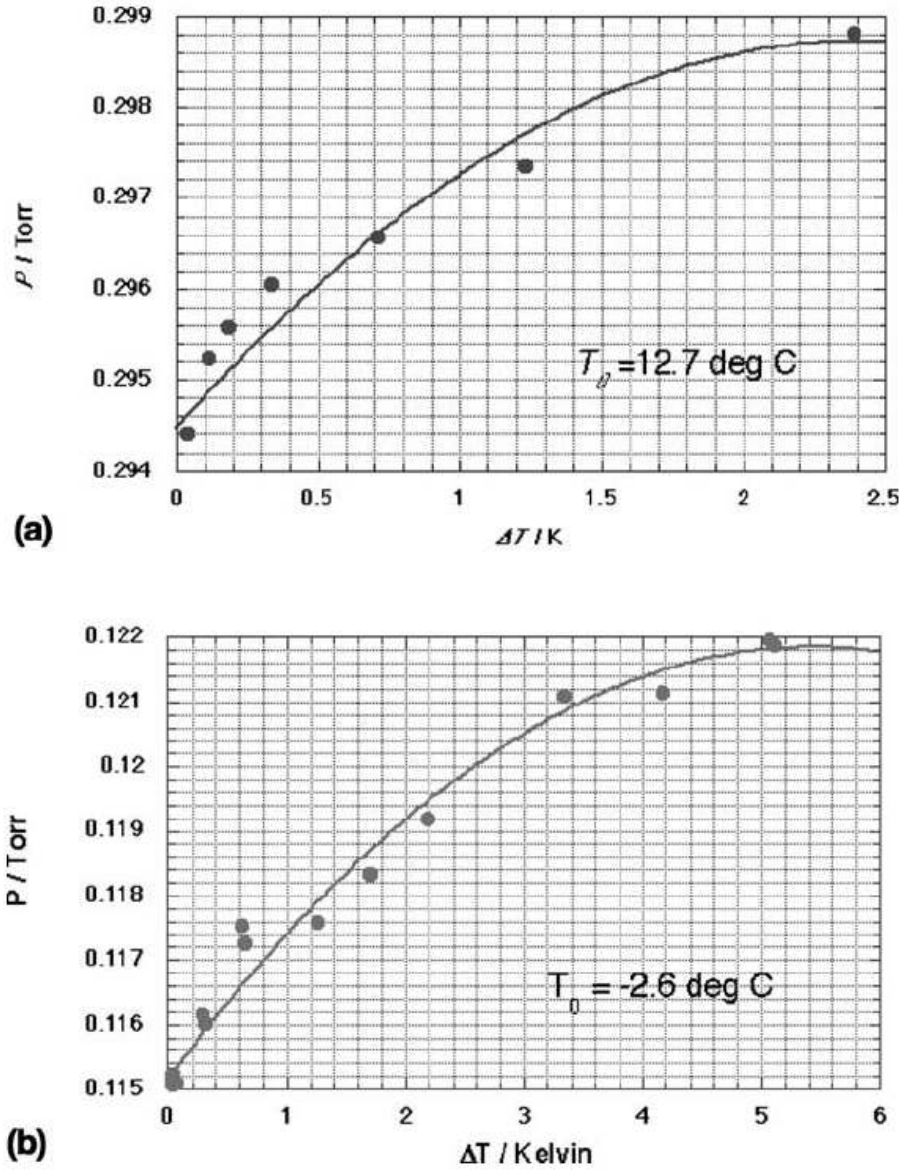

Figure 1.14. Typical curvature seen in the aniline experiments [30].

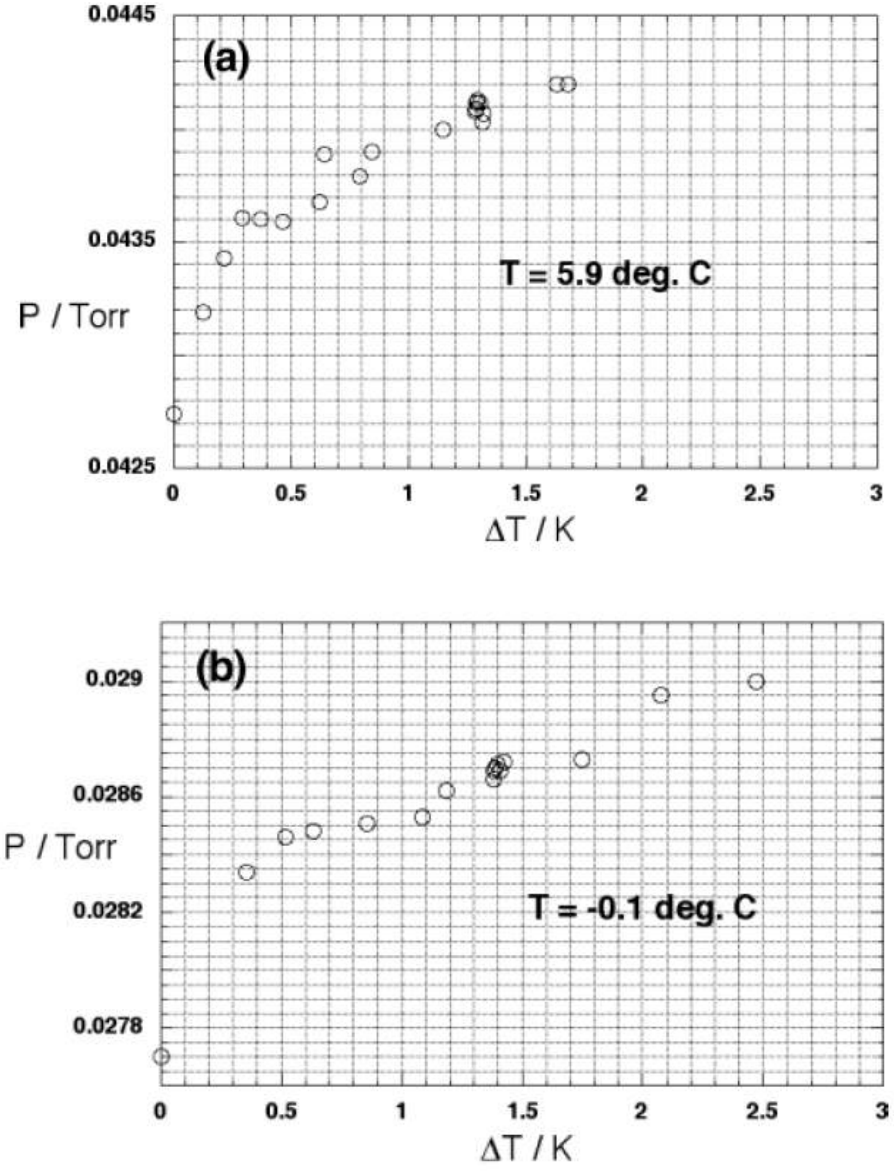

Figure 1.15. Typical curvature at higher temperatures seen in the n-heptanol experiments [33].

A referee for the n-heptanol paper suggested that the cause of this curvature might be a form of turbulence resulting from 'persistence of velocity' during collisions. Experimental work was carried out in our research group repeating the *n*-heptanol work in a metal cell instead of the glass cell to see if this removed the turbulence from the system, but the initial results were negative. Recent experiments by Dr Chris Pursell [35], in our research group, with pure water in a metal Onsager cell showed that curvature still remained, although the resulting graph for ΔT vs. ΔP appears to be a piecewise graph, similar to Fig. 1.15, made up of two straight sections with differing gradients, instead of a curve as previously assumed. Current theoretical work indicates that the reduced gradient of ΔP versus ΔT plots at large ΔT is the

consequence of gas-kinetic temperature jumps at the dry upper plate, which reduce the effective temperature difference across the gas layer adjacent to the liquid (see *section1.3.1*).

1.3.4 Observations with Sulfuric Acid

Sulfuric acid/water vapour was the first two-component system to be studied in the glass Onsager cell [34]. Measurements for two-component systems were needed because the original problem of the CO_2 and water involves a two-component system, and because a two-component system can tolerate negative ΔT values without condensation, because the vapour pressure is always lower than the equilibrium vapour pressure of the volatile component at the temperature of the upper plate. This experiment confirmed that Equation 1.22 holds for negative ΔT values. No curvature was found in the ΔP vs. ΔT plots, probably because the water vapour pressure was always very low.

The surface concentration of free water molecules in concentrated sulfuric acid is very small [46]. This is because of the formation of hydrates with one or more water molecules bonded to a sulfuric acid molecule [46]. As there is more hydrate formation at the higher concentrations, the hydrate dissociation energy adds to the usual heat of vaporization. Therefore it was expected that an increase in $|Q^*|$ might be observed at higher concentrations of sulfuric acid. Contrary to this hypothesis, the value of $|Q^*|$ fell with increasing acid concentration [34] (Figure 1.16). The reason was that the rate of dissociation of the hydrates became a significant rate-determining step in the evaporation process. The dissociation process was independent of the temperature gradient at the liquid surface, so the measured $|Q^*|$ value was reduced.

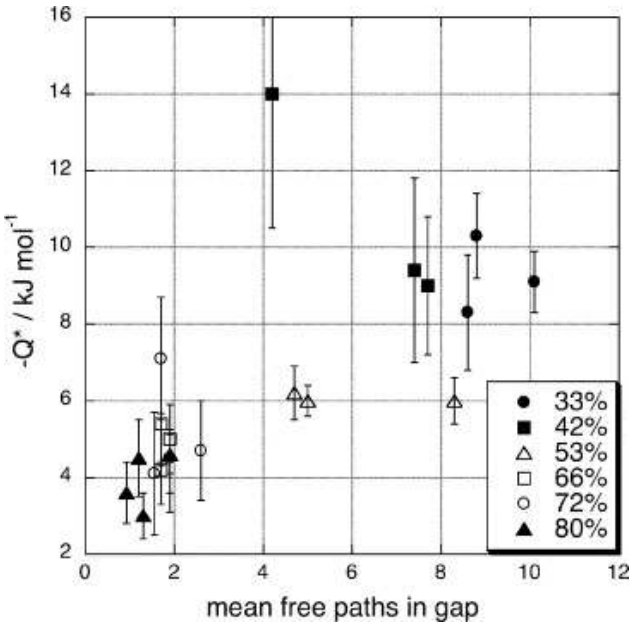

Figure 1.16. |Q*| vs. n_λ for sulfuric acid[34].

1.4 Glycerol-Water Mixtures

Further studies of the two-component systems were required, because the only such system studied so far has been sulfuric acid-water. For comparison of the CO_2-water system with other two-component systems, in order to check for inconsistencies and individual behaviour, there must be a range of systems to compare with. The sulfuric acid system was not a simple one, in that $|Q^*|$ decreased as the sulfuric acid concentration increased and so it was not a good standard for comparison. Hence it was decided that a study of the glycerol-water system would be useful. In glycerol-water mixtures, the vast majority of the vapour leaving the surface is water [47], which eliminates the problem of measuring differing species in the matter fluxes from the liquid surface.

Water does not form a complex with glycerol as strongly as with sulfuric acid, with hydration energies in the order of 4 kJ mol^{-1} for glycerol and 29 kJ mol^{-1} for sulfuric acid [46]. Therefore, there should be significant differences in the dependence of Q^* on water concentration for this experiment, because dissociation of the hydrates is not likely to be rate determining. Important complexes are formed in the glycerol-water system [48, 49] and are of the form AB and AB_6, where A is glycerol and B is water. If the AB complex becomes the major component and the dissociation step becomes rate determining for evaporation at high glycerol concentrations, then

$|Q^*|$ should again be found to decrease with decreasing water concentration. Marcus [50] used data from the literature to calculate the maximum excess enthalpy of glycerol-water mixtures, which occurred at a mole fraction of around 0.4, and obtained a value of -0.6 kJ mol^{-1} at 25°C. Hence there is no strong interactions between the glycerol and water molecules and we can predict that the variation of $|Q^*|$ with the number of mean free paths in the 2 mm gap should be similar to the results found with the one-component systems [30, 33].

This experiment is testing whether the effective temperature gradient for the glycerol-water system exists within the range of two mean free paths from the surface of the liquid as proposed in *section 1.3.1*. This will be apparent through the resulting $|Q^*|$ vs. mean free path plots which will show a rise in $|Q^*|$ near the liquid surface starting at the point where the effective temperature gradient occurs. Also, this experiment will examine the effect of increasing glycerol concentration on the resulting $|Q^*|$ values. This effect of concentration should be dramatically smaller when compared to the effect observed in the sulfuric acid experiments. This is because the coordination interactions between the glycerol and water molecules are weaker. If there is a significant effect on $|Q^*|$ from the glycerol-water complexes, then complexes of water and CO_2 may need to be taken into account when calculating the flux of CO_2 from the water surface.

Chapter 2:

Experimental

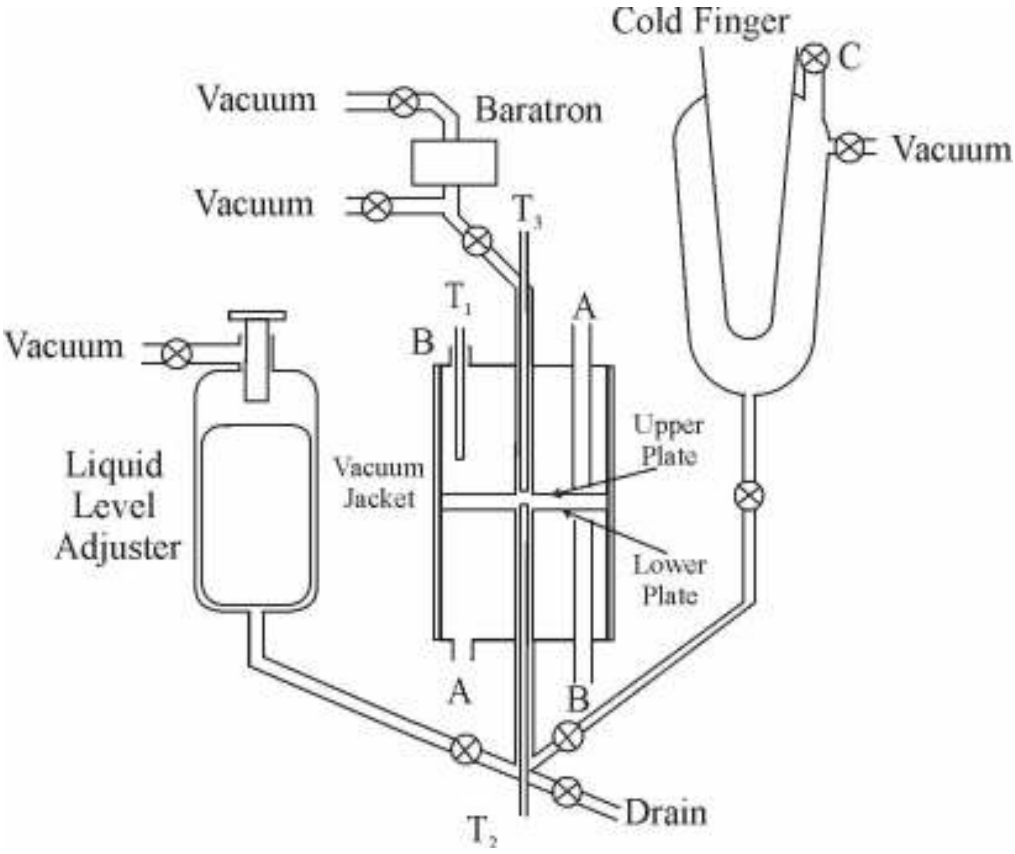

Figure 2.1. Onsager Cell with degassing chamber and liquid level adjuster.

To measure Q^* for water vapour over glycerol-water mixtures, the temperature difference across the vapour layer was varied while keeping the liquid-surface temperature constant, and pressure readings were taken via the Baratron above the Onsager cell. The temperature difference was given by T_{vap}-T_{liq}, where T_{vap} is actually the temperature, T_3, of the vapour at the level of the upper plate. For equation (1.22), $\Delta T=T_{vap}-T_{liq}$, T and P are the temperature and pressure when $\Delta T=0$ and $\Delta P=P_{vap}-P_{vap}^{\ 0}$ (where $P_{vap}^{\ 0}$ is the pressure when $\Delta T=0$). The apparatus for measuring Q^* for water vapour over the glycerol-water mixture was the same that had been used for previous experiments [30, 33, 34] with only slight modifications (Figure 2.1). The experimental set up consisted of three main compartments: the experimental cell, the liquid level adjuster and the degassing chamber, all of which were connected

to a Pyrex high-vacuum system which incorporated two large cold traps and a diffusion pump.

2.1 Experimental Cell

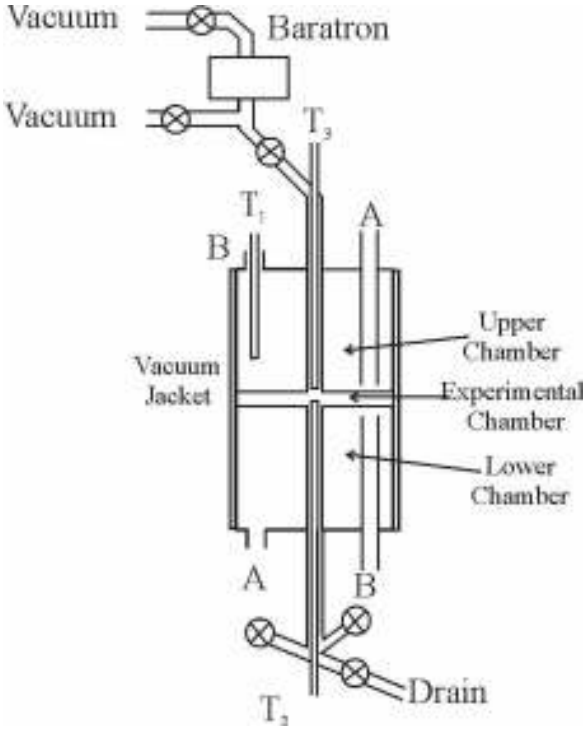

Figure 2.2. Pyrex glass Onsager cell.

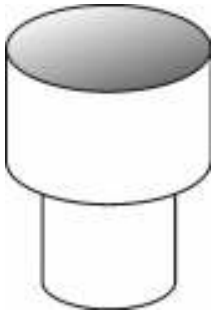

Figure 2.3. Hollow copper cylinder which holds the dry ice in the circulating bath.

The Pyrex glass cell was made by Robert MacGregor in the departmental glass workshop. The cell comprised three compartments, the upper, lower and experimental chambers. The three chambers were surrounded by a vacuum jacket. Including the vacuum jacket, the cell was 70 mm in diameter and 130 mm high.

The upper and lower chambers were connected to a Julabo FP50 circulating bath via insulated rubber tubing. The bath liquid used was ethanol. The Julabo bath's lowest stable temperature was -45 °C. To obtain the lower temperatures required for some of the experiments a hollow copper cylinder (Figure 2.3) was made in the

chemistry department's mechanical workshop. This cylinder was insulated with a layer of cotton wool, 2.5 cm thick, held in place with duct tape. An insulated lid was made from a cork ring, plus cotton wool and duct tape. In use, the cylinder was half filled with ethanol and the thinner end was placed in the circulating bath. Dry ice was put inside the cylinder as required (usually every 20-25 mins during an experimental run) to enable lower regulated temperatures to be obtained.

The Inlets, labelled A, in the upper and lower baths denote where the bath liquid entered the compartments before exiting via inlets B. Heaters, controlled by a computer, were connected to inlets A. The heaters and control electronics were made in the departmental glass, electronics and mechanical workshops. These heaters controlled the liquid and vapour temperatures in the experiment, with reference to chosen thermistor voltages, by a QuickBasic program written by Professor Leon Phillips.

The central experimental chamber comprises two 60 mm diameter glass plates with 8 mm diameter glass tubes attached to the centre for the entry of thermistors, liquid and vapour. The two plates were spaced 8 mm apart, and the lower plate's tube was connected to the liquid reservoir of the liquid level adjuster, while the upper plate tube was connected to the Baratron. The Baratron was a MKS 223B 0.2 torr differential gauge, the reference side connected to the high-vacuum line. The output voltage from the Baratron was monitored continuously with a 12-bit A/D board (PCLD-780) and plotted as a 5-point running average.

The thermistors T_2 and T_3 were placed in small 2 mm glass tubes which ran down the middle of the central 8 mm glass tubing. The sensor proportion of the upper thermistor (T_3) was at the level of the upper plate. The sensor proportion of the bottom thermistor (T_2) was half way between the two plates, so that when the liquid was at the right depth the temperature taken would refer to the surface of the liquid. The thermal conductivity of the liquid was larger than that of the vapour by at least a factor of 8.5. Previous tests had shown that the measured value of Q^* was not strongly dependent on the depth of immersion of the thermistor when this was varied over a range of 1-2 mm. All the thermistors, including T_1 were coated with thermal grease before being inserted into the 2 mm glass tubing, to provide greater contact with the glass for better heat transfer. The thermistors were incorporated into a circuit with an ordinary resistor and the voltage drop was read by the computer via the 12-bit A/D board every three seconds. Two 12-bit D/A outputs on the same board were used

to drive the heater-control circuit. The slow response of the T_3 thermistor was overcome by using the T_1 thermistor immersed in the upper bath solution for temperature control. T_3 was used to monitor the approach to a stable temperature of the vapour at the level of the upper plate (*see section 2.4.2*).

.

2.2 Preparation of Mixtures

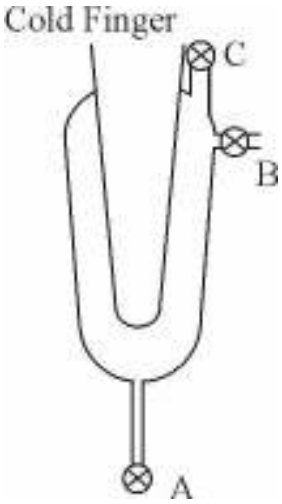

Figure 2.4. Glass degassing system.

The degassing system (Figure 2.4) was used to remove dissolved gas from the liquid in preparation for the experimental runs. It had a cold finger in the centre for liquid nitrogen and three greaseless stopcocks. Stopcock C leads to the vacuum system, stopcock B connects to a funnel which is used for adding liquid and stopcock A leads to the liquid level adjuster and measurement cell. Mixtures of distilled water and analytical reagent grade 99.5 % glycerol were degassed by a number of freeze--pump-thaw-boil cycles in the degassing chamber. Every time a mixture was exposed to the atmosphere, because of breakages or leaks, the process had to be repeated. Each degassing cycle consisted of boiling the mixture with heat provided by a hand-held heat gun. After cooling for 10 minutes, the mixture was then frozen by pouring liquid nitrogen into the cold finger. After freezing, the solid mixture was exposed to the vacuum via tap C for 5 minutes. This cycle was repeated 5-6 times. The Baratron connected to the vacuum line down-stream from the degassing chamber was used to monitor progress. If there was no increase in pressure when the frozen liquid was opened to the vacuum then the process was complete. Nevertheless, one or two

further cycles were completed after a nil pressure increase result, to ensure that all dissolved gas had been expelled.

2.3 Transferring a degassed mixture to the cell

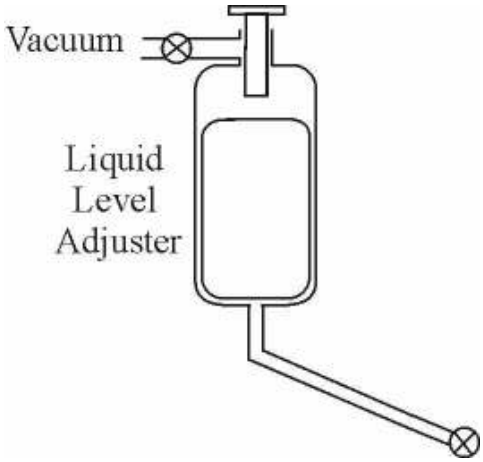

Figure 2.5. Glass liquid level adjuster.

From the degassing chamber the mixture was allowed to flow down the glass tubing and up into the liquid level adjuster and cell. The liquid level adjuster consisted of a hollow glass cylinder inside a slightly larger glass compartment, to which a modified greaseless stopcock was attached at the top.

The hollow cylinder rose to the top of the compartment as the mixture flowed up from the bottom. The modified stopcock had a plunger which could be used to push the cylinder down, so forcing more mixture into the cell. It could also be raised to allow the mixture to leave the cell but, for the mixture to be lowered in the cell the drain was generally preferred because the mixtures were very viscous and the liquid level adjuster worked only very slowly in reverse. To ensure that the entire bottom plate was covered, the best view was obtained by looking from below through the lower temperature-control compartment, while the circulating bath was turned off; this gave a clear view of the extent of covering of the bottom plate by the mixture. The mixture level was adjusted to a point where, when viewed slightly below the surface, the tip of the thermistor touched the tip of its own reflection. This height was 3 mm from the top plate, δ in equation (1.21).

Care had to be taken to ensure that the liquid did not touch the top plate and leave droplets, for then the cell would have to be washed out and degassed and a new mixture put in the cell. With liquid on the top plate, false pressure measurements

would be obtained. With aniline and n-heptanol, liquid on the top plate was not such a problem because heating of the top plate caused any droplets to evaporate from the top plate and condense below. This did not work with the glycerol/water or sulfuric acid/water mixtures because an involatile, strongly hygroscopic residue would be left.

An extra stopcock was installed between the liquid level adjuster and the cell, because when the mixture was cooled, the vapour pressure was reduced, pulling more mixture from the liquid level adjuster, with the likelihood of getting liquid on the top plate. Closing the stopcock prevented this.

2.4 Taking Measurements

2.41. Preparation

In preparation for taking Q^* results at a different mixture composition, the system was first washed out with distilled water (7-8 repeated rinsings for most of the apparatus and about 20 for the main cell) and then pumped dry. The system was degassed by pumping under high vacuum for two days, to remove all the gas adsorbed on the glass and in the Baratrons, before the mixture was introduced into the degassing chamber. Careful visual inspection of the main cell was needed to ensure that it was dry. Running liquid from the circulating bath at 40°C through the main cell during pumping helped with evaporating the water.

Before each experimental run the zero-pressure base-line of the Baratron was monitored and adjusted with both sides of the Baratron open to the vacuum. Also, built into the computer programme was a facility for entry of the Baratron zero, as obtained by roughly averaging ~10 minutes of pressure readings. Typical computer Baratron adjustments were about 0.0002 torr. Baratron pressure drifts during experimental runs were checked by returning to the same ‘reference’ temperature values about every third or (sometimes) fourth point. The program which analysed the data fitted the reference values to a quadratic function of time (the drift was not usually linear) and corrected all the pressure readings accordingly.

2.4.2 Experimental Procedure

The ethanol bath for each experimental run was set to a temperature at least 6 °C lower than the base liquid temperature required for the run. This was to counter the gain of heat from the surroundings as the ethanol travelled to the cell via insulated

tubing and to allow the inlet heaters to control the final temperature. This allowed readings with ΔT up to -2 °C to be taken.

The experiment was run by a QuickBasic programme written by Professor Phillips. This programme recorded the voltages from the three thermistors and the voltage from the Baratron. These voltages were converted to temperature and pressure readings on a single combined graph on the computer screen. Individual pressure values corresponded to a ten point moving average. The programme displayed both the voltage input from the thermistors and the result of conversion from voltage to temperature, using calibration formulas based on a separate series of measurements using a Tinsley Pt100 platinum resistance thermometer.

For the first measurement in the run, the pressure was first allowed to equilibrate over 30 mins after the Baratron was opened to the cell. All sets of measurements after the first set during the run were left to equilibrate for a minimum of 15 mins. After the pressure had equilibrated, a number of criteria had to be met before taking each point:

- T_1 within ±0.0005 volts of required voltage (approx ±0.05 °C)
- T_2 within ±0.001volts of required voltage (approx ±0.1 °C)
- T_1, T_2, T_3 and P stable

The vapour temperature could be allowed to vary more than the liquid temperature, because the vapour pressure was very sensitive to the liquid surface temperature and relatively less sensitive to the vapour temperature.

For each of these requirements to be met, each set of points could take up to 10 minutes therefore lengthening the total equilibration time. Each set of measurements consisted of taking ten points which consisted of T_1, T_2, T_3, P, point number and time (seconds). ΔT varied between different sets of points between ± 2 °C in approximately 0.5 °C steps. The temperature steps were approximate because the required voltages were adjusted in 0.01 V steps.

Every third set of points taken was referenced back to ΔT=0. To get the drift of the pressure during the experimental run, sets 1, 4, 7, 10 and 13 were always set to ΔT=0. Including the reference sets, each run was typically made up of thirteen set of points with ΔT equalling -2, -1.5, -1, -0.5, 0, 0.5, 1, 1.5 and 2.

2.4.3 Calculating Q*

By using another QuickBasic programme written by Professor Phillips, the sets of data were manipulated to find Q^* for the experimental run. Each set of ten points were averaged to get to get one ΔP value for each change in vapour temperature. Q^* was calculated in two ways: by a linear fit to graphs of ΔP vs. ΔT, and by averaging individual points. All of the Q^* values I have plotted in the results section were calculated via linear fit to the P versus T graphs. The gradient ($\Delta P/\Delta T$) fits into equation (1.22) to calculate Q^*. To calculate Q^* via individual points, the reference temperature and pressure at ΔT=0 was used as T_0 and P_0 for all points. With the exception of the five ΔT=0 points, which give highly incorrect values as small pressure deviations when divided by almost zero (ΔT) resulted in Q^* values of $\pm$ 300 kJ mol^{-1}, resulting Q^* values were then averaged to get a single value with a student t analysis of the standard deviation and 95 % confidence limits. Although only the linear values are reported, individual Q^* values were useful for checking for consistency in a run.

Average each set of 10 points

↓

Calculated the temperature drift using the reference values

↓

Adjust the averaged points using the temperature drift

↓

Calculated Q* via linear fit

↓

Calculate Q* via individual points

↓

Check for consistency in Q* from both methods

2.4.4. Sources of Error

The measured temperature and pressure changes were all small, so there was a lot of room for error. Typical sources of problems in this experiment ranged from diffusion pump problems, to small leaks which were nearly impossible to find, through unforeseen condensation on the top plate, to unpredictable vagaries of the temperature-regulation system. In some of the graphs in the results section the reader will notice that there seems to be a non-linear drop of pressure at the tail end of the ΔP vs. ΔT graphs, near the value of ΔT=-2. This was believed to be because of condensation. This condensation applied mostly to the graphs where the base

temperature was -46 °C. This is because at that low temperature a drop in the target thermistor of 0.04 volts created a ΔT of –(3-4) °C, compared to a drop of -2 °C when the base temperature was at -34 °C. This arised from the voltage/temperature conversion for the thermistors not being linear.

The condensation caused the pressure to drop due to the presence of liquid at a lower temperature, which allowed the vapour to condense more readily than on a dry surface. If ΔT remained small, condensation would not occur. The condensation was easily recognised as the pressure would first settle during the fifteen minute equilibrating stage and then rapidly fall. The condensation, which was hard to get rid of, would affect the lower readings of ΔT. Consequently, voltage changes of -0.0075 and -0.0125 V were put in place of the normal settings of -0.003 and -0.004 V, which gave temperature changes of around -1 and -2 °C instead of -3 to -4 °C. This often would not affect the upper ΔT as quick recognition of condensation enabled rapid adjustment to a large positive ΔT in order to remove the condensation.

Even so, there were many bad runs because of failure to quickly notice the condensation occurring, which then required a few hours where the top plate was heated extensively while keeping the bottom liquid as cool as possible.

Chapter 3:
Results and Discussion

3.1 ΔT vs. ΔP Graphical Results (see appendix 5.1-5.6)

Each of the ΔT vs. ΔP graphs was the result of a single experimental run which in return gives one Q^* result per graph, to be plotted against the distance δ in terms of mean free paths. It was intended that Q^* would be recorded for each of the five concentrations at three different temperatures, -32, -34 and -46 °C and to repeat each temperature twice. Therefore if all the runs were successful there would be nine points on each of the ΔT vs. ΔP graphs. These temperatures were chosen because the lowest temperature the bath could conveniently hold was -40 °C; for ΔT to be as low as -2 °C while still keeping the lower plate warm, -34 °C was found to be the lowest workable temperature. Using dry ice in the copper cylinder submerged into the rotating bath liquid, enabled the bath to cool to -52 °C. The lowest working range (46 °C) was 6 °C higher than the absolute lowest temperature. Any temperature higher than -32 °C would result in a pressure higher than the Baratron's working range.

Results were taken at -40 °C for the 94.5 % glycerol mixture because this concentration was the most likely to be able to have approximately a distance of 1 mean free path between the upper plate and the surface of the liquid. This would give extra information on the $|Q^*|$ graph where the slope was starting to change rapidly.

The 75 % glycerol mixture resulted in vapour pressures at -32 °C outside the accurate working range of our Baratron. Therefore data was only taken at -34 and -46 °C. Also, for the 75 % glycerol mixtures at -46 °C there was an apparent large increase of $|Q^*|$ (to around 40 kJ mol^{-1}). This was unexpected as ΔH_{vap} was calculated to only be 39 kJ mol^{-1}. To confirm this result, the cell was cleaned out and a new solution of 75 % glycerol was made and put into the cell, with care taken to avoid any liquid getting on the top plate. Runs 1-5 used the first solution, while runs 6-10 used the second solution. The second set of results agreed with the first set of results, so there is an unsolved problem here, which could not be solved in the time available.

After the drift of the reference temperatures were taken into account *(section 2.4.2)* most of the resulting graphs were linear. This lack of curvature showed that condensation played no part in those experiments. In some of the graphs there is a large scatter, which occasionally leads to apparent slight curvature at low ΔT. Unless there is some glycerol on the upper plate, condensation can only occur if the vapour pressure of water or ice at the temperature of the top plate is exceeded. This was not the case. All results with a R^2 value less than 0.85 were discarded as being too greatly affected by scatter.

These linear plots were then used to calculate Q^* both from the mean of individual points and also by finding the slope. The assumption was made that the Q^* values calculated via a line of best fit gave a more accurate value and these are the values listed. The values obtained from the mean and standard deviation of the individual points were used to check the line of best fit value. The values when ΔT=0 were not included in the mean of the individual points because of the large uncertainties associated with small values of ΔT and ΔP.

By substitution of the gradient in equation (1.22), the calculation of Q^* becomes:

$$Q^* = \frac{RT^2}{P}\left(\frac{\Delta P}{\Delta T}\right) \tag{3.1}$$

where T and P are listed on each graph as T^0 and P^0 respectively and $(\Delta P/\Delta T)$ is the gradient of the respective graph. Note that the Q^* values and their confidence intervals in Appendices 5.8 and 5.9 were calculated using a QuickBasic program written by Professor Leon Phillips, and may differ slightly from those in the Appendix 5.1-5.5, which were recalculated later using Microsoft Excel, with a different routine for obtaining the linear fit.

For comparison of the resulting Q^* values with ΔH_{vap}, the ΔH_{vap} values were calculated by use of the Clausius-Clapeyron Equation:

$$\frac{d\ ln(P)}{dT} = \frac{\Delta H_{vap}}{RT^2} \tag{3.2}$$

which rearranges to give

$$\frac{d\ ln(P)}{d\left(\frac{1}{T}\right)} = \frac{-\Delta H_{vap}}{R} \tag{3.3}$$

By plotting $ln(P)$ vs. $1/T$ with the temperature ranging from 252 to 276 K, I calculated ΔH_{vap} for each of the mixtures (see *appendix 5.7*).

3.2 |Q*| Graphical Results (appendix 5.9)

These graphs show my measured $|Q^*|$ values versus the number of mean free paths in the 2 mm gap between the surface of the liquid and top plate (calculated for H_2O with a collision diameter of 3×10^{-8} cm).

The 80%, 85% and 90% graphs all show a slight rise in $|Q^*|$ as the mean free path decreased, as predicted (see *section 1.3.1*). As all three graphs have their lowest points near or just inside the 2 x mean-free-path distance, there should not be a large rise in $|Q^*|$ values until the mean free paths decrease further into the Knudsen layer. All the high mean free path $|Q^*|$ values lie around the 5-8 kJ mol^{-1} region which is almost an order of magnitude smaller than the calculated ΔH_{vap}. In the 90 % glycerol results there is a lot of scatter at the higher mean free path end of the graph; this is put down to experimental error.

As mentioned above, the results from the 94.5 % glycerol-water mixture was measured over a range of four temperatures instead of three because of the likelihood of this concentration having $\beta > \delta$. At the higher numbers of mean free paths $|Q^*|$ is approximately 10 kJ mol^{-1}. The values for $|Q^*|$ become increasingly scattered as the mean free paths decrease. This scattering makes it difficult to observe any increase in the $|Q^*|$ values, although a slight rise in $|Q^*|$ can still be seen. This increase in $|Q^*|$ seems steeper than the increase of $|Q^*|$ seen for the previous three concentrations of 80, 85 and 90% glycerol mixtures. This result suggests that δ has either come close to or just become slightly lower than β. This cannot be confirmed as present as further experimental runs are required at a lower temperature with lower scattering in the observed $|Q^*|$ values. Combining data from the four concentrations result in Figure 3.1 where in the higher mean free path region the differing concentrations give similar $|Q^*|$. This similarity in values between the differing concentrations provides some evidence for the lack of dependence of Q^* on glycerol concentration. In Figure 3.1, the increase of $|Q^*|$ as δ decreases is more evident. This can be seen even with the large amount of scattering in the results. Although a curved line of best fit through this region will not necessarily be an accurate representation of what is occurring, it

does shows the anticipated increase of Q^* at low numbers of mean free paths (Figure 3.2).

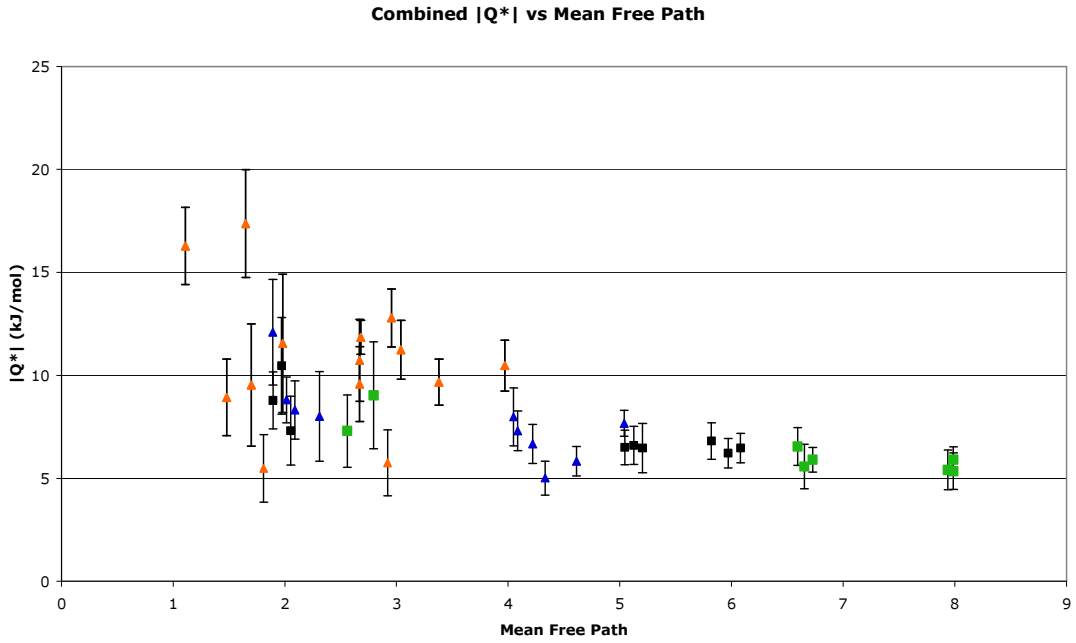

Figure 3.1. Combined |Q*| values of the 80 (green squares), 85 (black squares), 90 (blue triangles) and 94.5% (orange triangles) glycerol-water mixtures.

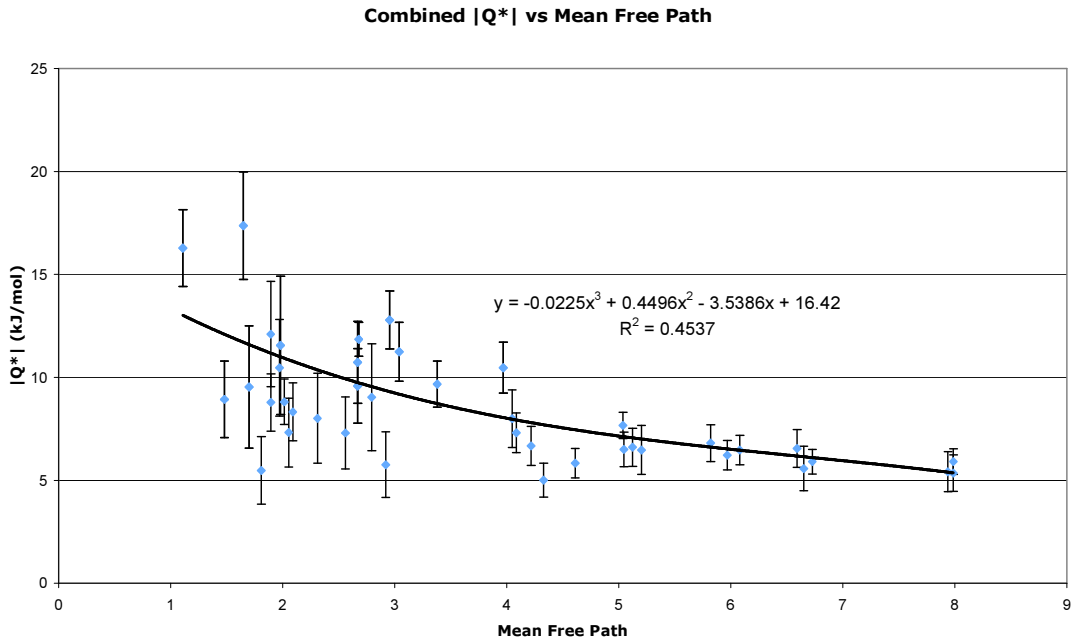

Figure 3.2. Calculated curve through the combined |Q*| values of the 80, 85, 90 and 94.5% glycerol-water mixtures.

The 75 % glycerol solution results do not agree with the results from other concentrations (Figure 3.3). At the higher mean free path region, the $|Q^*|$ values agree with the other concentrations, with values less than 10 kJ mol^{-1}, when δ falls to 2-3 mean free paths, the value of $|Q^*|$ rises dramatically. This differs from the predicted effect, where there is a small steady increase in the value of $|Q^*|$ until the 1-2 mean free path region. This rise in Q^* commences at a higher mean free path distance then previously expected. The current theory suggests that when δ reaches zero $Q^* = -\Delta H_{vap}$. The calculated $-\Delta H_{vap}$ for the 75 % mixture is 39 kJ mol^{-1} but the last two $|Q^*|$ values around 2.5 mean free paths are 39 kJ mol^{-1} or higher. As noted earlier, this remains an unsolved problem.

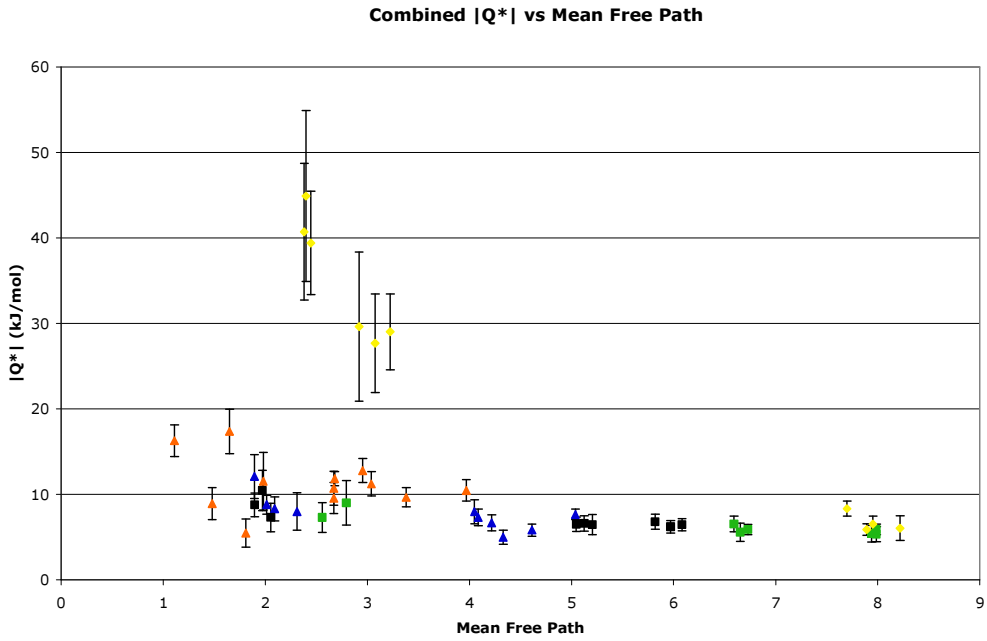

Figure 3.3.Combined |Q*| values of the 75 (yellow diamonds), 80 (green squares), 85 (black squares), 90 (blue triangles) and 94.5% (orange triangles) glycerol-water mixtures.

Chapter 4:
Conclusion

Unlike the previous Onsager heat of transport experiments with aniline and n-heptanol, the ΔT vs. ΔP plots were linear, as in the sulfuric acid experiments. The reason for this is still obscure, although it can be noted that temperature-jump theory (which provides a highly plausible explanation for the bent plots obtained with one-component systems at large numbers of mean free paths in the vapour gaps) breaks down when the gap is only a few mean free paths.

Comparison of the measured $|Q^*|$ values, at different concentrations over the range 94.5 % to 80 %, shows very little dependence of $|Q^*|$ on the concentration of the glycerol-water mixture. This contrasts with the results seen with the earlier sulfuric acid measurements where the $|Q^*|$ values decreased with increasing acid concentration. The decrease in $|Q^*|$ for sulfuric acid is attributed to the strong complexes formed between the water and acid molecules. The absence of such a decrease for the glycerol-water mixtures for these concentration suggests that, as anticipated, the glycerol-water complexes do not have a significant impact on the resulting $|Q^*|$ values. The odd results obtained with the 75 % solution are as yet unexplained and further work on this system is required.

It has been reported that the major complexes found in the glycerol-water system are AB and AB_6 [48, 49]. Therefore, if $|Q^*|$ were to decrease because of dissociation becoming rate determining, a resulting drop of $|Q^*|$ would occur at the concentrations 83 % and 46 % glycerol for the AB and AB_6 complexes respectively. The results do not show a drop in $|Q^*|$ between 80 % and 85 % which suggests that this is not happening. However, there is a drop from the 75 % to 80 % results, which can suggest that something close to this coordinating effect is occurring, but not as simple as dissociation becoming rate determining. Despite these results for a glycerol-water mixture, complexes formed by CO_2 and water will almost certainly need to be take this into account in the planned experiments with CO_2.

The distance in mean free paths over which the effective temperature gradient occurs is found by observing where the resulting curve of $|Q^*|$ starts to greatly increase with e decreasing distance from the liquid surface. In the results from the

glycerol-water system there is insufficient clarity to make an accurate observation of where this increase of $|Q^*|$ starts. It is only possible to conclude that the increase starts in the 2-4 mean free path region, and that only if the 75 % glycerol results are not taken into account. As this result suggests that the effective temperature gradient is 2 to 4 mean free paths away from the liquid surface, it shows that the previous theory (that the effective temperature gradient was fully in the 2 mean free path range) to be incorrect. Even so, it shows that the effective temperature gradient extends a distance on the order of a few mean free paths away from the liquid surface. This temperature gradient depends on the liquid surface, which at present is not fully understood for the glycerol-water solutions.

These results still support the argument that there is a steep temperature gradient close to the liquid surface, which needs to be accounted for in modelling calculations.

The calculated values of $|Q^*|$ for 80 % to 94.5 % glycerol are in the range of 5 to 10 kJ mol^{-1}. This agrees with the previous work with the sulfuric acid. This agreement of $|Q^*|$ values is expected as the measured flux out of the liquid layer consists mostly of water and therefore should be similar between the two experiments. The glycerol-water $|Q^*|$ values are slightly higher than the sulfuric acid results because of the difference in the binding energies involved in the different complexes formed in the different solution as described in the introduction (*section 1.4*). The *n*-heptanol and aniline $|Q^*|$ values are different because the matter leaving and entering the liquid surface is not water and hence has different $|Q^*|$ values. This does not give any concrete estimates as to the expected value of the $|Q^*|$ for the flux of CO_2 from the oceans with the exception of the fact that all measured $|Q^*|$ values measured in our research group are in the range 2 to 50 kJ mol^{-1}. Values for CO_2/water would be expected to be in this range.

The problem with these results of the glycerol-water system as mentioned earlier is that the results from the very high values calculated for the concentration of 75 %. Glycerol-water do not fit the pattern. Although this might be an effect of the complexes of glycerol-water having an effect on the $|Q^*|$ values and so the values of $|Q^*|$ at higher concentrations have decreased, as seen with the previous sulfuric acid experiment, that does not seem to be the case. In the sulfuric acid experiment an increase of the ΔH_{vap} corresponded to the decrease of $|Q^*|$ as the strength of the lower order acid-water complexes binding to water increased. This observed increase of ΔH_{vap} was not seen in the glycerol-water solutions (Figure 4.1). Therefore, further

measurements of the glycerol system are required to find out what was different about the 75 % glycerol mixture.

Further measurements of this system over a wider range of concentrations and temperatures did not happen because of time constraints and the lack of a Baratron that would measure a high enough pressure and yet still have the accuracy of the Baratron that was used. Therefore, further investigations of these systems require such a Baratron, as the pressure changes are minute. A wider range of concentrations and temperatures should be investigated. A cooler circulating bath would also help lower the temperature, which would allow more concentrations to be measured inside the effective temperature layer, giving better insight into the exact workings of the fluxes to and from the liquid surfaces.

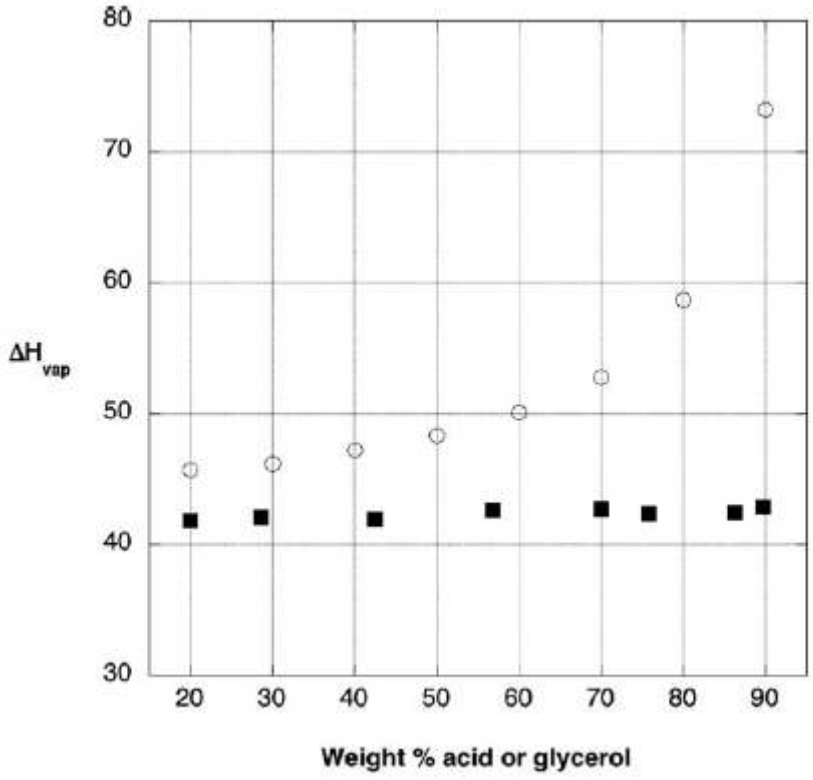

Figure 4.1. Comparison between the ΔH_{vap} of sulfuric acid (white circles) and glycerol-water (black squares) solutions[51].

Appendix

5.1 ΔP vs. ΔT for 75% Glycerol-Water Mixtures

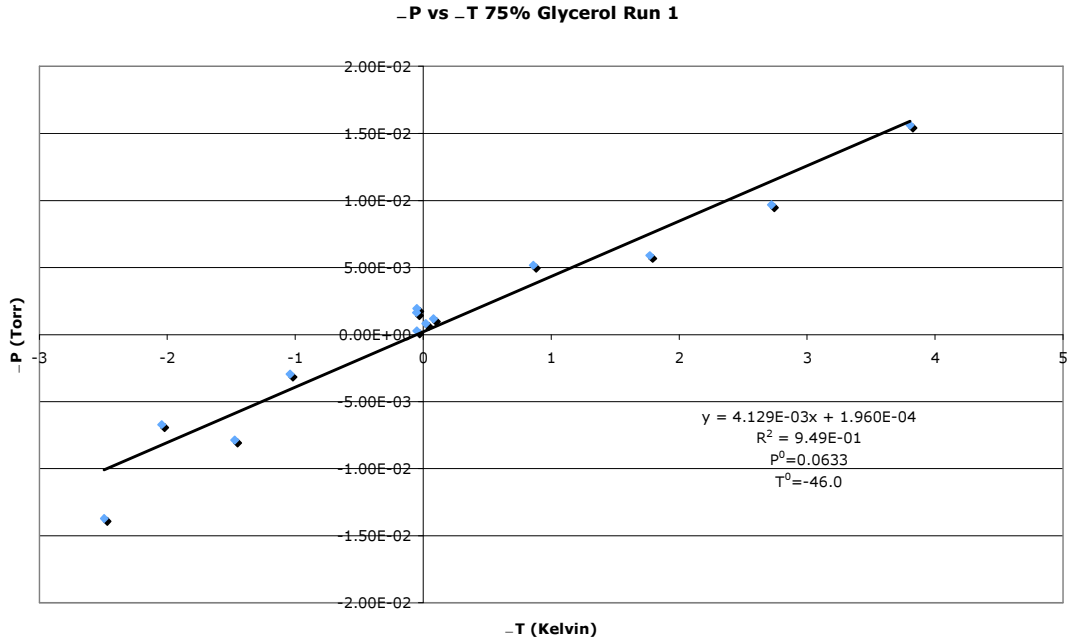

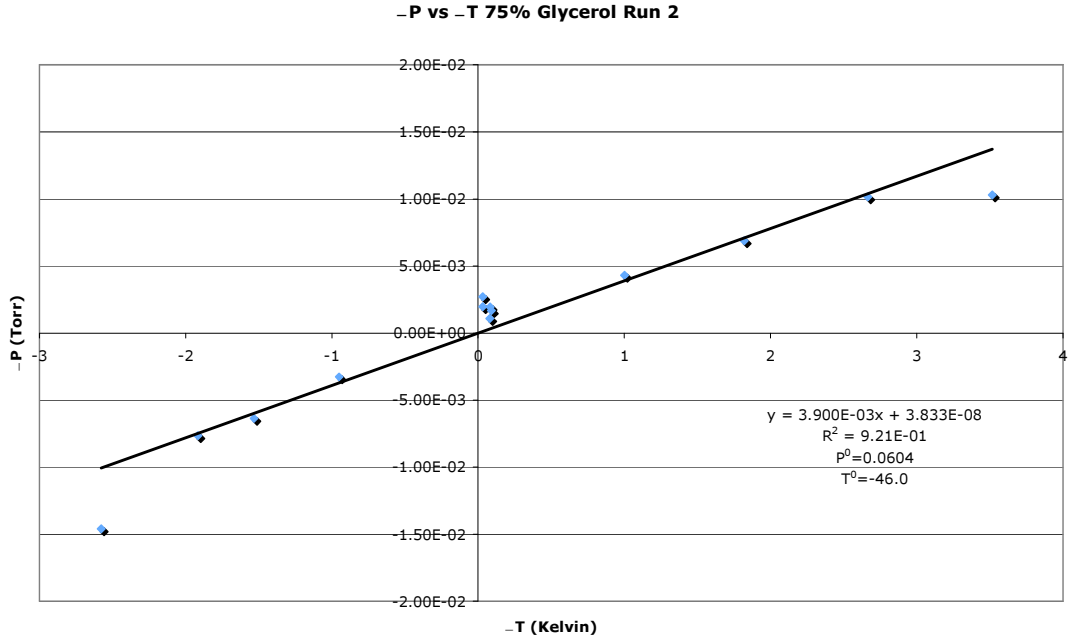

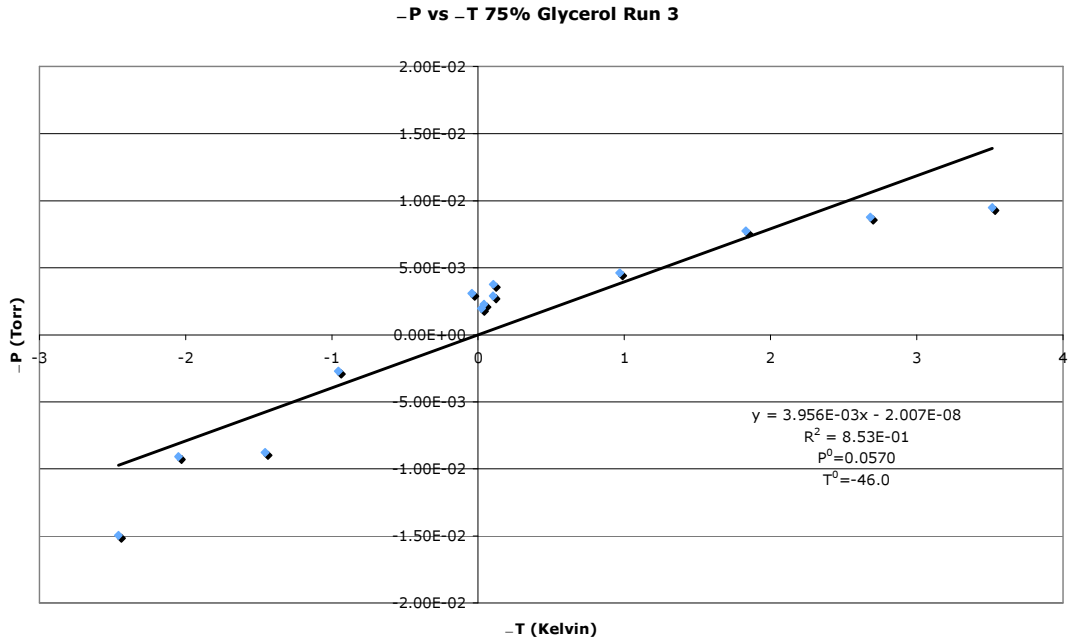
_P vs _T 75% Glycerol Run 3
2.00E-02
1.50E-02
1.00E-02
5.00E-03
0.00E+00
-5.00E-03
-1.00E-02
-1.50E-02
-2.00E-02
-3
-2
-1
0
1
2
3
4
_P (Torr)
_T (Kelvin)
y = 3.956E-03x - 2.007E-08
R2 = 8.53E-01
P0=0.0570
T0=-46.0

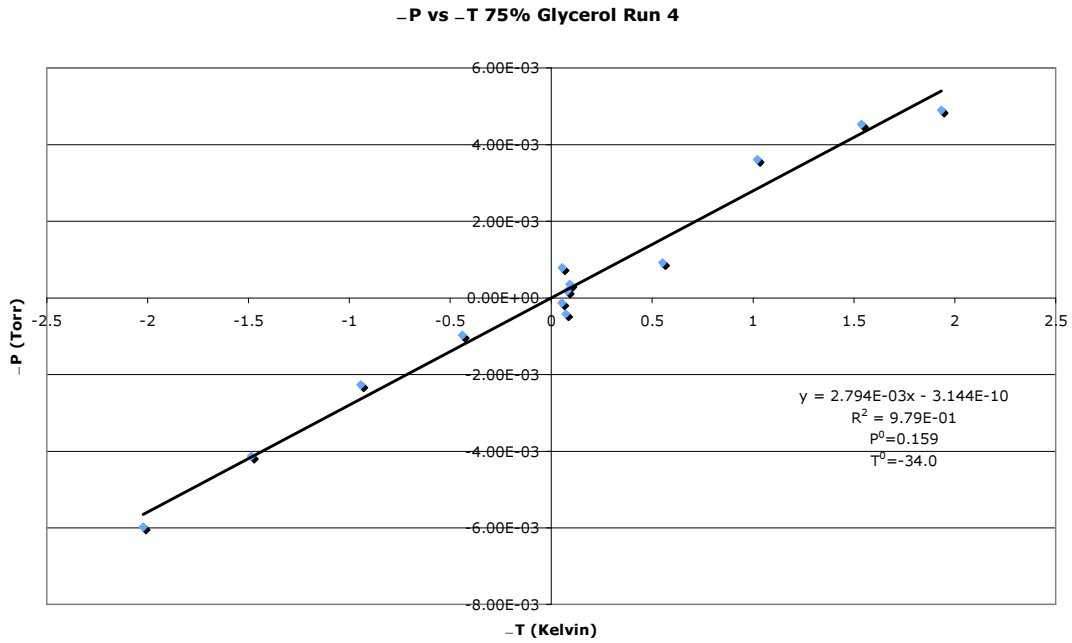
_P vs _T 75% Glycerol Run 4
6.00E-03
4.00E-03
2.00E-03
0.00E+00
-2.00E-03
-4.00E-03
-6.00E-03
-8.00E-03
-2.5
-2
-1.5
-1
-0.5
0
0.5
1
1.5
2
2.5
_P (Torr)
_T (Kelvin)
y = 2.794E-03x - 3.144E-10
R2 = 9.79E-01
P0=0.159
T0=-34.0

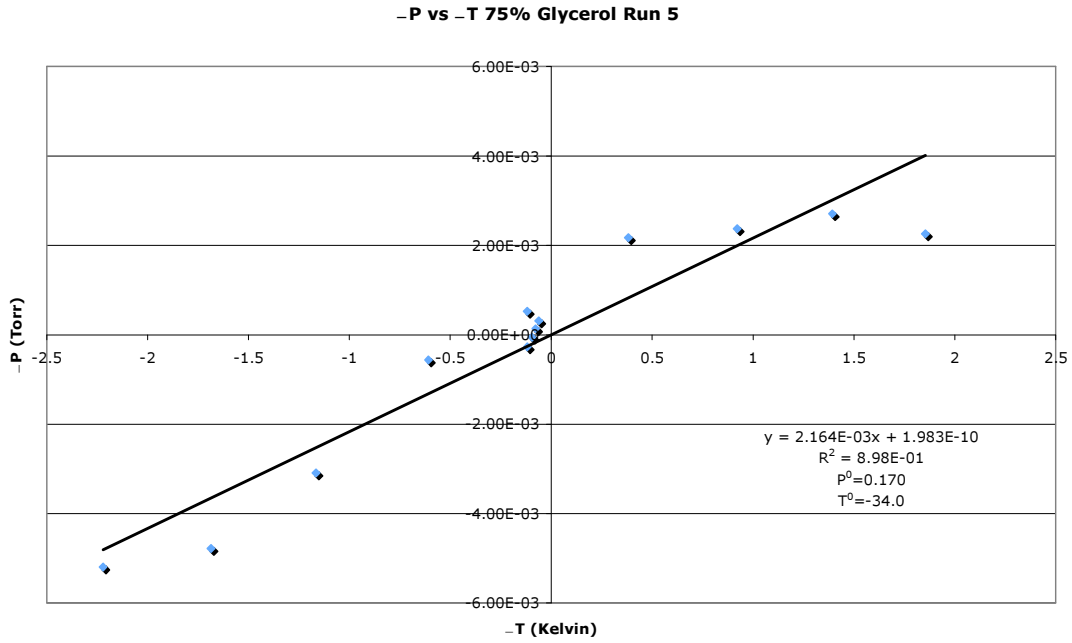
_P vs _T 75% Glycerol Run 5
6.00E-03
4.00E-03
2.00E-03
0.00E+00
-2.00E-03
-4.00E-03
-6.00E-03
-2.5
-2
-1.5
-1
-0.5
0
0.5
1
1.5
2
2.5
_P (Torr)
_T (Kelvin)
y = 2.164E-03x + 1.983E-10
R2 = 8.98E-01
P0=0.170
T0=-34.0

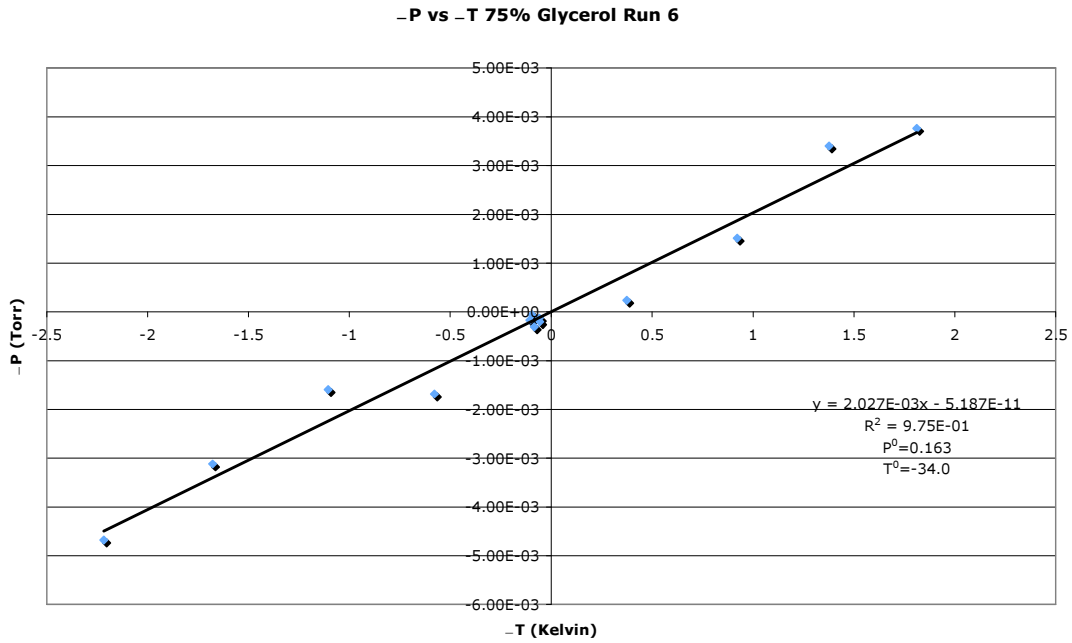
_P vs _T 75% Glycerol Run 6
5.00E-03
4.00E-03
3.00E-03
2.00E-03
1.00E-03
0.00E+00
-1.00E-03
-2.00E-03
-3.00E-03
-4.00E-03
-5.00E-03
-6.00E-03
-2.5
-2
-1.5
-1
-0.5
0
0.5
1
1.5
2
2.5
_P (Torr)
_T (Kelvin)
y = 2.027E-03x - 5.187E-11
R2 = 9.75E-01
P0=0.163
T0=-34.0

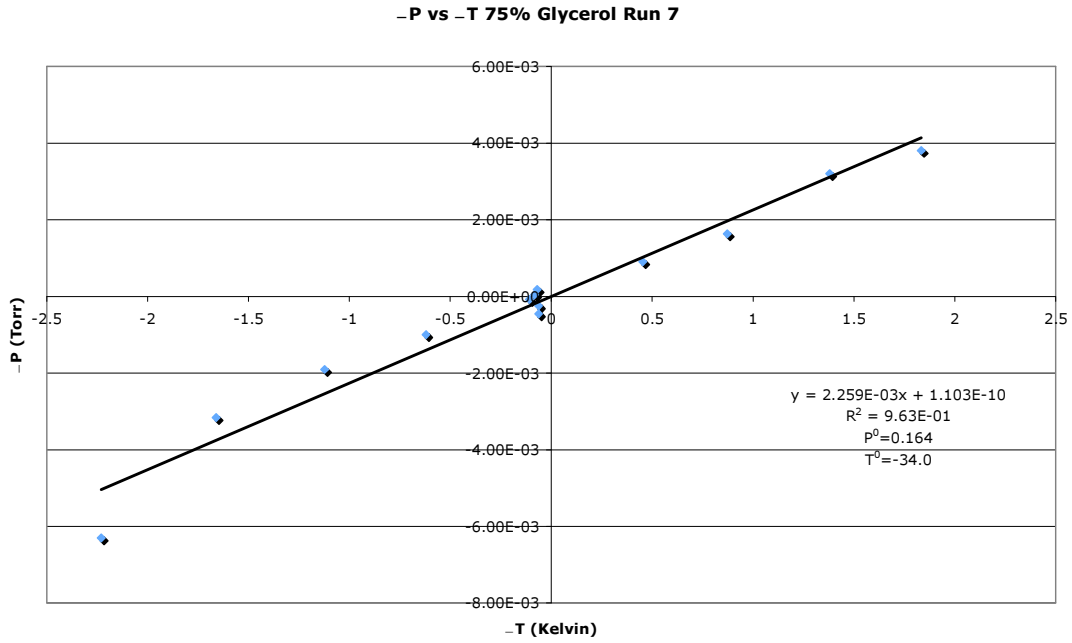
_P vs _T 75% Glycerol Run 7
6.00E-03
4.00E-03
2.00E-03
0.00E+00
-2.00E-03
-4.00E-03
-6.00E-03
-8.00E-03
-2.5
-2
-1.5
-1
-0.5
0
0.5
1
1.5
2
2.5
_P (Torr)
_T (Kelvin)
y = 2.259E-03x + 1.103E-10
R2 = 9.63E-01
P0=0.164
T0=-34.0

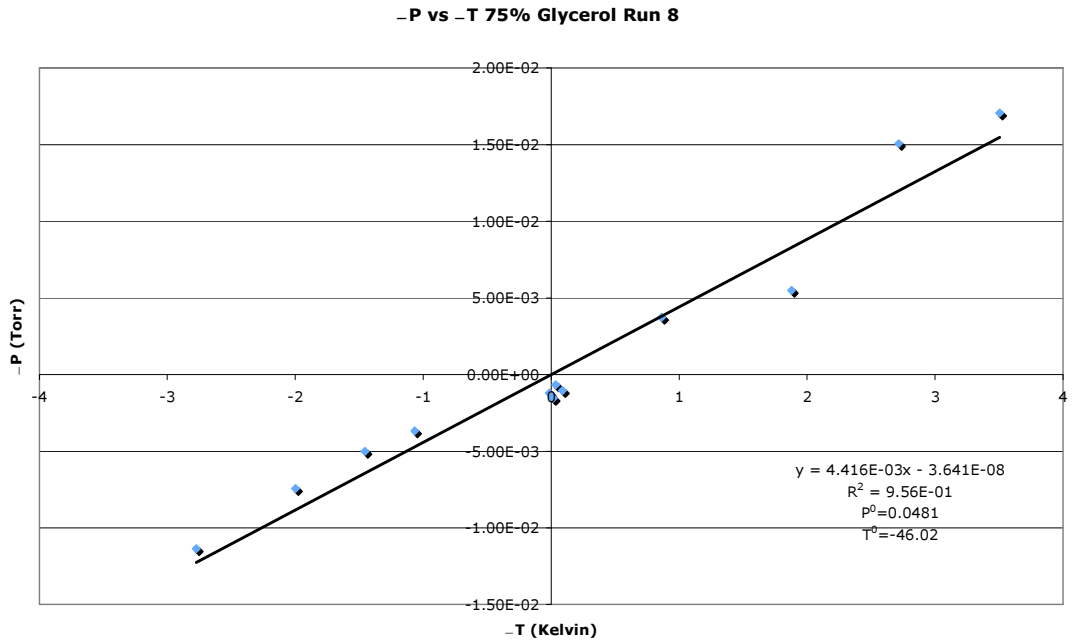
_P vs _T 75% Glycerol Run 8
2.00E-02
1.50E-02
1.00E-02
5.00E-03
0.00E+00
-5.00E-03
-1.00E-02
-1.50E-02
-4
-3
-2
-1
0
1
2
3
4
_P (Torr)
_T (Kelvin)
y = 4.416E-03x - 3.641E-08
R2 = 9.56E-01
P0=0.0481
T0=-46.02

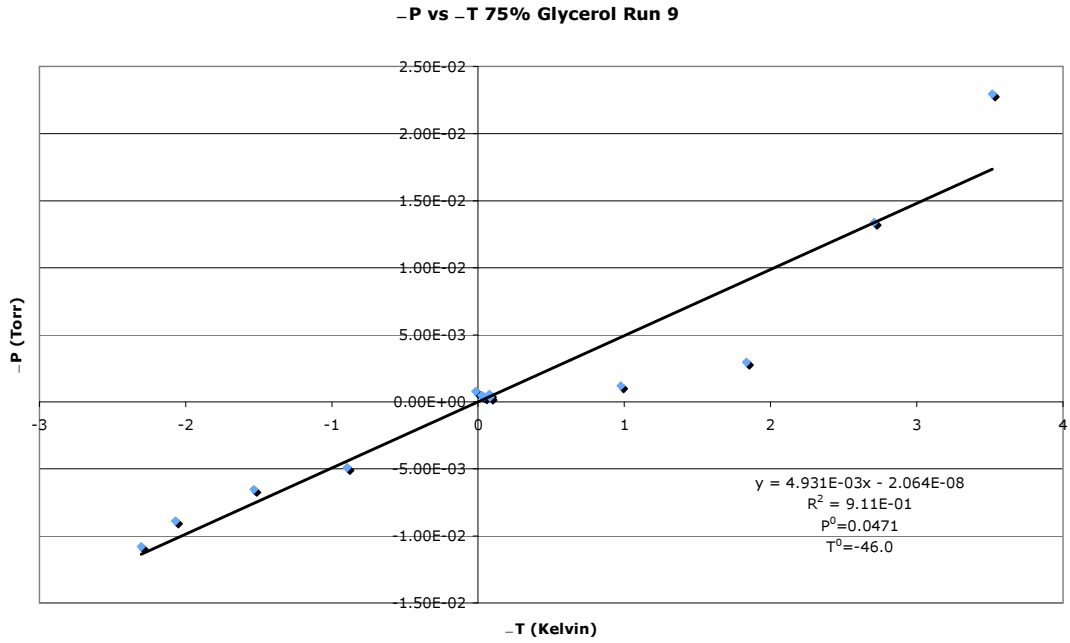
_P vs _T 75% Glycerol Run 9
2.50E-02
2.00E-02
1.50E-02
1.00E-02
5.00E-03
0.00E+00
-5.00E-03
-1.00E-02
-1.50E-02
-3
-2
-1
0
1
2
3
4
_P (Torr)
_T (Kelvin)
y = 4.931E-03x - 2.064E-08
R2 = 9.11E-01
P0=0.0471
T0=-46.0

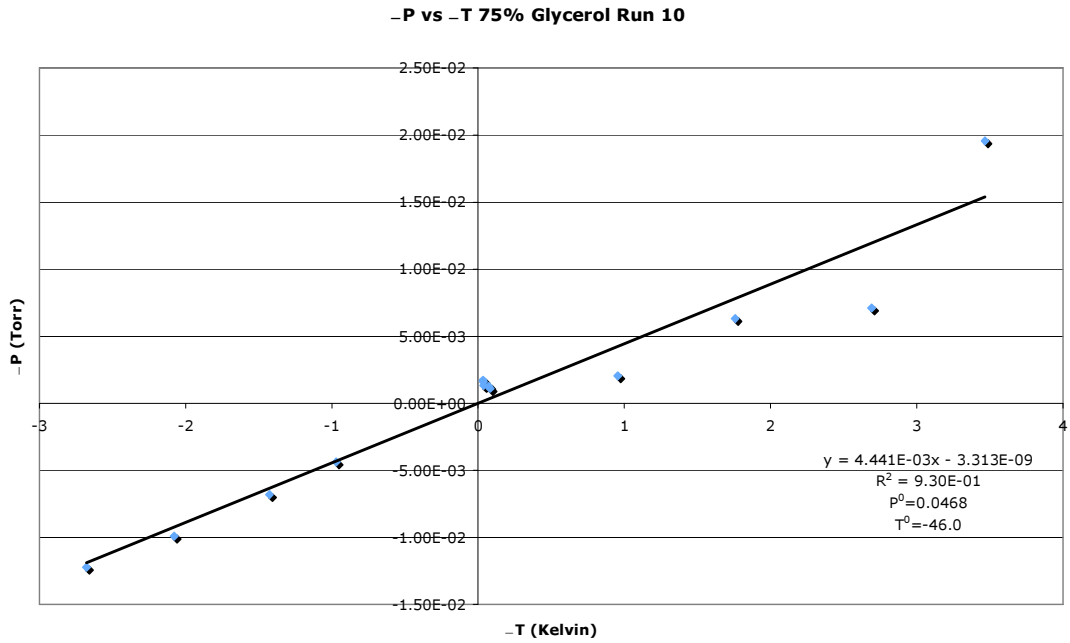
_P vs _T 75% Glycerol Run 10
2.50E-02
2.00E-02
1.50E-02
1.00E-02
5.00E-03
0.00E+00
-5.00E-03
-1.00E-02
-1.50E-02
-3
-2
-1
0
1
2
3
4
_P (Torr)
_T (Kelvin)
y = 4.441E-03x - 3.313E-09
R2 = 9.30E-01
P0=0.0468
T0=-46.0

5.2 ΔP vs. ΔT for 80% Glycerol-Water Mixtures

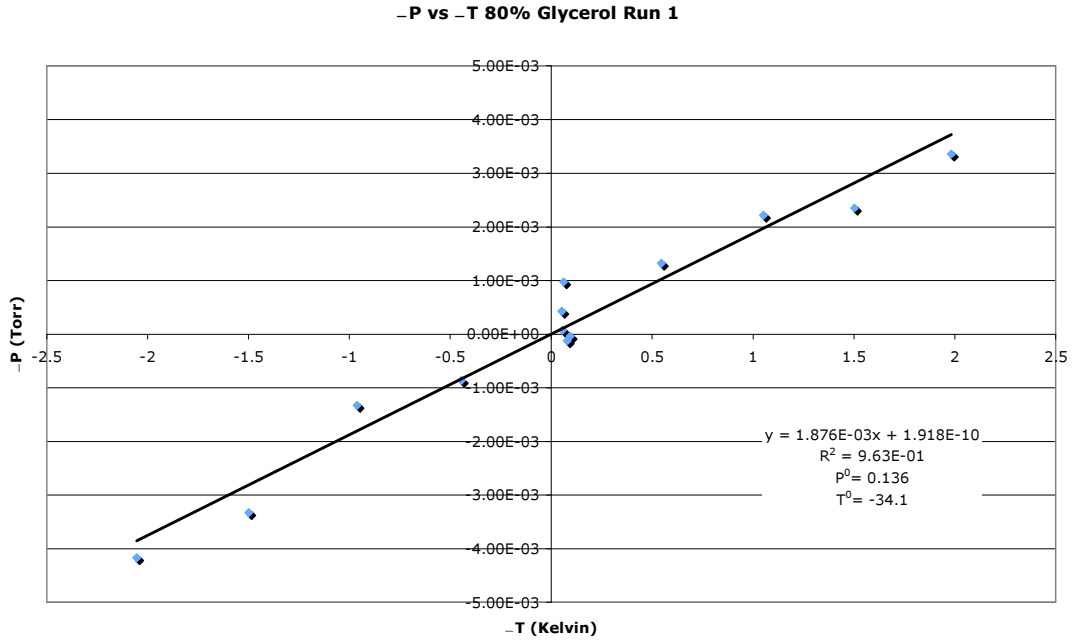

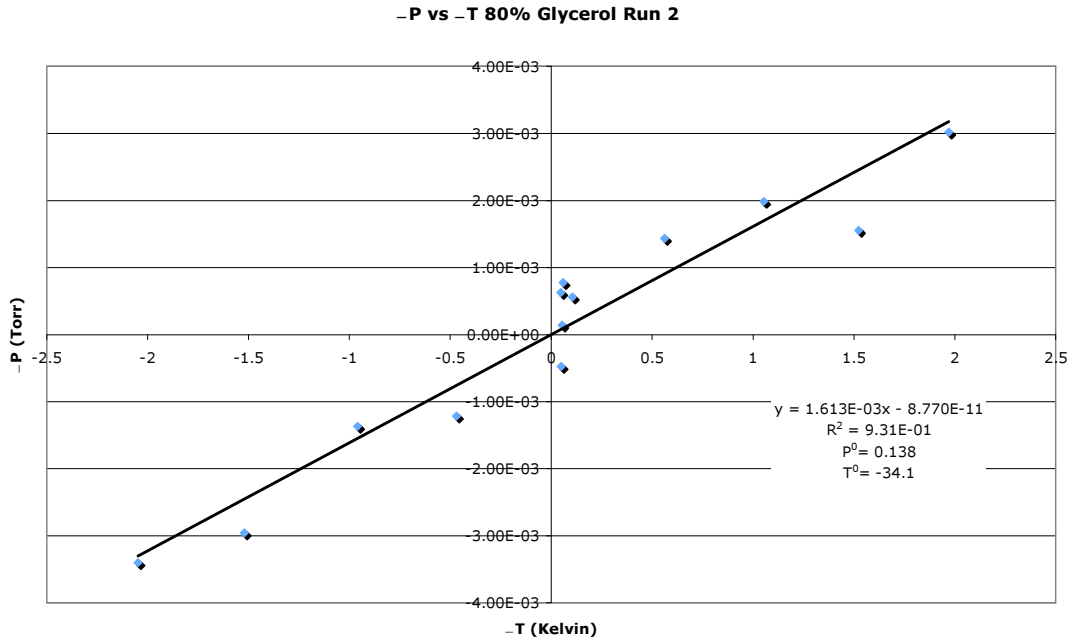

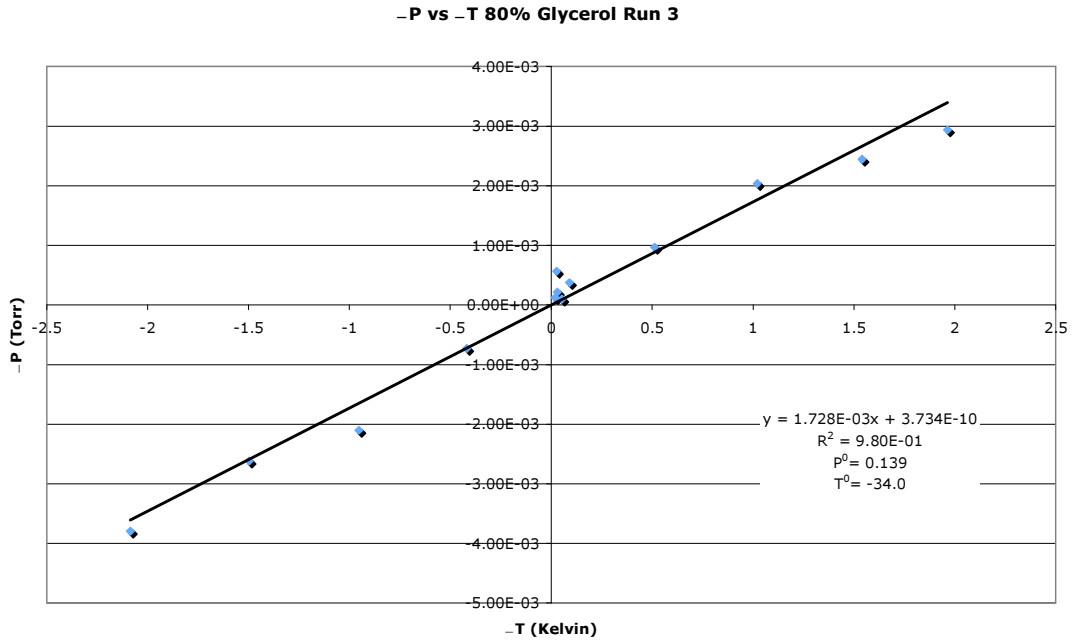
_P vs _T 80% Glycerol Run 3
4.00E-03
3.00E-03
2.00E-03
1.00E-03
0.00E+00
-1.00E-03
-2.00E-03
-3.00E-03
-4.00E-03
-5.00E-03
-2.5
-2
-1.5
-1
-0.5
0
0.5
1
1.5
2
2.5
_P (Torr)
_T (Kelvin)
y = 1.728E-03x + 3.734E-10
R2 = 9.80E-01
P0= 0.139
T0= -34.0

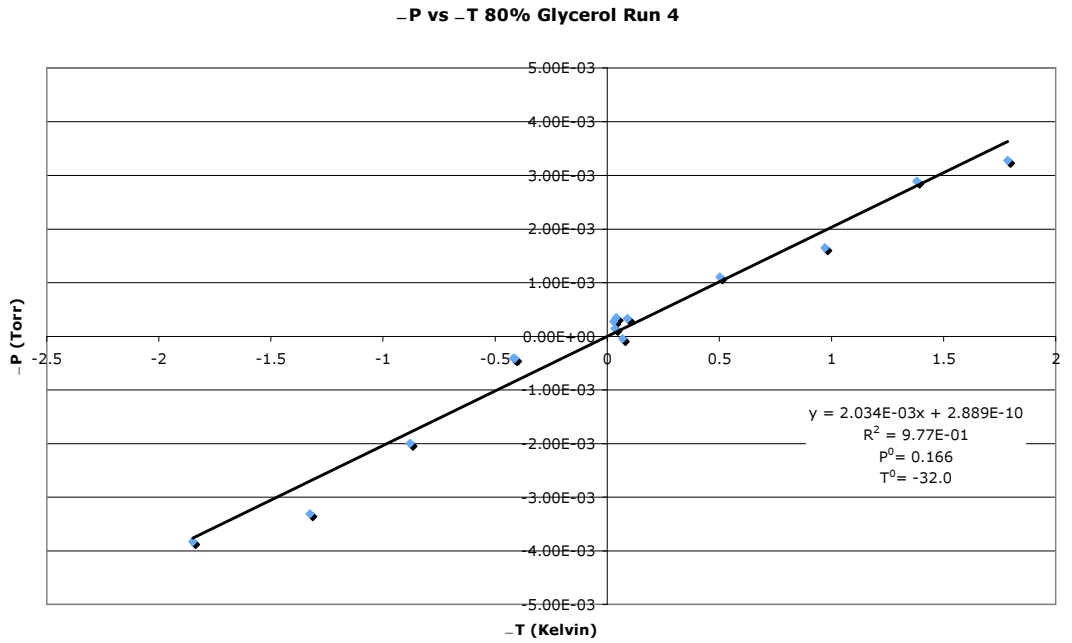
_P vs _T 80% Glycerol Run 4
5.00E-03
4.00E-03
3.00E-03
2.00E-03
1.00E-03
0.00E+00
-1.00E-03
-2.00E-03
-3.00E-03
-4.00E-03
-5.00E-03
-2.5
-2
-1.5
-1
-0.5
0
0.5
1
1.5
2
_P (Torr)
_T (Kelvin)
y = 2.034E-03x + 2.889E-10
R2 = 9.77E-01
P0= 0.166
T0= -32.0

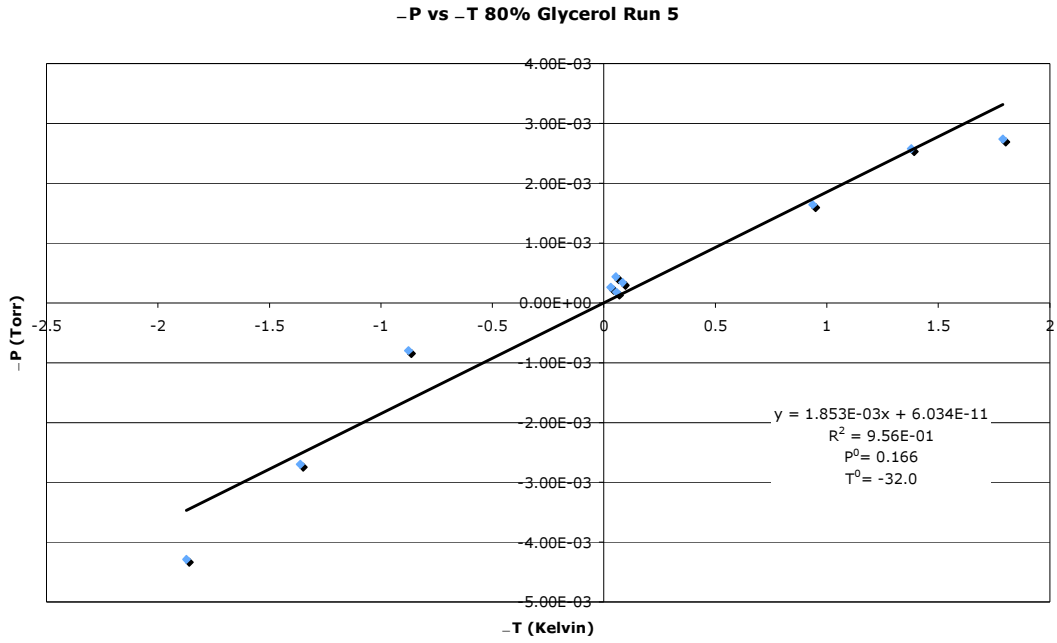
_P vs _T 80% Glycerol Run 5
4.00E-03
3.00E-03
2.00E-03
1.00E-03
0.00E+00
-1.00E-03
-2.00E-03
-3.00E-03
-4.00E-03
-5.00E-03
-2.5
-2
-1.5
-1
-0.5
0
0.5
1
1.5
2
_P (Torr)
_T (Kelvin)
y = 1.853E-03x + 6.034E-11
R2 = 9.56E-01
P0= 0.166
T0= -32.0

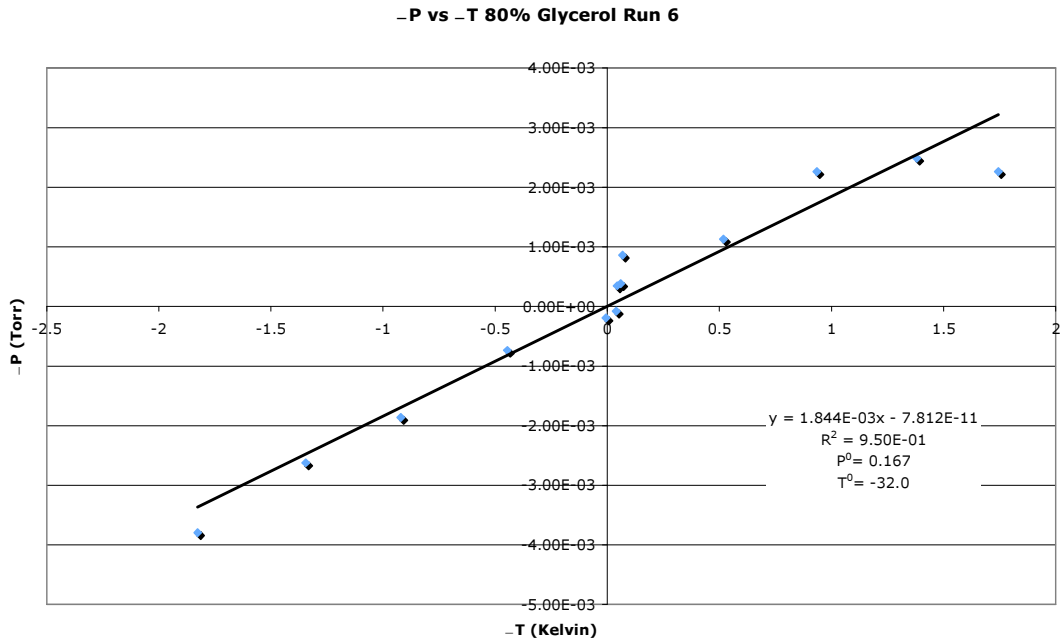
_P vs _T 80% Glycerol Run 6
4.00E-03
3.00E-03
2.00E-03
1.00E-03
0.00E+00
-1.00E-03
-2.00E-03
-3.00E-03
-4.00E-03
-5.00E-03
-2.5
-2
-1.5
-1
-0.5
0
0.5
1
1.5
2
_P (Torr)
_T (Kelvin)
y = 1.844E-03x - 7.812E-11
R2 = 9.50E-01
P0= 0.167
T0= -32.0

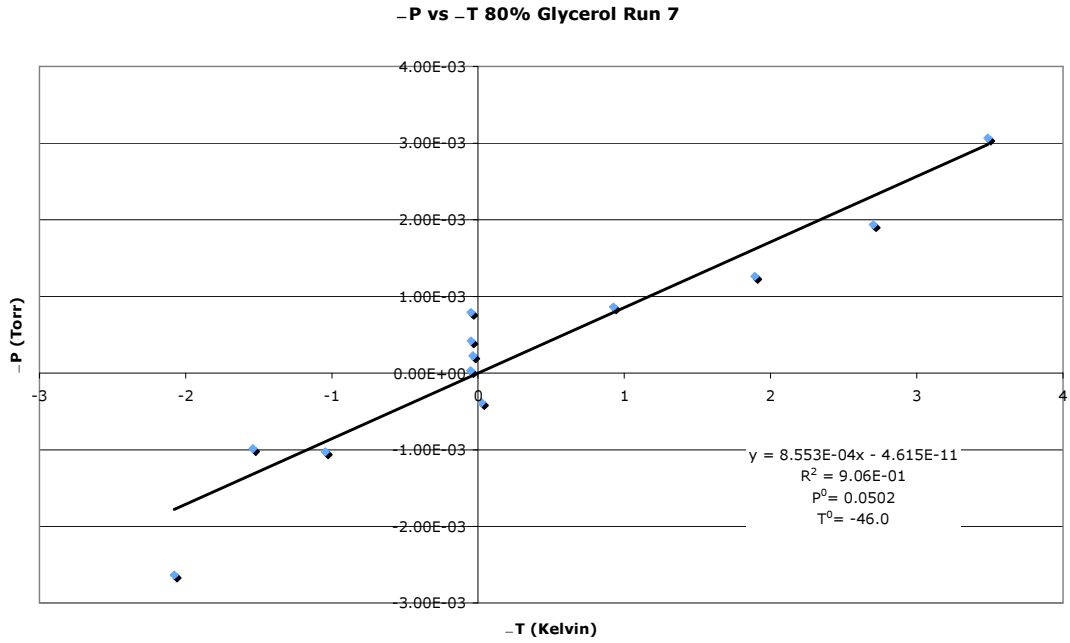
_P vs _T 80% Glycerol Run 7
4.00E-03
3.00E-03
2.00E-03
1.00E-03
0.00E+00
-1.00E-03
-2.00E-03
-3.00E-03
-3
-2
-1
0
1
2
3
4
_P (Torr)
_T (Kelvin)
y = 8.553E-04x - 4.615E-11
R2 = 9.06E-01
P0= 0.0502
T0= -46.0

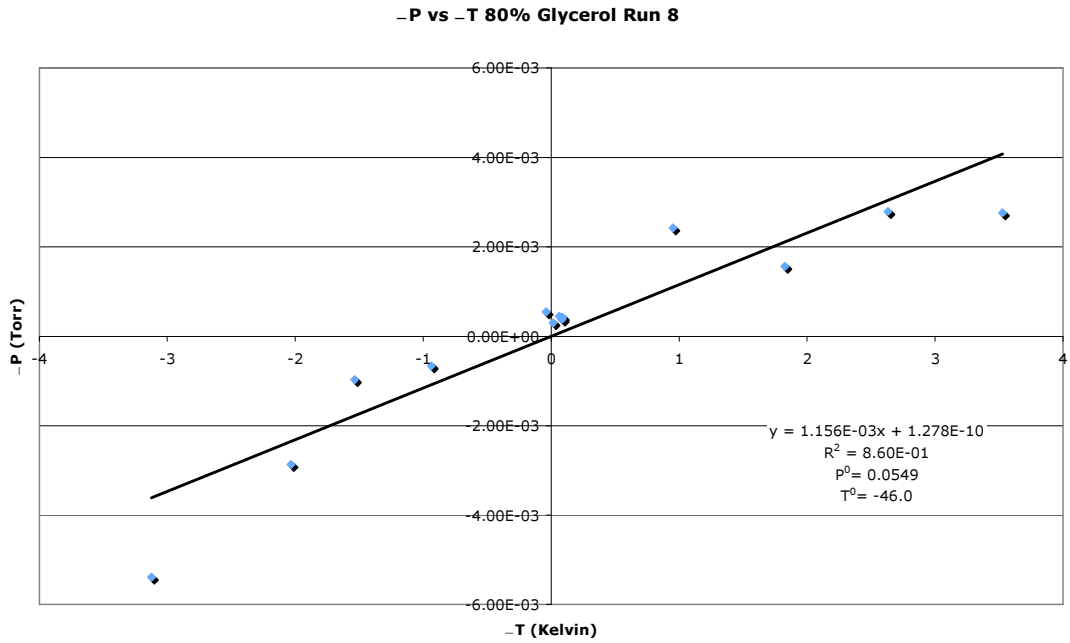
_P vs _T 80% Glycerol Run 8
6.00E-03
4.00E-03
2.00E-03
0.00E+00
-2.00E-03
-4.00E-03
-6.00E-03
-4
-3
-2
-1
0
1
2
3
4
_P (Torr)
_T (Kelvin)
y = 1.156E-03x + 1.278E-10
R2 = 8.60E-01
P0= 0.0549
T0= -46.0

5.3 ΔP vs. ΔT for 85% Glycerol-Water Mixtures

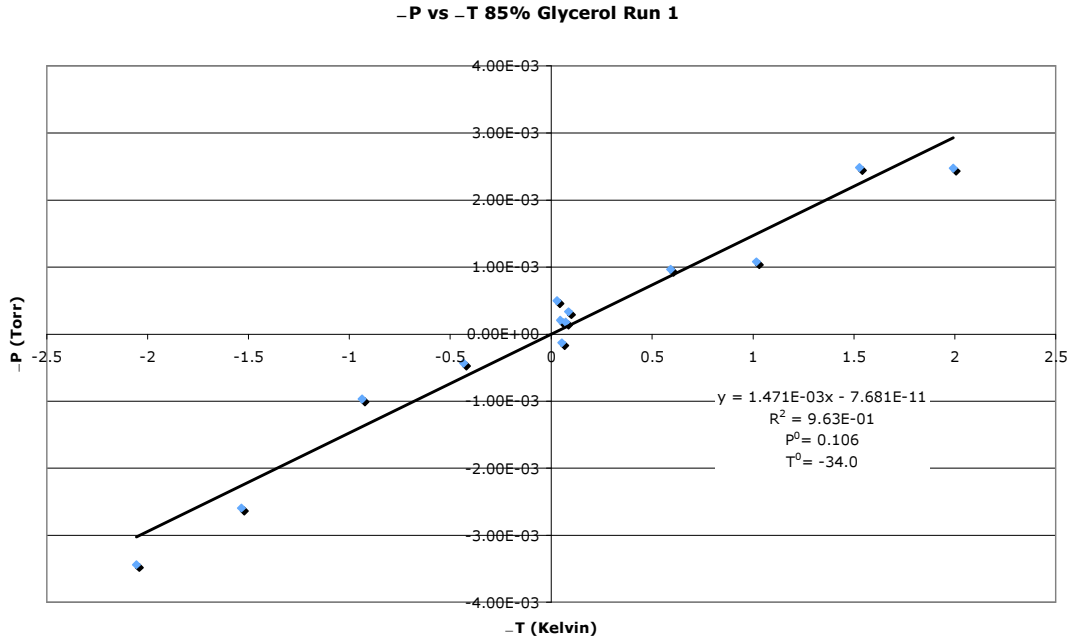

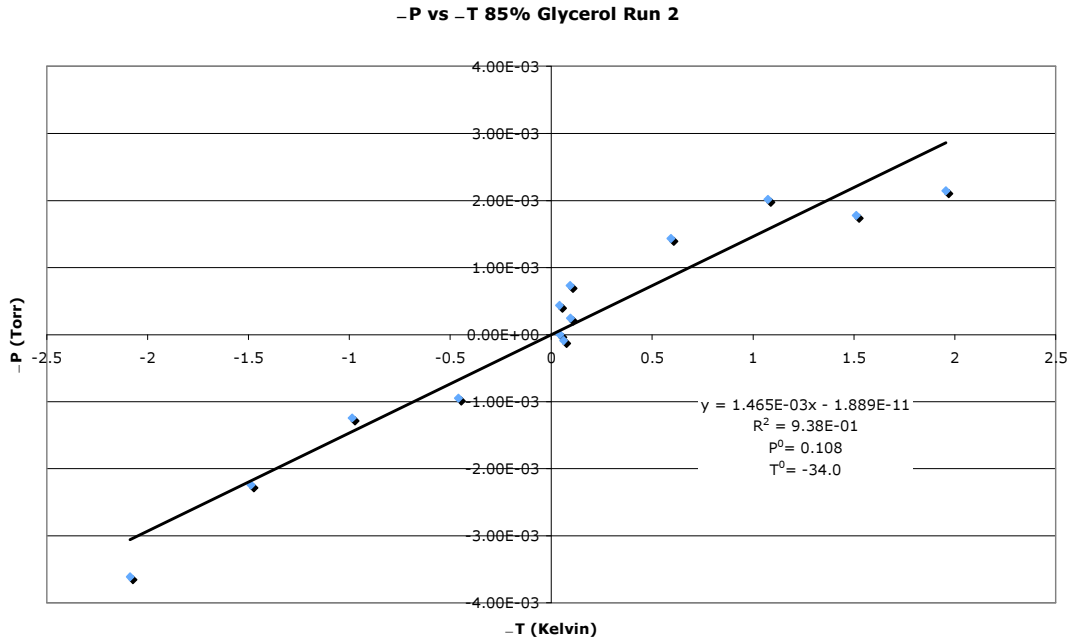

_P vs _T 85% Glycerol Run 3

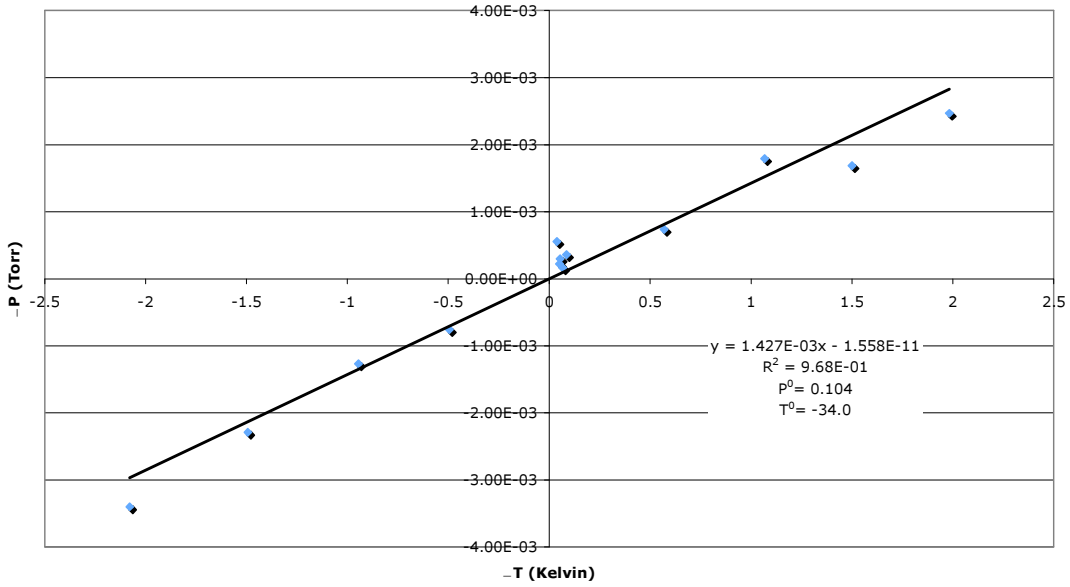

_P vs _T 85% Glycerol Run 4

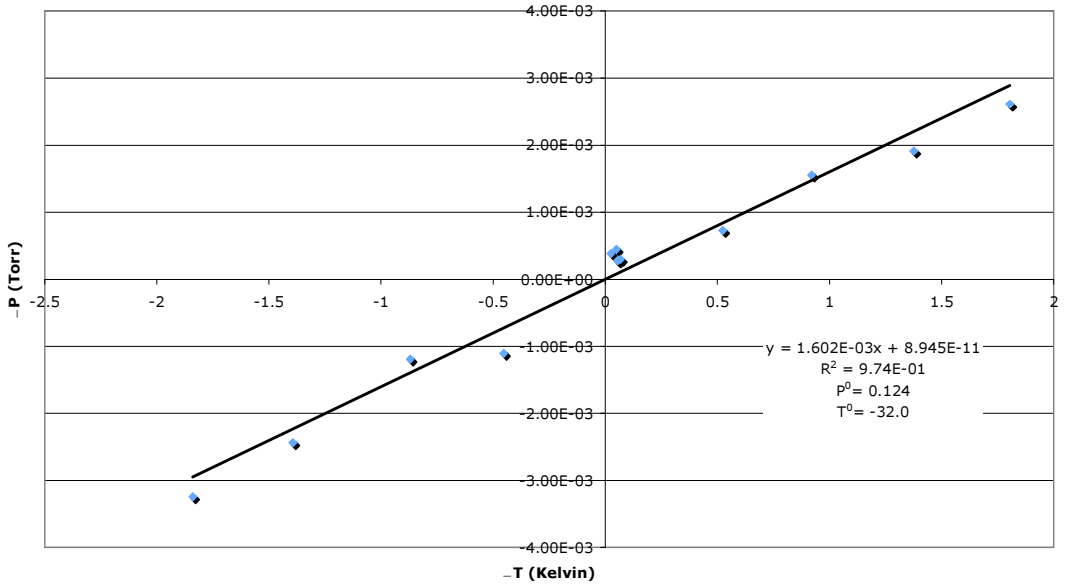

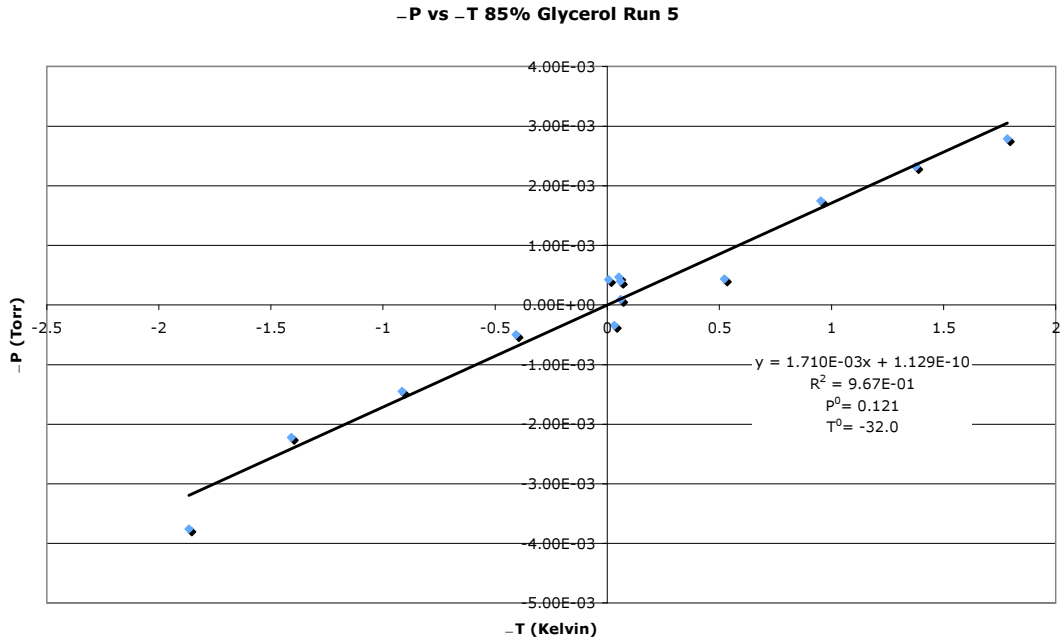
_P vs _T 85% Glycerol Run 5
4.00E-03
3.00E-03
2.00E-03
1.00E-03
0.00E+00
-1.00E-03
-2.00E-03
-3.00E-03
-4.00E-03
-5.00E-03
-2.5
-2
-1.5
-1
-0.5
0
0.5
1
1.5
2
_P (Torr)
_T (Kelvin)
y = 1.710E-03x + 1.129E-10
R2 = 9.67E-01
P0= 0.121
T0= -32.0

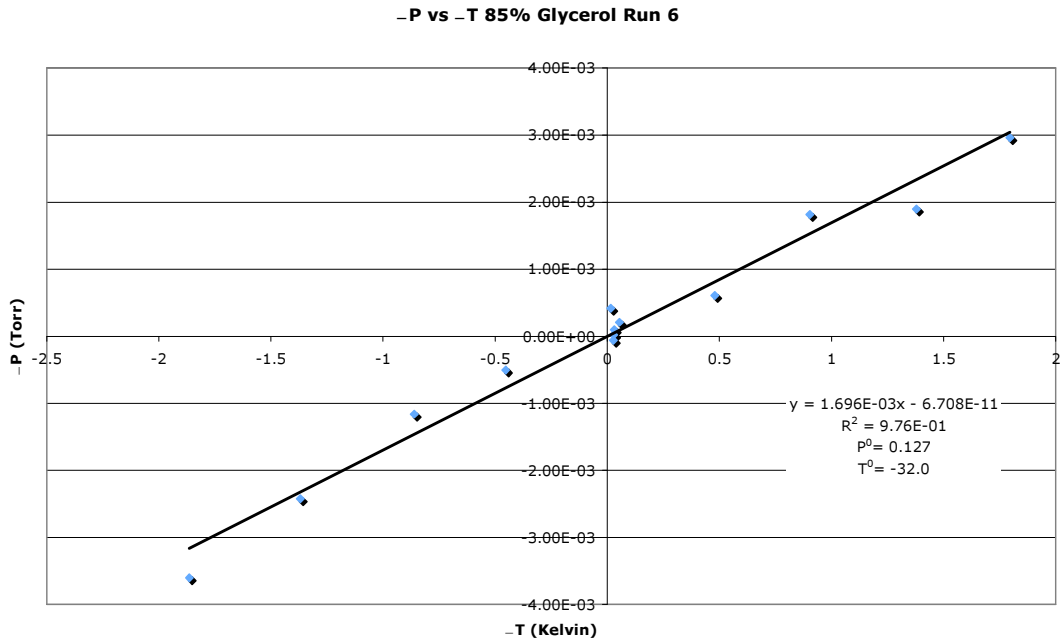
_P vs _T 85% Glycerol Run 6
4.00E-03
3.00E-03
2.00E-03
1.00E-03
0.00E+00
-1.00E-03
-2.00E-03
-3.00E-03
-4.00E-03
-2.5
-2
-1.5
-1
-0.5
0
0.5
1
1.5
2
_P (Torr)
_T (Kelvin)
y = 1.696E-03x - 6.708E-11
R2 = 9.76E-01
P0= 0.127
T0= -32.0

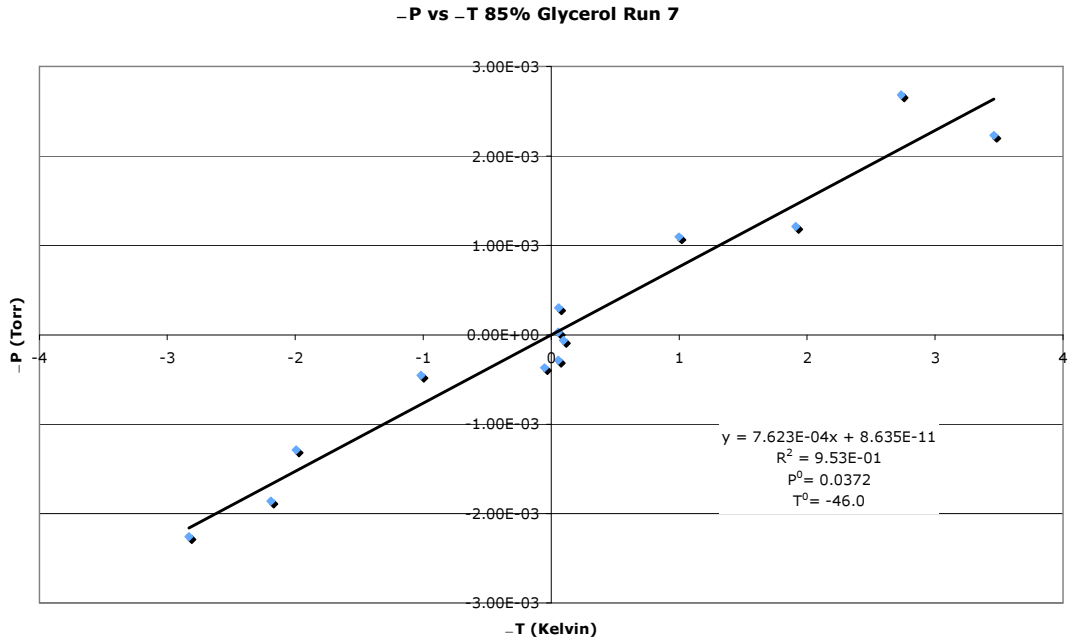
_P vs _T 85% Glycerol Run 7
3.00E-03
2.00E-03
1.00E-03
0.00E+00
-1.00E-03
-2.00E-03
-3.00E-03
-4
-3
-2
-1
0
1
2
3
4
_P (Torr)
_T (Kelvin)
y = 7.623E-04x + 8.635E-11
R2 = 9.53E-01
P0= 0.0372
T0= -46.0

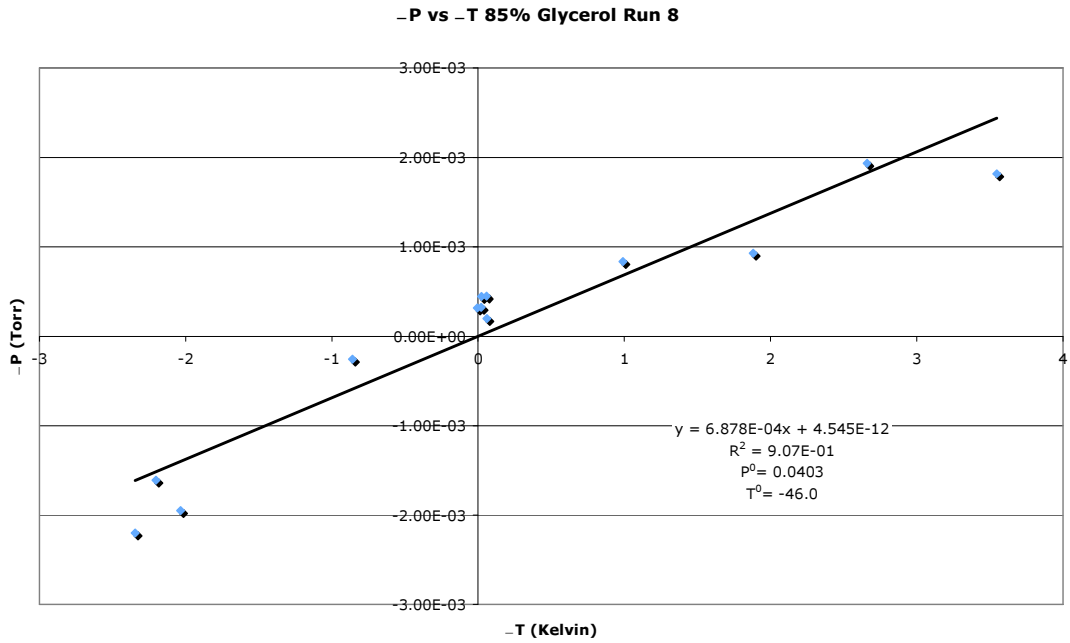
_P vs _T 85% Glycerol Run 8
3.00E-03
2.00E-03
1.00E-03
0.00E+00
-1.00E-03
-2.00E-03
-3.00E-03
-3
-2
-1
0
1
2
3
4
_P (Torr)
_T (Kelvin)
y = 6.878E-04x + 4.545E-12
R2 = 9.07E-01
P0= 0.0403
T0= -46.0

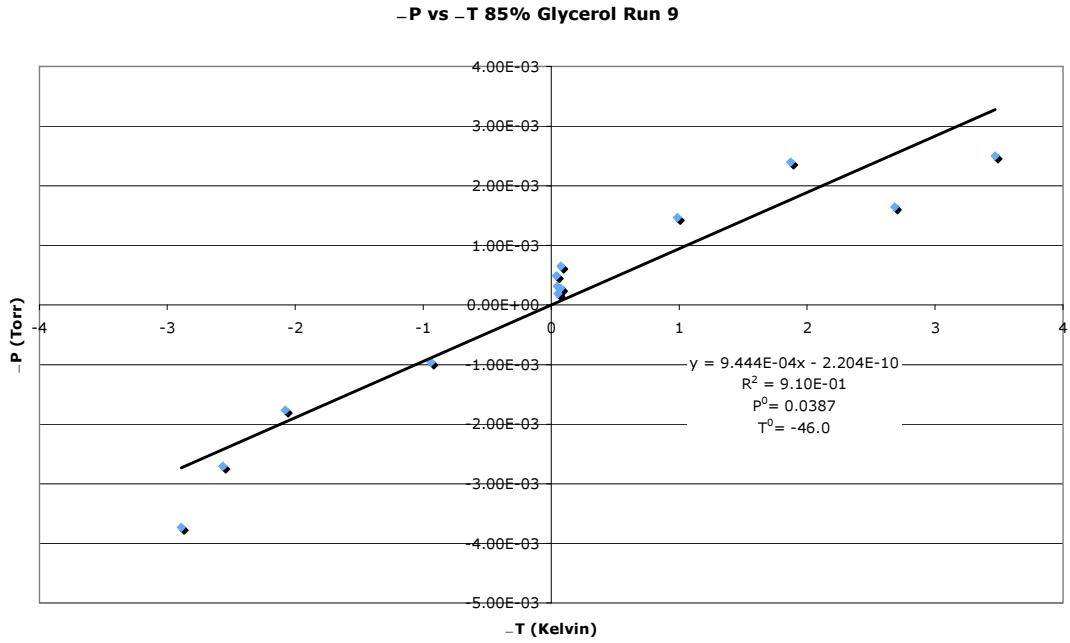
_P vs _T 85% Glycerol Run 9
4.00E-03
3.00E-03
2.00E-03
1.00E-03
0.00E+00
-1.00E-03
-2.00E-03
-3.00E-03
-4.00E-03
-5.00E-03
-4
-3
-2
-1
0
1
2
3
4
_P (Torr)
_T (Kelvin)
y = 9.444E-04x - 2.204E-10
R2 = 9.10E-01
P0= 0.0387
T0= -46.0

5.4 ΔP vs. ΔT for 90% Glycerol-Water Mixtures

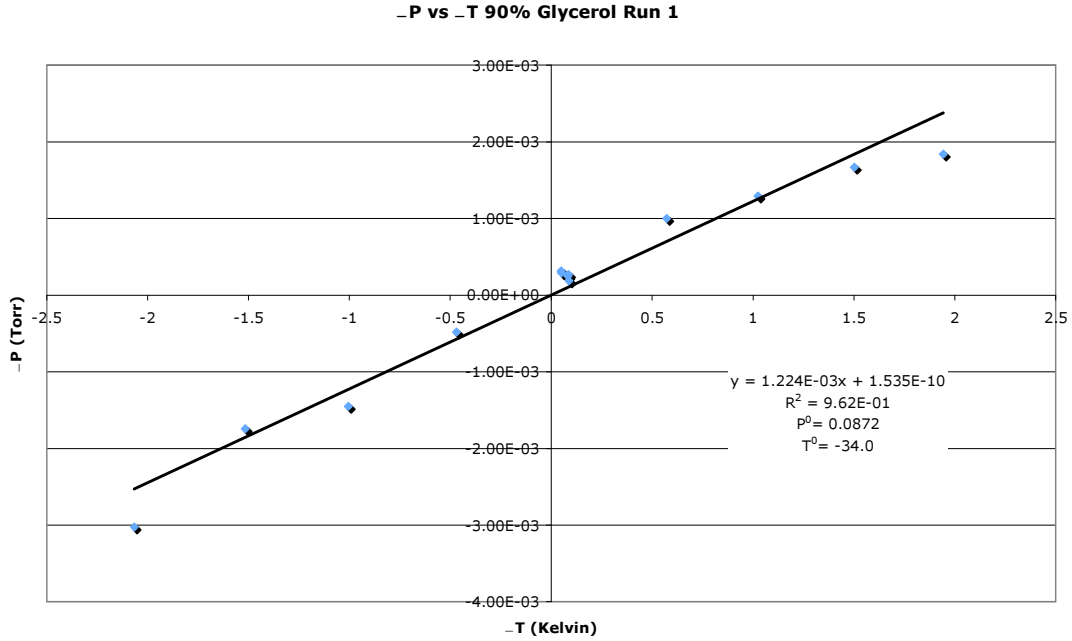

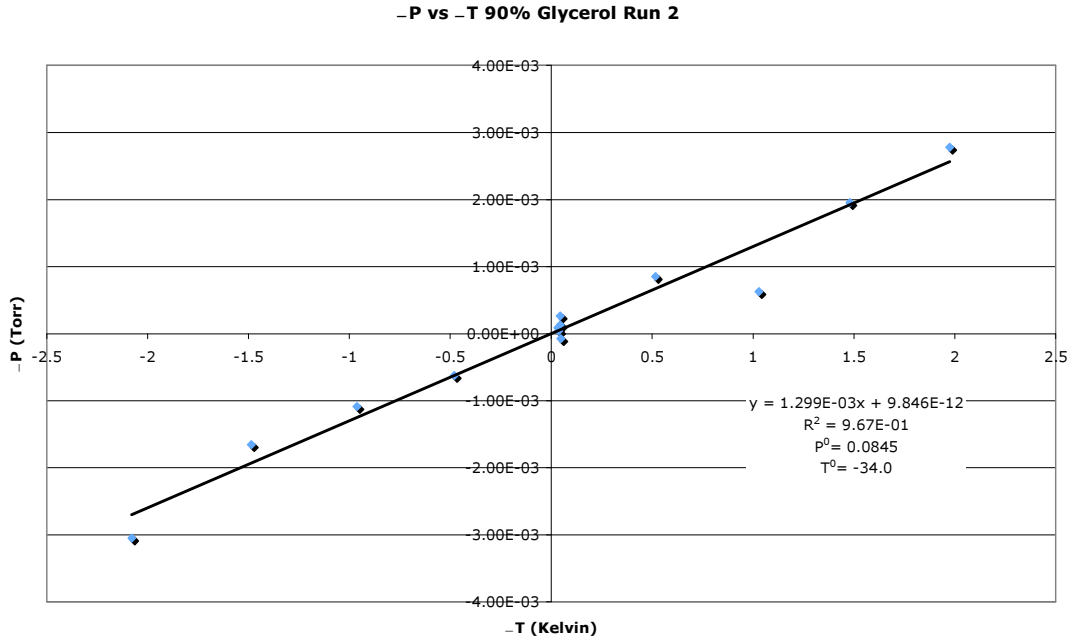

_P vs _T 90% Glycerol Run 3

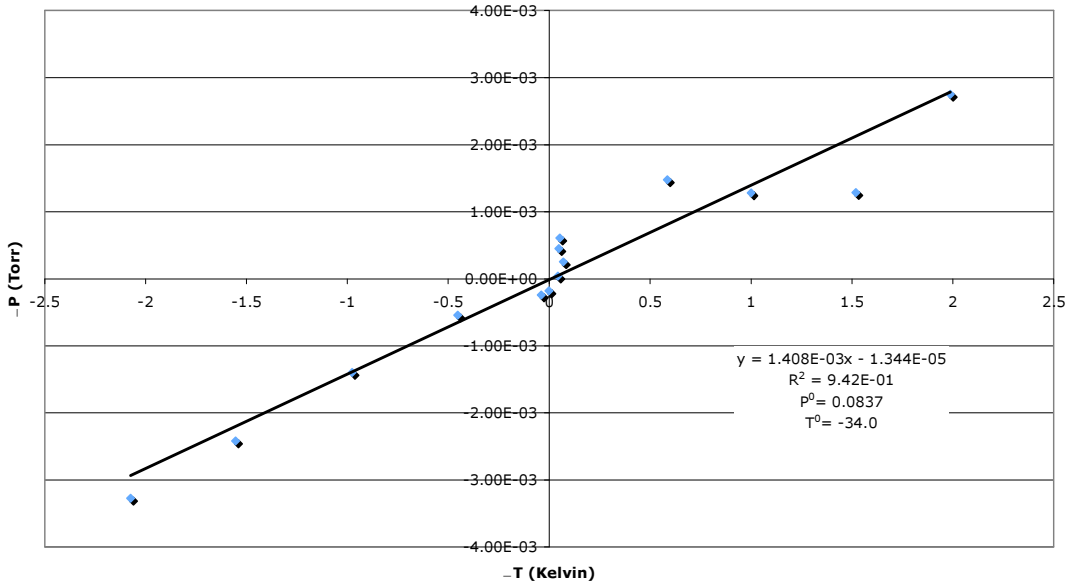

_P vs _T 90% Glycerol Run 4

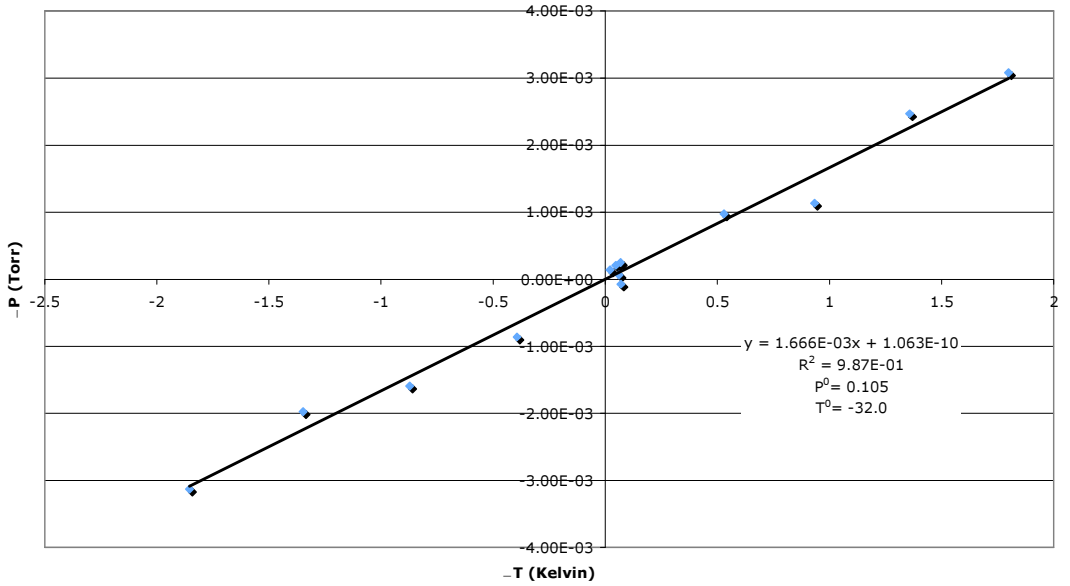

_P vs _T 90% Glycerol Run 5

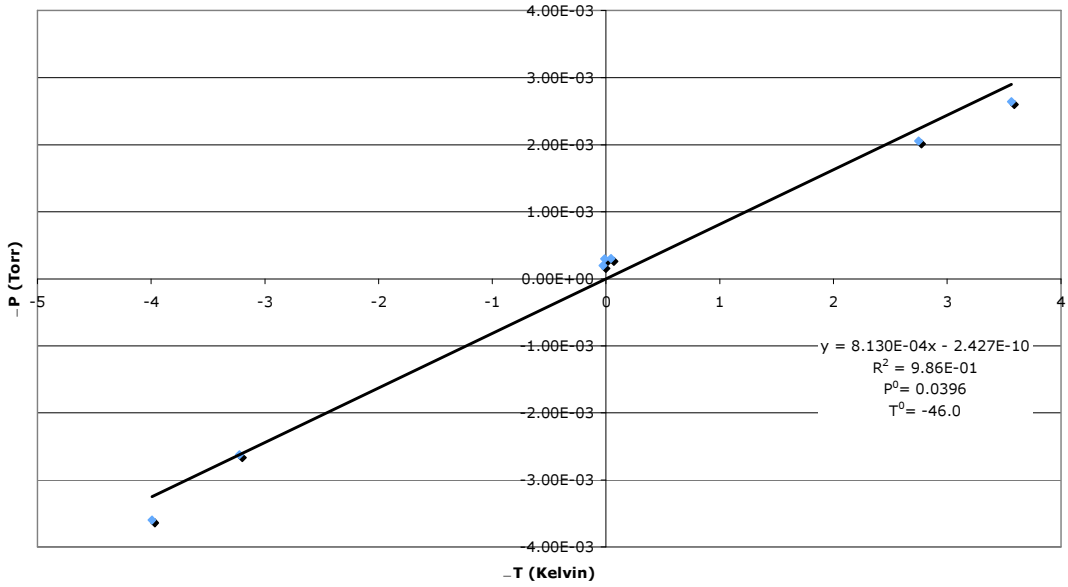

_P vs _T 90% Glycerol Run 6

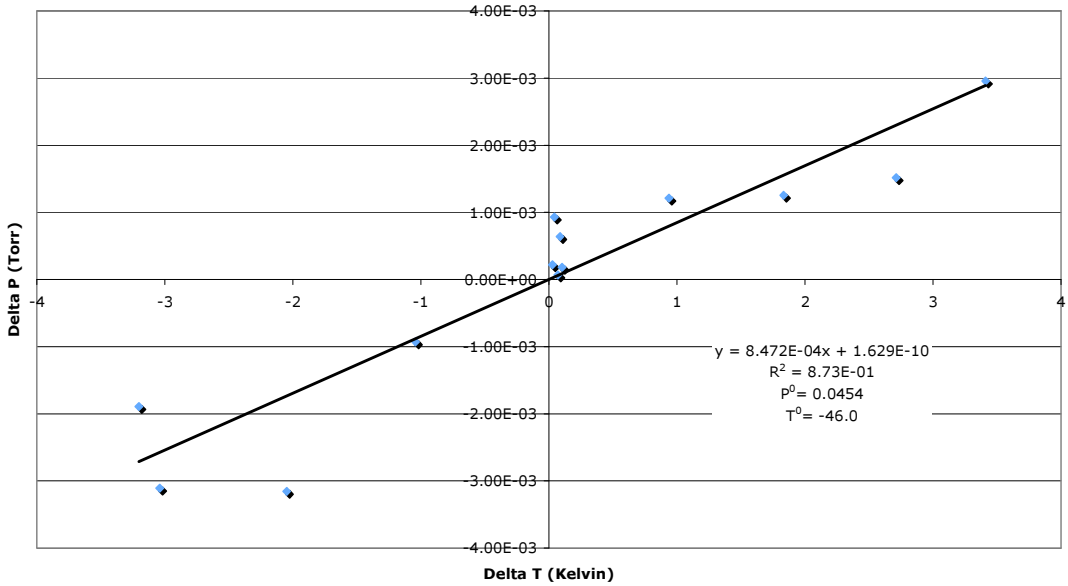

_P vs _T 90% Glycerol Run 7

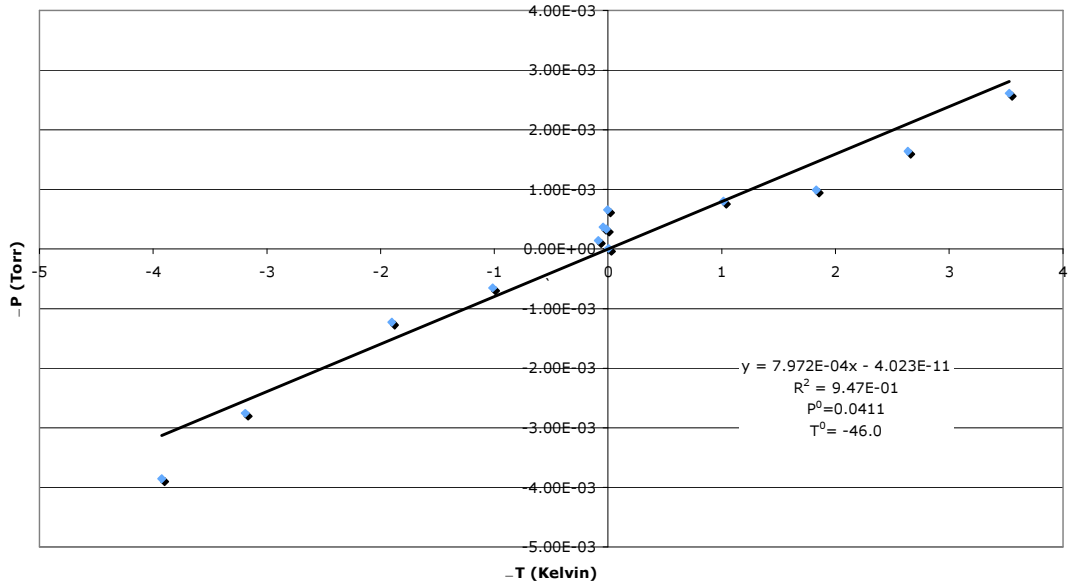

_P vs _T 90% Glycerol Run 8

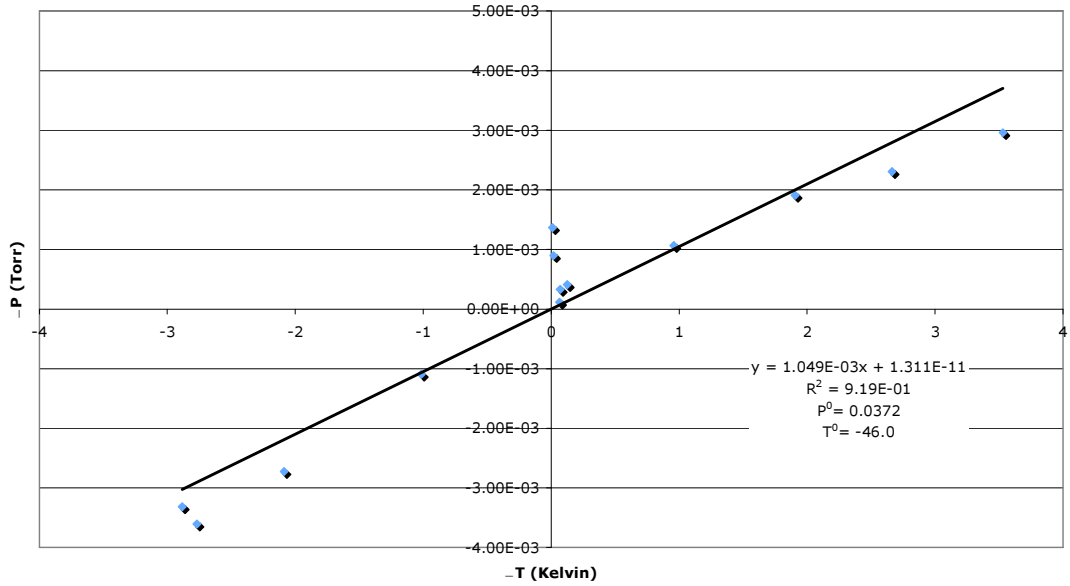

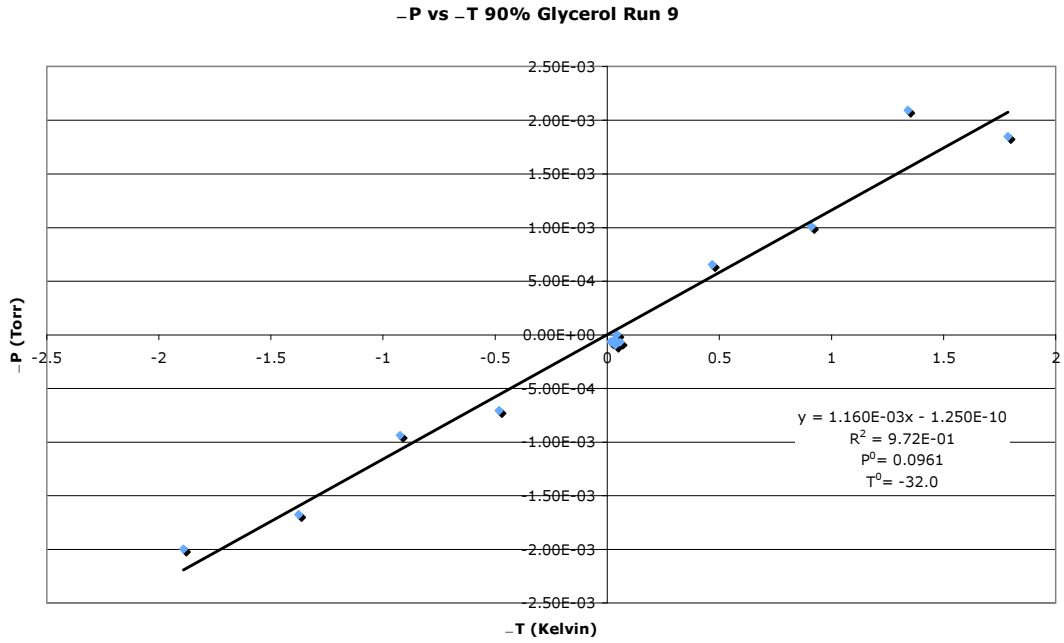
_P vs _T 90% Glycerol Run 9
2.50E-03
2.00E-03
1.50E-03
1.00E-03
5.00E-04
0.00E+00
-5.00E-04
-1.00E-03
-1.50E-03
-2.00E-03
-2.50E-03
-2.5
-2
-1.5
-1
-0.5
0
0.5
1
1.5
2
_P (Torr)
_T (Kelvin)
y = 1.160E-03x - 1.250E-10
R2 = 9.72E-01
P0= 0.0961
T0= -32.0

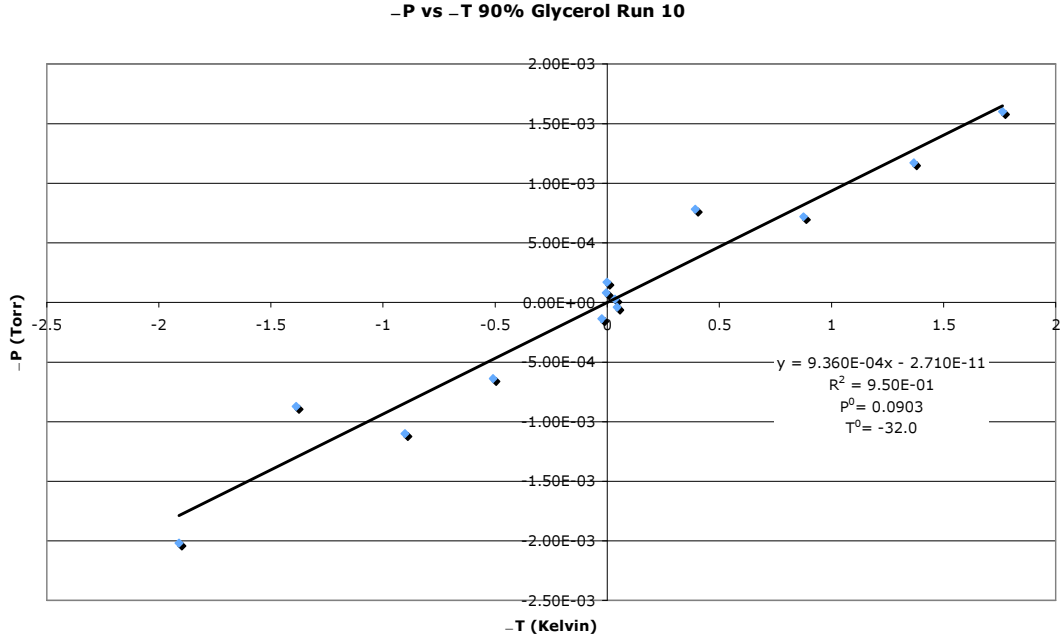
_P vs _T 90% Glycerol Run 10
2.00E-03
1.50E-03
1.00E-03
5.00E-04
0.00E+00
-5.00E-04
-1.00E-03
-1.50E-03
-2.00E-03
-2.50E-03
-2.5
-2
-1.5
-1
-0.5
0
0.5
1
1.5
2
_P (Torr)
_T (Kelvin)
y = 9.360E-04x - 2.710E-11
R2 = 9.50E-01
P0= 0.0903
T0= -32.0

5.5 ΔP vs. ΔT for 94.5% Glycerol-Water Mixtures

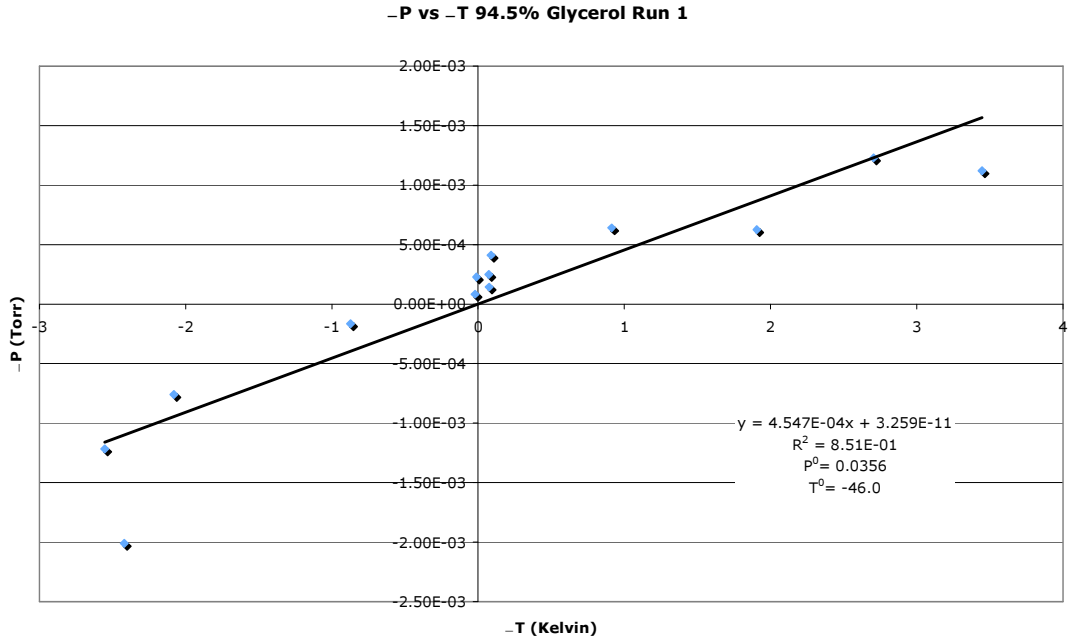

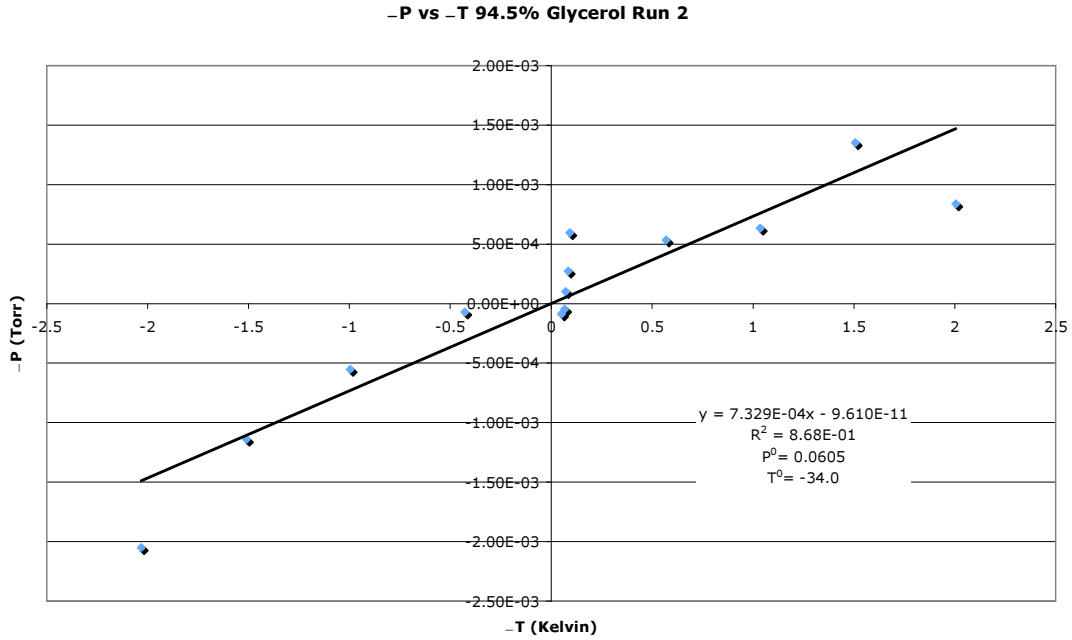

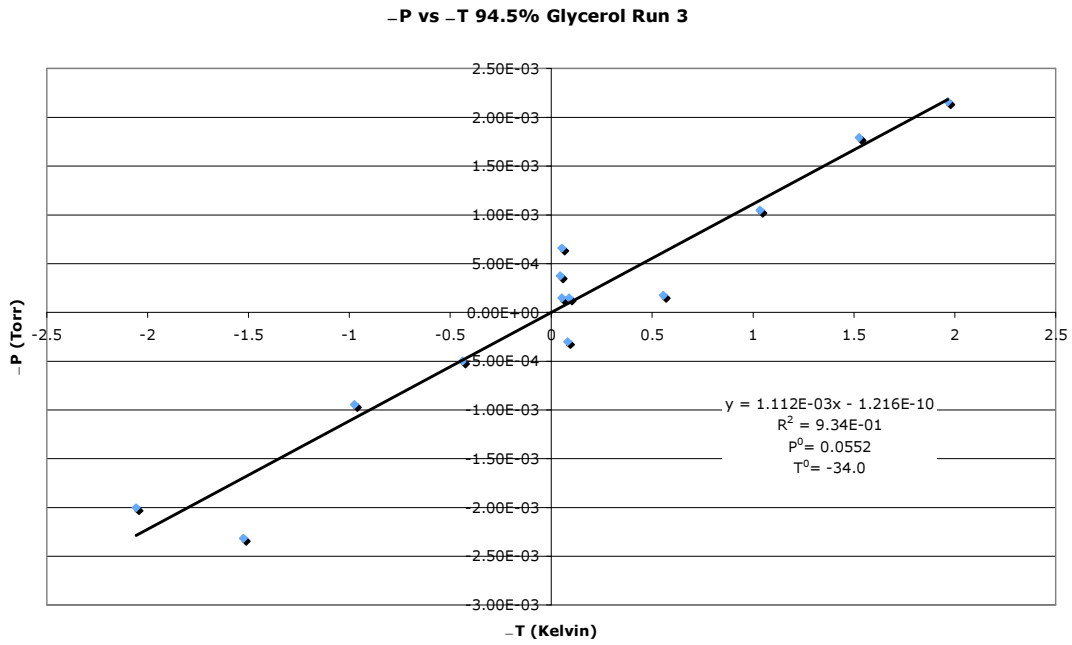
_P vs _T 94.5% Glycerol Run 3
2.50E-03
2.00E-03
1.50E-03
1.00E-03
5.00E-04
0.00E+00
-5.00E-04
-1.00E-03
-1.50E-03
-2.00E-03
-2.50E-03
-3.00E-03
-2.5
-2
-1.5
-1
-0.5
0
0.5
1
1.5
2
2.5
_P (Torr)
_T (Kelvin)
y = 1.112E-03x - 1.216E-10
R2 = 9.34E-01
P0= 0.0552
T0= -34.0

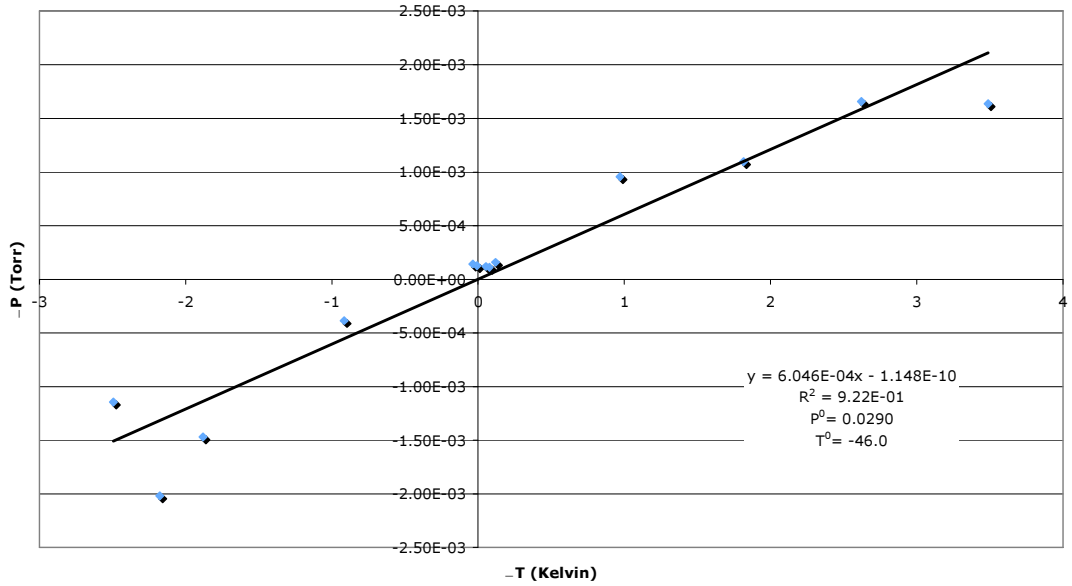
_P vs _T 94.5% Glycerol Run 4
2.50E-03
2.00E-03
1.50E-03
1.00E-03
5.00E-04
0.00E+00
-5.00E-04
-1.00E-03
-1.50E-03
-2.00E-03
-2.50E-03
-3
-2
-1
0
1
2
3
4
_P (Torr)
_T (Kelvin)
y = 6.046E-04x - 1.148E-10
R2 = 9.22E-01
P0= 0.0290
T0= -46.0

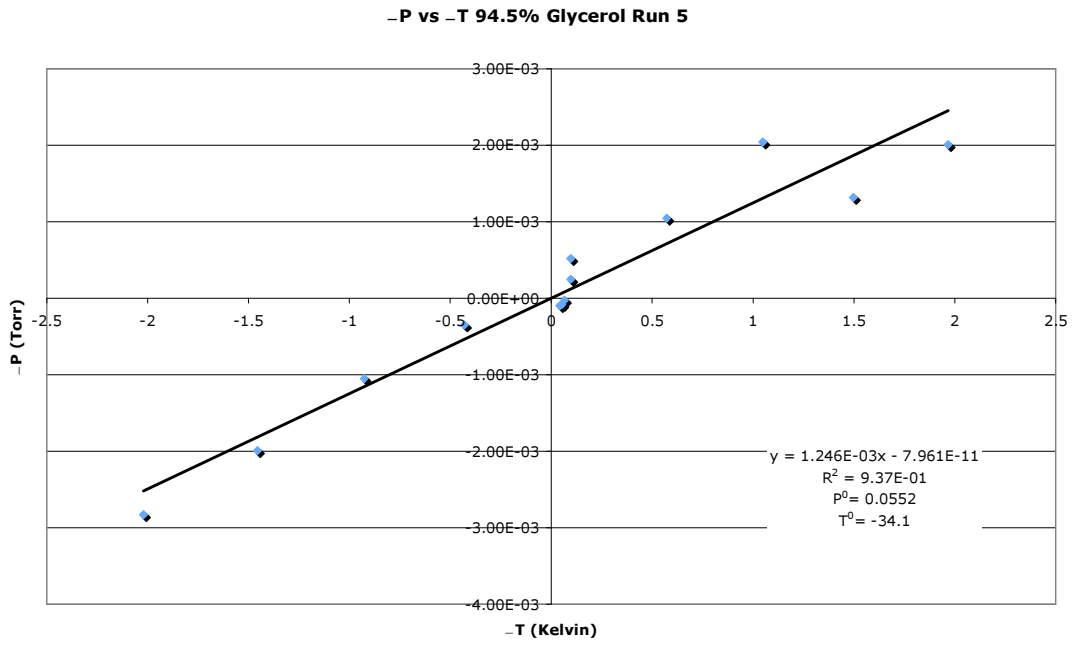
_P vs _T 94.5% Glycerol Run 5
3.00E-03
2.00E-03
1.00E-03
0.00E+00
-1.00E-03
-2.00E-03
-3.00E-03
-4.00E-03
-2.5
-2
-1.5
-1
-0.5
0
0.5
1
1.5
2
2.5
_P (Torr)
_T (Kelvin)
y = 1.246E-03x - 7.961E-11
R2 = 9.37E-01
P0= 0.0552
T0= -34.1

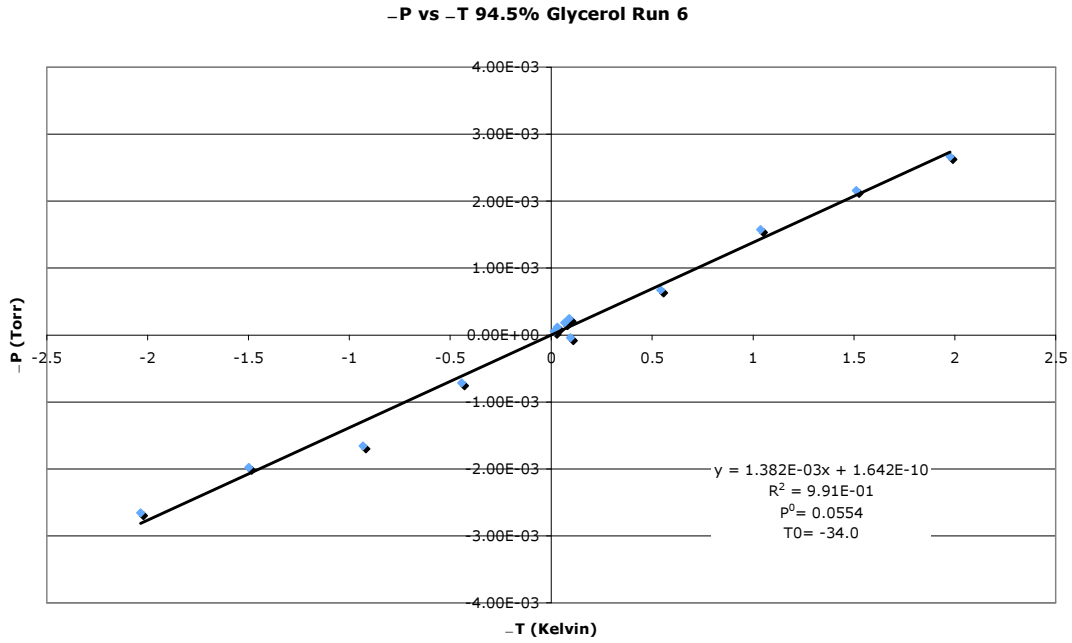
_P vs _T 94.5% Glycerol Run 6
4.00E-03
3.00E-03
2.00E-03
1.00E-03
0.00E+00
-1.00E-03
-2.00E-03
-3.00E-03
-4.00E-03
-2.5
-2
-1.5
-1
-0.5
0
0.5
1
1.5
2
2.5
_P (Torr)
_T (Kelvin)
y = 1.382E-03x + 1.642E-10
R2 = 9.91E-01
P0= 0.0554
T0= -34.0

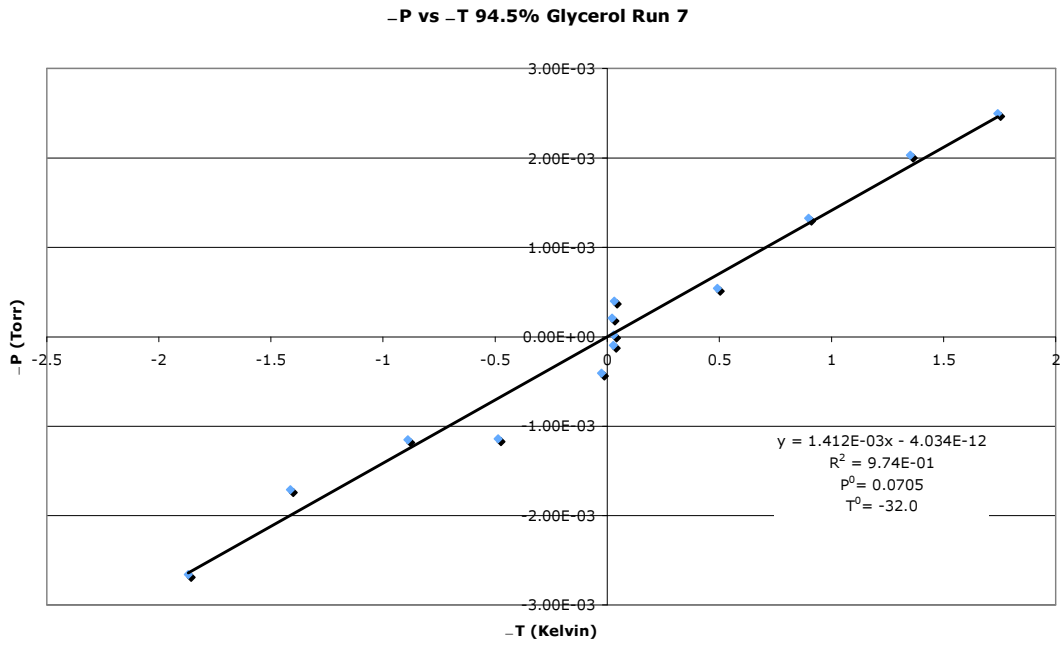
_P vs _T 94.5% Glycerol Run 7
3.00E-03
2.00E-03
1.00E-03
0.00E+00
-1.00E-03
-2.00E-03
-3.00E-03
-2.5
-2
-1.5
-1
-0.5
0
0.5
1
1.5
2
_P (Torr)
_T (Kelvin)
y = 1.412E-03x - 4.034E-12
R2 = 9.74E-01
P0= 0.0705
T0= -32.0

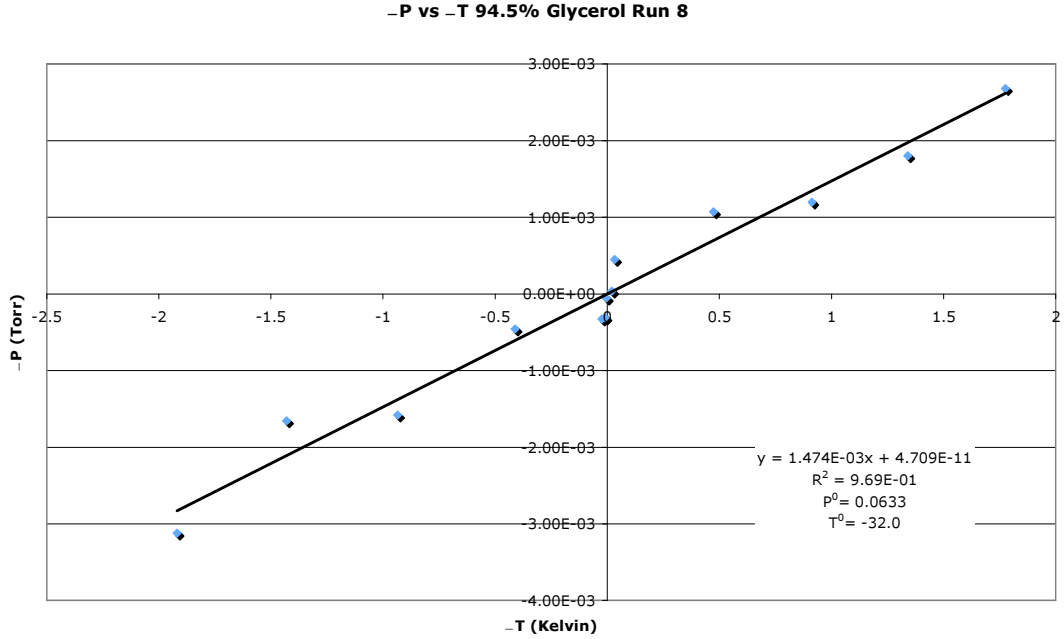
_P vs _T 94.5% Glycerol Run 8
3.00E-03
2.00E-03
1.00E-03
0.00E+00
-1.00E-03
-2.00E-03
-3.00E-03
-4.00E-03
-2.5
-2
-1.5
-1
-0.5
0
0.5
1
1.5
2
_P (Torr)
_T (Kelvin)
y = 1.474E-03x + 4.709E-11
R2 = 9.69E-01
P0= 0.0633
T0= -32.0

_P vs _T 94.5% Glycerol Run 9

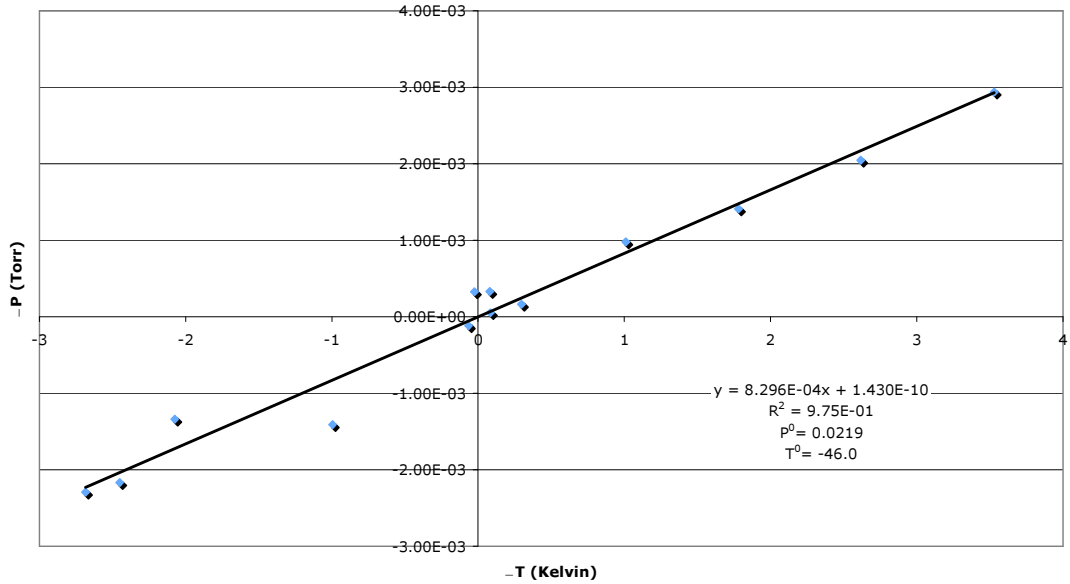

_P vs _T 94.5% Glycerol Run 10

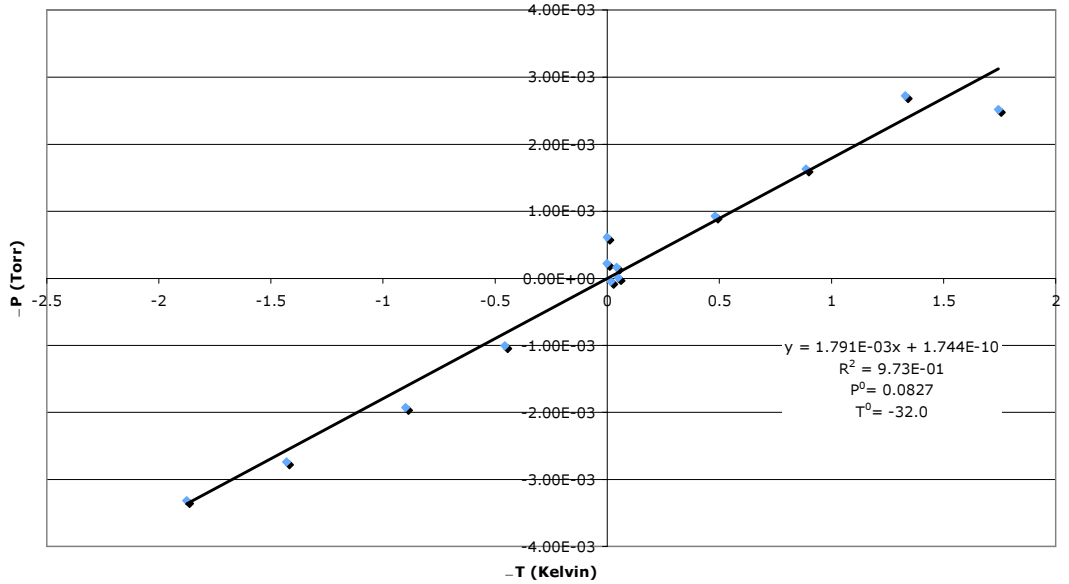

_P vs _T 94.5% Glycerol Run 11

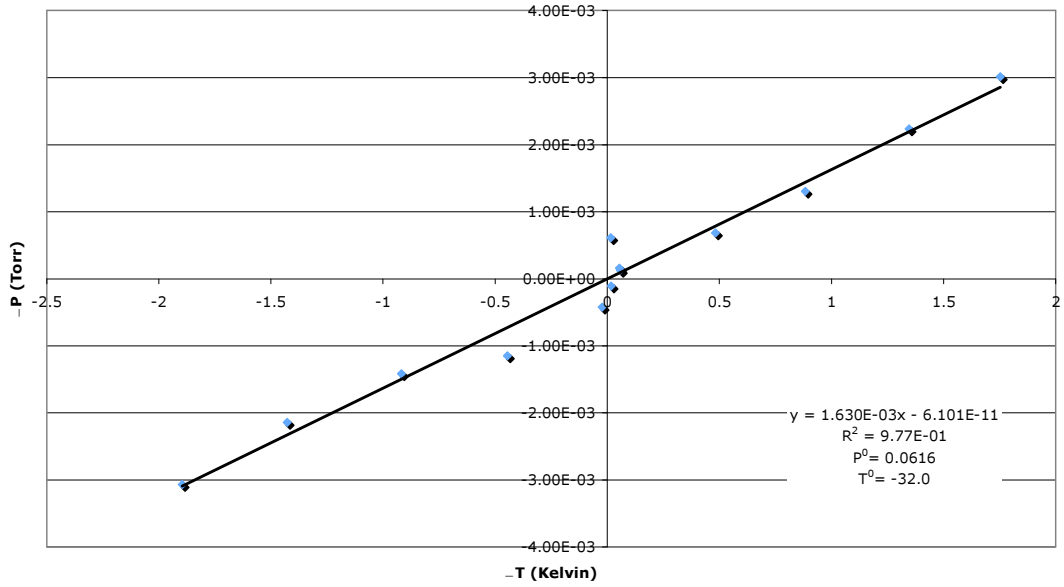

_P vs _T 94.5% Glycerol Run 12

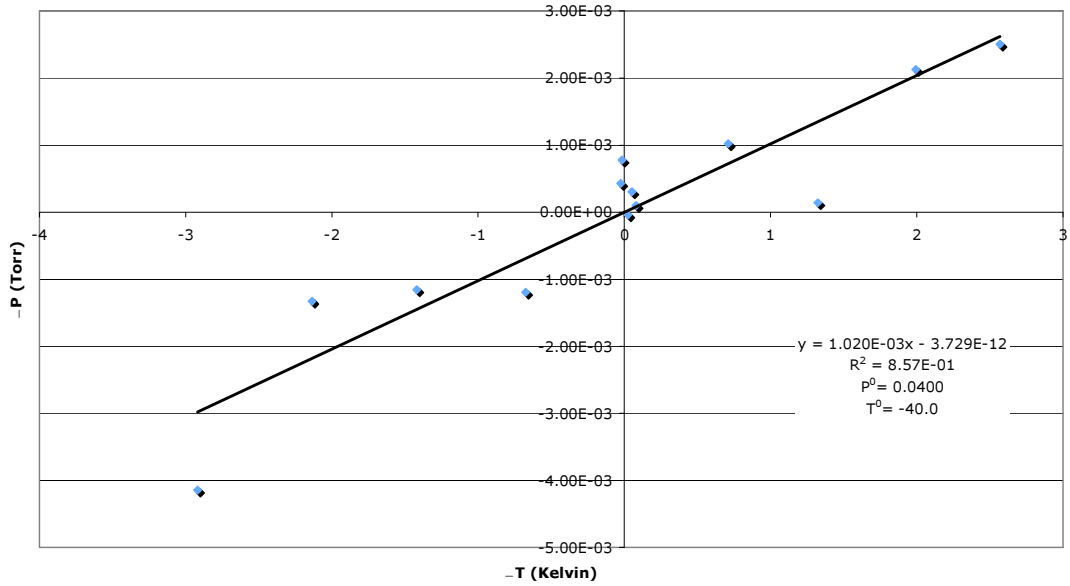

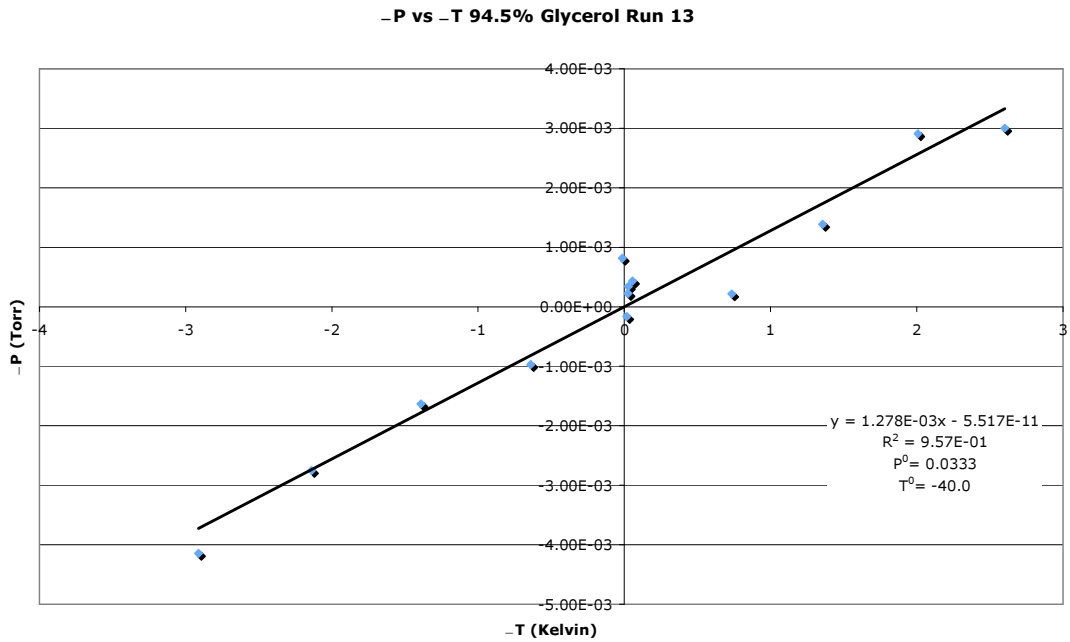
_P vs _T 94.5% Glycerol Run 13
4.00E-03
3.00E-03
2.00E-03
1.00E-03
0.00E+00
-1.00E-03
-2.00E-03
-3.00E-03
-4.00E-03
-5.00E-03
-4
-3
-2
-1
0
1
2
3
_P (Torr)
_T (Kelvin)
y = 1.278E-03x - 5.517E-11
R2 = 9.57E-01
P0= 0.0333
T0= -40.0

5.6 ΔP vs. ΔT of Rejected Data

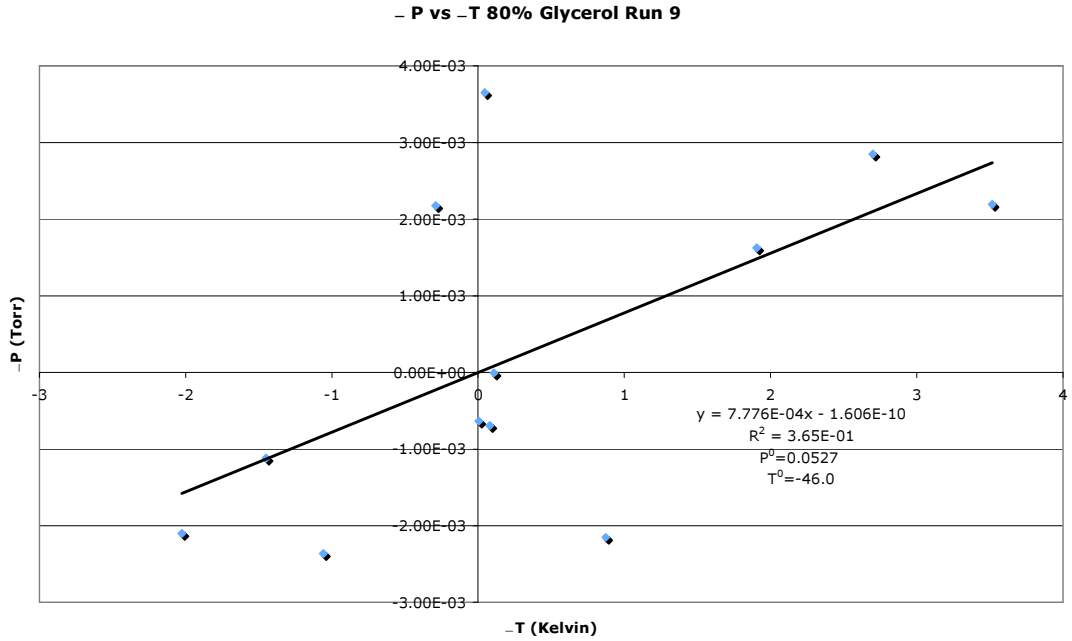

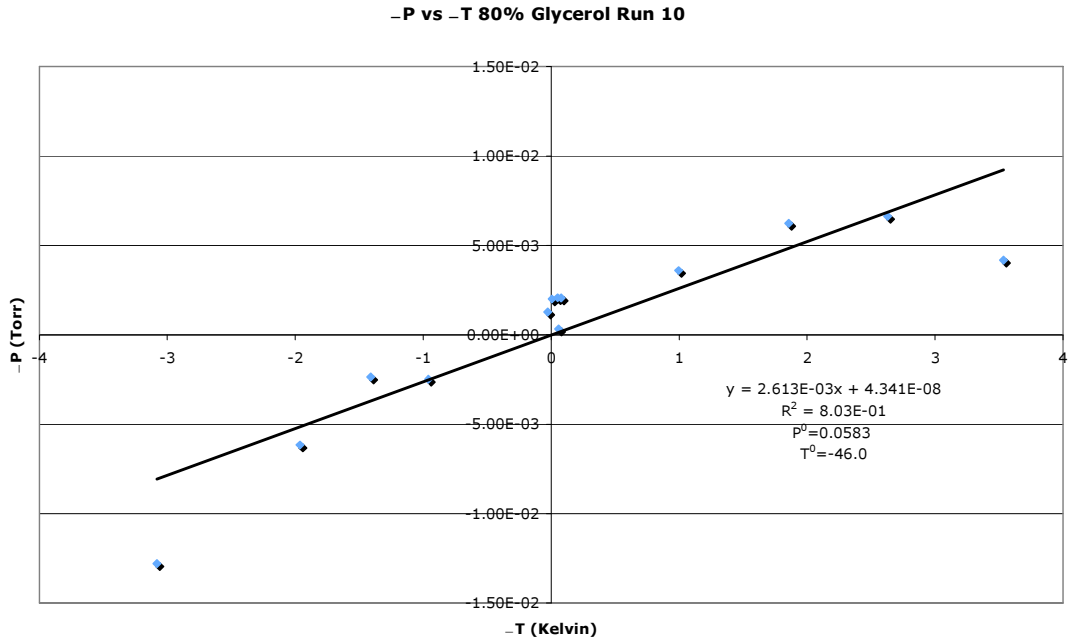

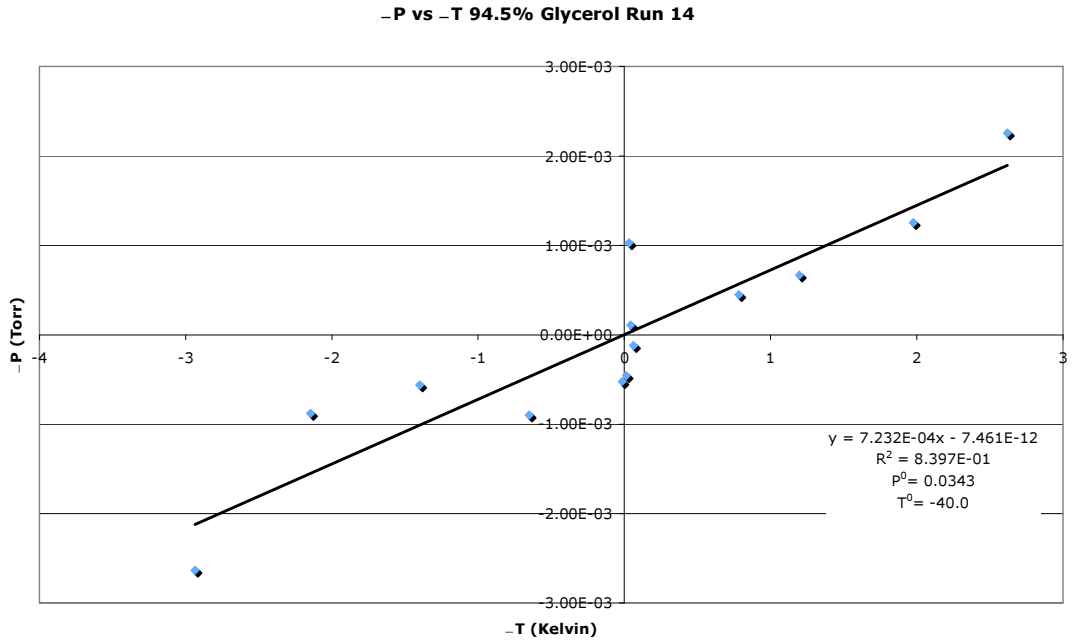
_P vs _T 94.5% Glycerol Run 14
3.00E-03
2.00E-03
1.00E-03
0.00E+00
-1.00E-03
-2.00E-03
-3.00E-03
-4
-3
-2
-1
0
1
2
3
_P (Torr)
_T (Kelvin)
y = 7.232E-04x - 7.461E-12
R2 = 8.397E-01
P0= 0.0343
T0= -40.0

5.7 ΔH_{vap} Calculation Graphs

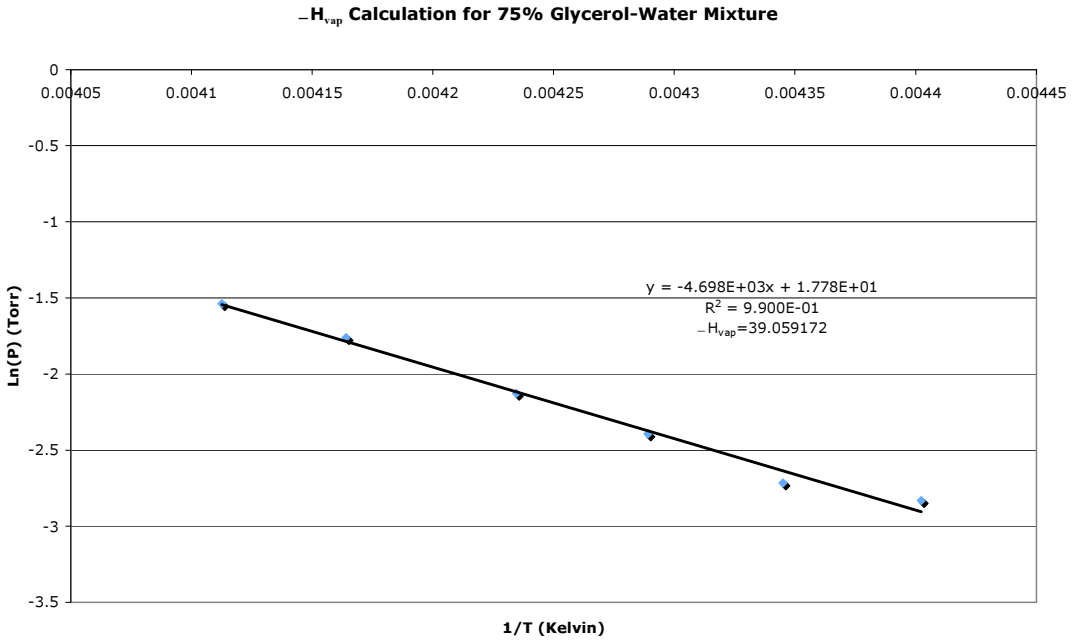

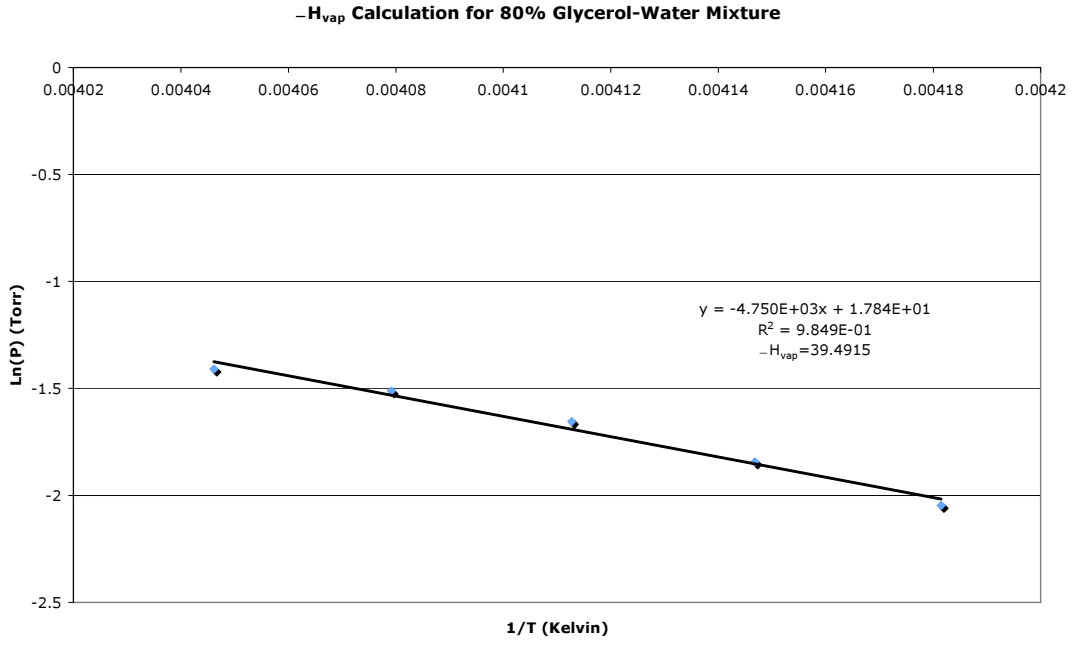

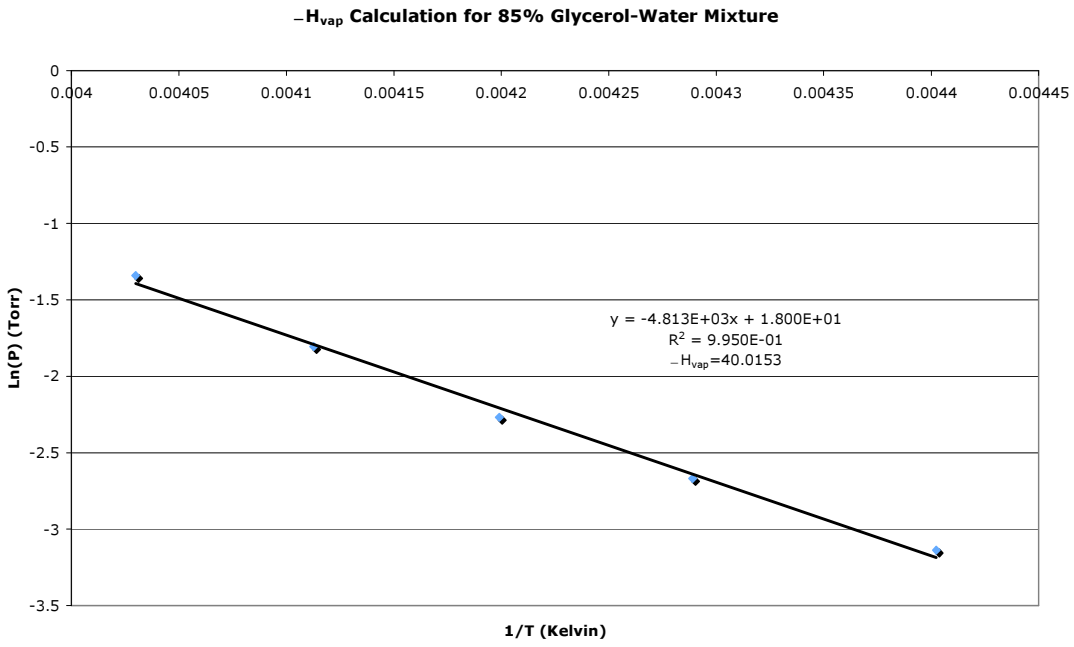
$-H_{vap}$ Calculation for 85% Glycerol-Water Mixture
0
0.004
0.00405
0.0041
0.00415
0.0042
0.00425
0.0043
0.00435
0.0044
0.00445
-0.5
-1
-1.5
-2
-2.5
-3
-3.5
Ln(P) (Torr)
y = -4.813E+03x + 1.800E+01
R^2 = 9.950E-01
$-H_{vap}$=40.0153
1/T (Kelvin)

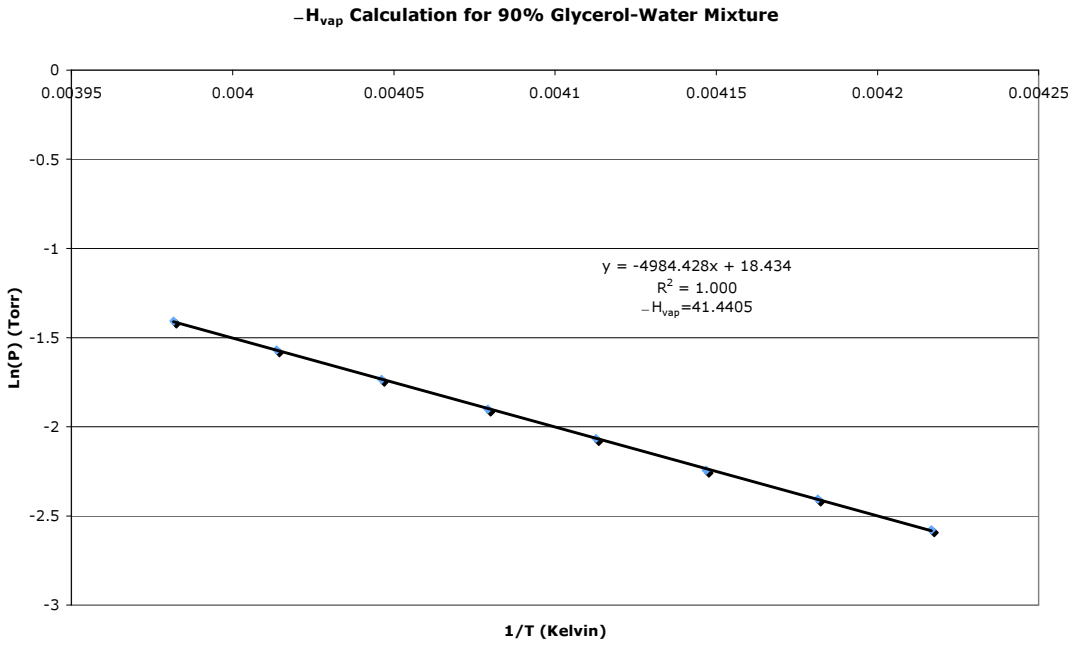
$-H_{vap}$ Calculation for 90% Glycerol-Water Mixture
0
0.00395
0.004
0.00405
0.0041
0.00415
0.0042
0.00425
-0.5
-1
-1.5
-2
-2.5
-3
Ln(P) (Torr)
y = -4984.428x + 18.434
R^2 = 1.000
$-H_{vap}$=41.4405
1/T (Kelvin)

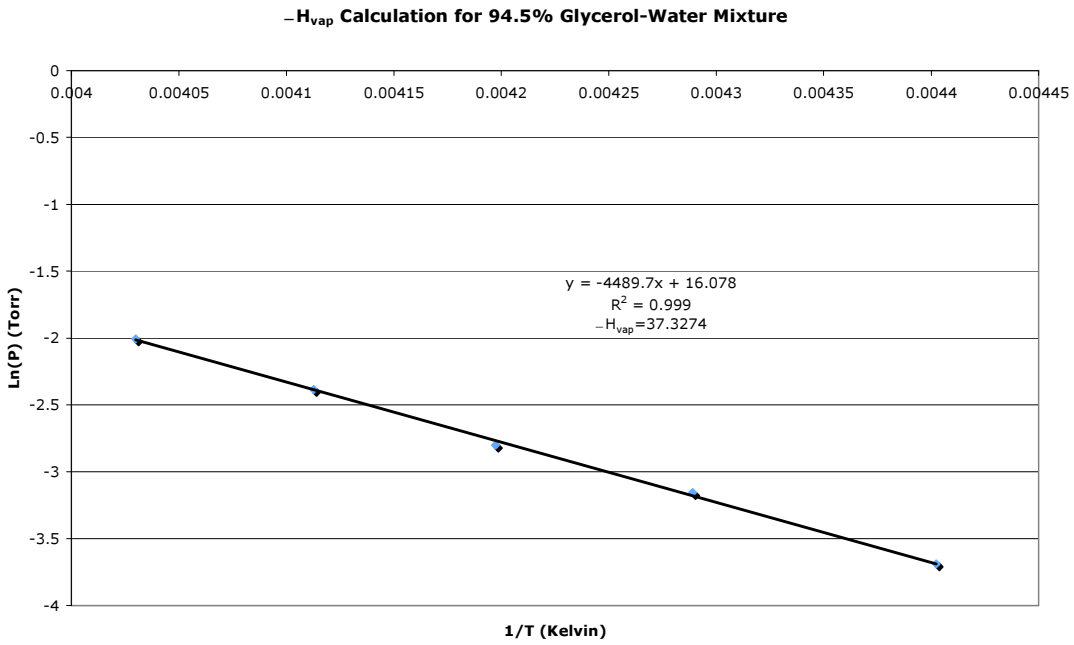
$-H_{vap}$ Calculation for 94.5% Glycerol-Water Mixture
0
-0.5
-1
-1.5
-2
-2.5
-3
-3.5
-4
0.004
0.00405
0.0041
0.00415
0.0042
0.00425
0.0043
0.00435
0.0044
0.00445
y = -4489.7x + 16.078
R^2 = 0.999
$-H_{vap}$=37.3274
Ln(P) (Torr)
1/T (Kelvin)

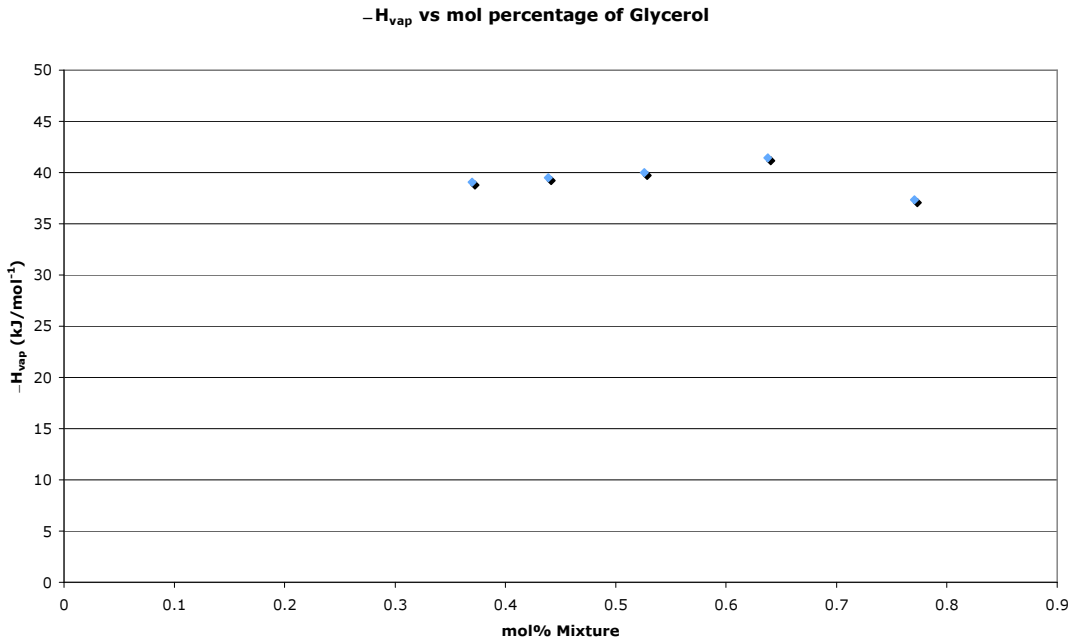
$-H_{vap}$ vs mol percentage of Glycerol
50
45
40
35
30
25
20
15
10
5
0
0
0.1
0.2
0.3
0.4
0.5
0.6
0.7
0.8
0.9
$-H_{vap}$ (kJ/mol^{-1})
mol% Mixture

5.8 |Q*| Calculation Tables

Table 5.1. Calculated Q* values for 75% Glycerol-Water Mixtures

Run #	|Q*| (kJ/mol^{-1})	95% confidence	Mean Free Paths
1	29.02	4.43	3.224
2	27.68	5.78	3.077
3	29.60	8.73	2.919
4	8.35	0.87	7.699
5	6.05	1.45	8.220
6	5.91	0.68	7.892
7	6.53	0.92	7.954
8	39.41	6.04	2.447
9	44.89	9.99	2.399
10	41.78	7.89	2.382

Table 5.2. Calculated Q* values for 80% Glycerol-Water Mixtures

Run #	|Q*| (kJ/mol^{-1})	95% confidence	Mean Free Paths
1	6.54	0.92	6.592
2	5.57	1.08	6.653
3	5.91	0.60	6.782
4	5.91	0.62	7.988
5	5.41	0.97	7.939
6	5.35	0.88	7.988
7	7.30	1.75	2.559
8	9.03	2.60	2.795

Table 5.3.Calculated Q* values for 85% Glycerol-Water Mixtures

Run #	|Q*| (kJ/mol^{-1})	95% confidence	Mean Free Paths
1	6.60	0.92	5.124
2	6.47	1.19	5.204
3	6.50	0.84	5.046
4	6.22	0.72	5.971
5	6.81	0.89	5.821
6	6.47	0.72	6.082
7	8.78	1.39	1.895
8	7.32	1.67	2.053
9	10.46	2.35	1.971

Table 5.4.Calculated Q* values for 90% Glycerol-Water Mixtures

Run #	|Q*| (kJ/mol^{-1})	95% confidence	Mean Free Paths
1	6.67	0.95	4.219
2	7.31	0.97	4.087
3	7.99	1.40	4.050
4	7.67	0.63	5.038
5	8.81	1.11	2.015
6	8.01	2.18	2.310
7	8.32	1.41	2.091
8	12.10	2.56	1.892
9	5.83	0.71	4.611
10	5.01	0.82	4.331

Table 5.5. Calculated Q* values for 94.5% Glycerol-Water Mixtures

Run #	|Q*| (kJ/mol^{-1})	95% confidence	Mean Free Paths
1	5.48	1.64	1.813
2	5.76	1.6	2.924
3	9.58	1.81	2.669
4	8.93	1.86	1.479
5	10.73	1.99	2.670
6	11.85	0.83	2.681
7	9.67	1.12	3.384
8	11.24	1.43	3.040
9	16.28	1.87	1.113
10	10.47	1.24	3.967
11	12.79	1.41	2.955
12	11.55	3.36	1.981
13	17.37	2.61	1.650

5.9 |Q*| Graphs

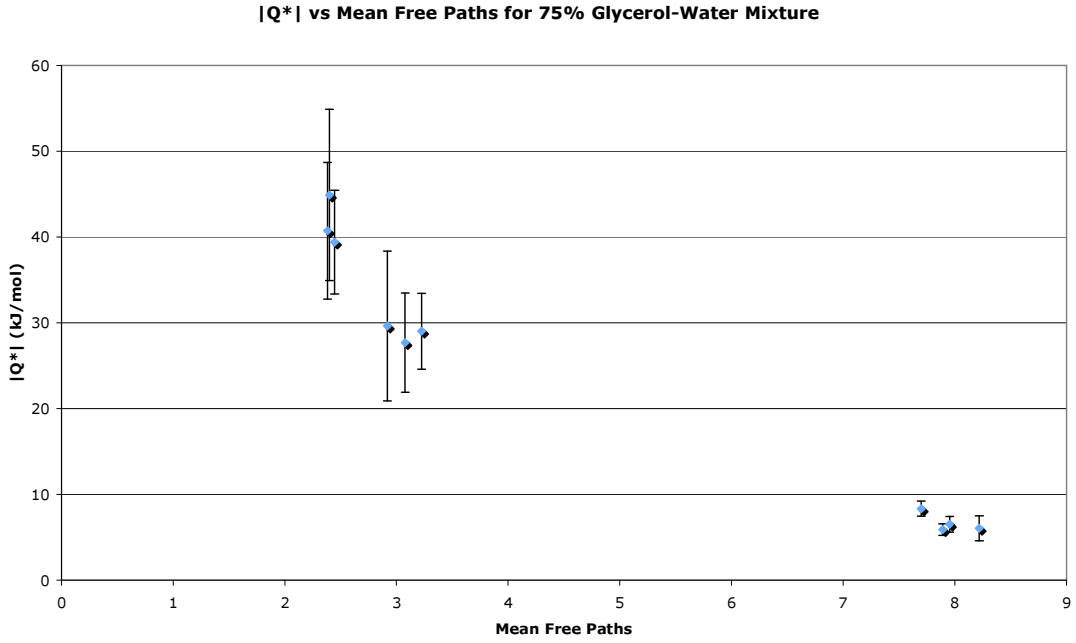
|Q*| vs Mean Free Paths for 75% Glycerol-Water Mixture
|Q*| (kJ/mol)
Mean Free Paths
0
10
20
30
40
50
60
0
1
2
3
4
5
6
7
8
9

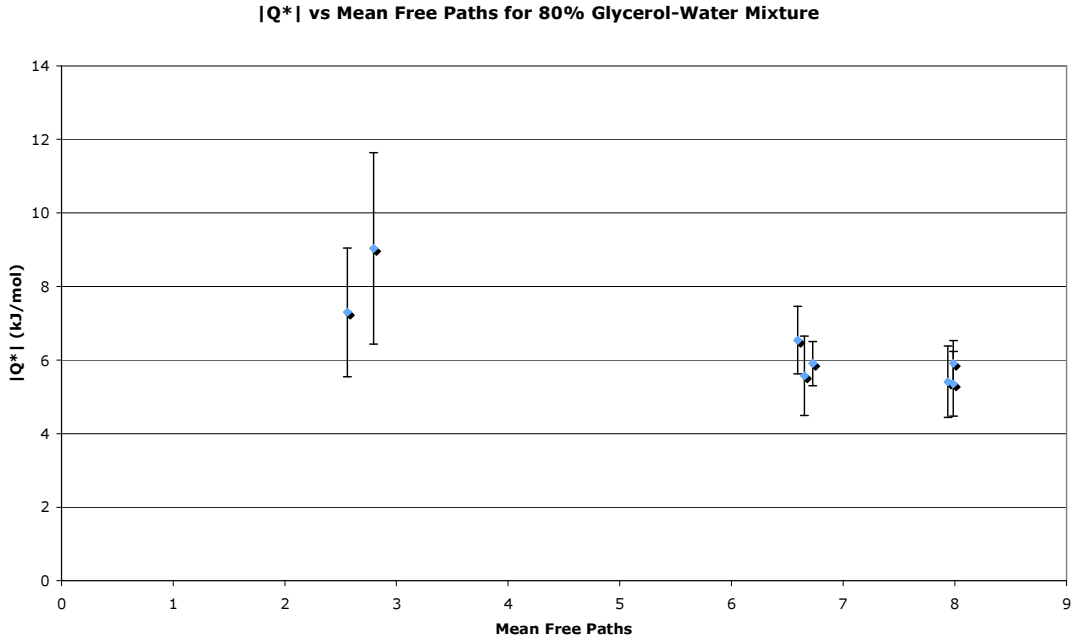
|Q*| vs Mean Free Paths for 80% Glycerol-Water Mixture
|Q*| (kJ/mol)
Mean Free Paths
0
2
4
6
8
10
12
14
0
1
2
3
4
5
6
7
8
9

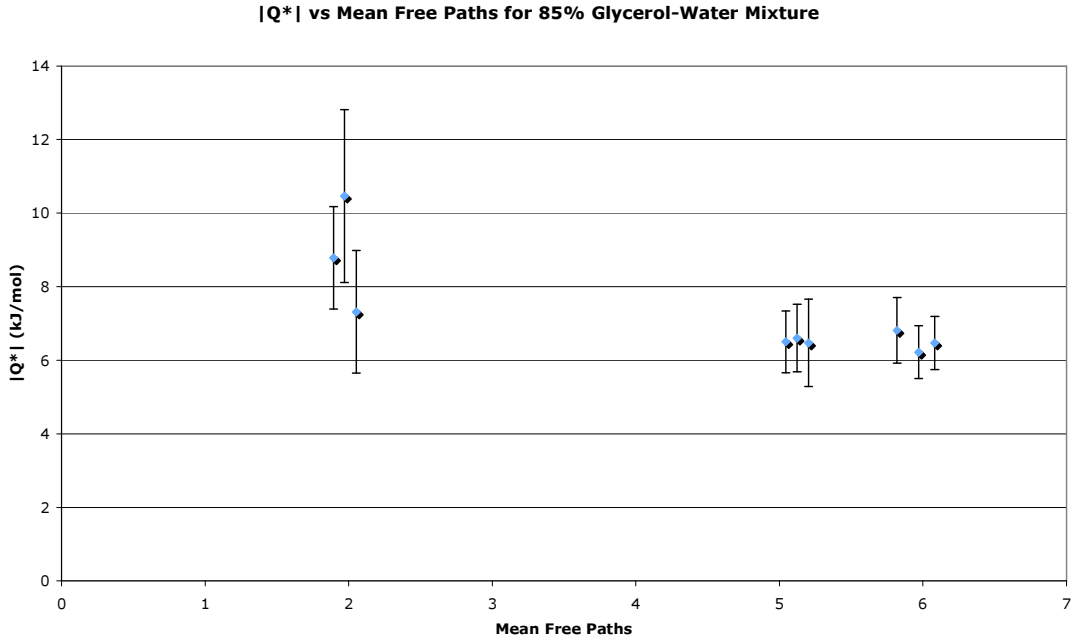
|Q*| vs Mean Free Paths for 85% Glycerol-Water Mixture
|Q*| (kJ/mol)
Mean Free Paths
0
2
4
6
8
10
12
14
0
1
2
3
4
5
6
7

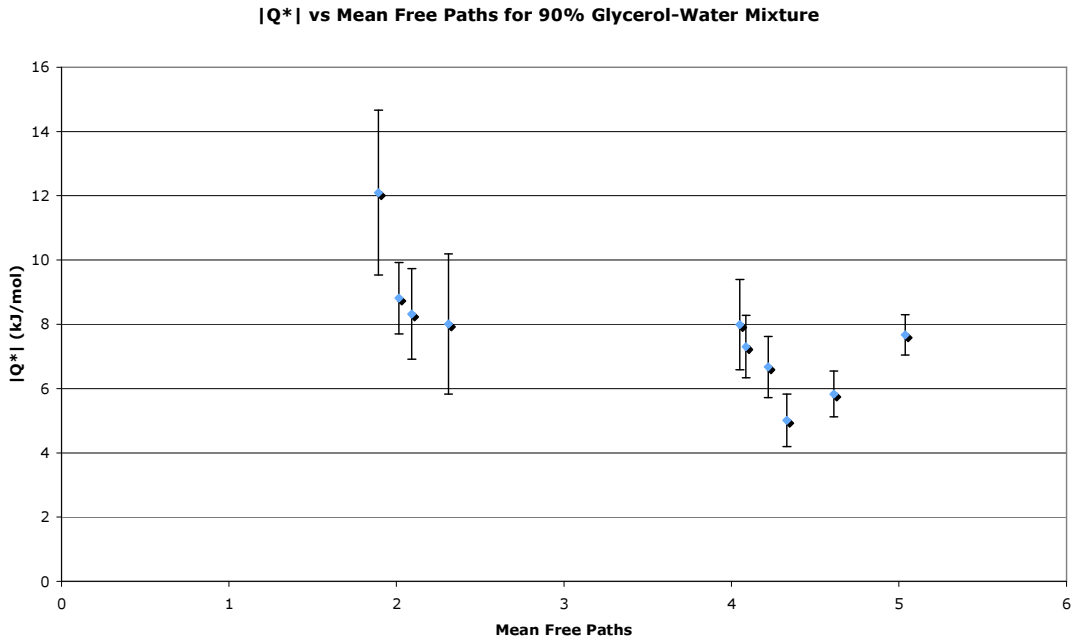
|Q*| vs Mean Free Paths for 90% Glycerol-Water Mixture
|Q*| (kJ/mol)
Mean Free Paths
0
2
4
6
8
10
12
14
16
0
1
2
3
4
5
6

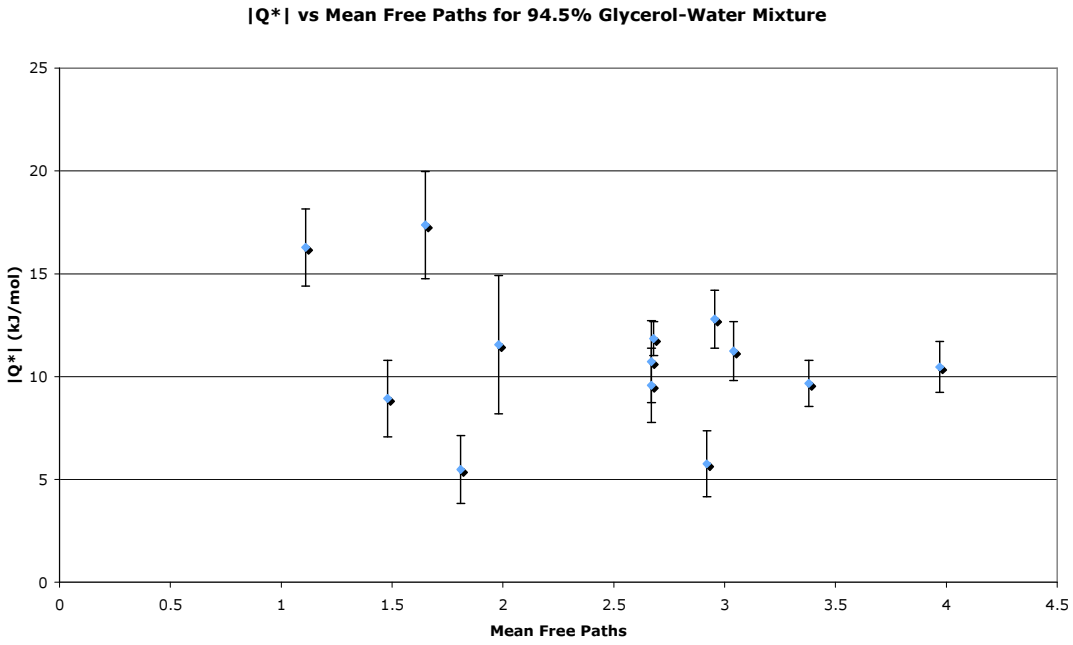
|Q*| vs Mean Free Paths for 94.5% Glycerol-Water Mixture
|Q*| (kJ/mol)
25
20
15
10
5
0
0
0.5
1
1.5
2
2.5
3
3.5
4
4.5
Mean Free Paths

References

1. Denbigh, K.G., *The Thermodynamics of the Steady State*. Monographs on Chemical Subjects, ed. Methuen. 1951, London: Methuen & Co. Ltd. 103.
2. Spanner, D.C., *The Active Transport of Water under Temperature Gradients.* Symp. Soc. Exp. Biol., 1954. **8**: p. 76-93.
3. Phillips, L.F., *Steady-state Heat and Matter Exchange at a Phase Interface.* J. Chem. Soc. Faraday Trans., 1991. **87**(14): p. 2187-2191.
4. Denbigh, K.G. and G. Raumann, *The thermo-osmosis of gases through a membrane. I. Theoretical.* Proc. R. Soc. London, 1952. **210**(Ser. A): p. 377-387.
5. Denbigh, K.G. and G. Raumann, *The thermo-osmosis of gases through a membrane. II. Experimental.* Proc. R. Soc. London, 1952. **210**(Ser. A): p. 518-533.
6. Rowley, R.L. and M.D. Hall, *Heats of transport from the diffusion thermoeffect in binary liquid mixtures of toluene, chlorobenzene and bromo benzene.* J. Chem. Phys., 1986. **85**(6): p. 3550-3555.
7. Phillips, L.F., *The role of the air-sea temperature difference in air-sea exchange.* Geophys. Res. Lett., 2004. **31**(L137301): p. 1-4.
8. Jones, E.P. and S.D. Smith, *A First Measurement of Sea-Air CO_2 Flux by Eddy Correlation.* J. Geophys. Res., 1977. **82**(37): p. 5990-5992.
9. Wanninkhof, R., *Relationship Between Wind Speed and Gas Exchange Over the Ocean.* J. Geophys. Res., 1992. **97**(C5): p. 7373-7382.
10. Watson, A.J., R.C. Upstill-Goddard, and P.S. Liss, *Air-sea gas exchange in rough and stormy seas measured by a dual-tracer technique.* Nature, 1991. **349**: p. 145-147.
11. Jacobs, C., W. Kohsiek, and W. Oost, *Air-sea fluxes and transfer velocity of CO2 over the North Sea: results from ASGAMAGE.* Tellus, 1999. **51B**(3): p. 629-641.
12. Iwata, T., K. Yoshikawa, K. Nishimura, Y. Higuchi, T. Yamashita, S. Kato, and E. Ohtaki, *CO2 flux measurement over the sea surface by eddy correlation and aerodynamic techniques.* J. Oceanography, 2004. **60**: p. 995-1000.
13. Webb, E.K., G.I. Pearman, and R. Leuning, *Correction of flux measurements for the density effects due to heat and vapour transfer.* Quart. J. R. Met. Soc., 1980. **106**: p. 85-100.
14. Kohsiek, W., *Water vapour cross-sensitivity of open ocean path H20/CO2 sensors.* Am. Met. Soc., 2000. **17**: p. 299-311.
15. Tsukamoto, O., S. Takahashi, and T. Kono, *Eddy-covariance CO_2 flux measurements over open ocean.* 2004.
16. Oost, W., *Report of the ASGAMAGE Workshop.* KNMI Scientific Report, 1998. **Royal Netherlands Meteorological Institute, De Bilt (also availible on internet: http://www.knmi.nl/asgamage.)**.
17. McGillis, W.R., J.B. Edson, J.E. Hare, and C.W. Fairall, *Direct covariance air-sea CO2 fluxes.* J. Geophys. Res., 2001. **106**(C8): p. 16,729-16,745.
18. McGillis, W.R., J.B. Edson, J.D. Ware, J.W.H. Dacey, J.E. Hare, C.W. Fairall, and R. Wanninkof, *Carbon dioxide flux techniques performed during GasEx-98.* Marine Chemistry, 2001. **75**: p. 267-280.
19. Phillips, L.F., *CO_2 Transport at the Air-Sea Interface: Effect of Coupling of Heat and Matter Fluxes.* Geophys. Res. Lett., 1991. **18**(7): p. 1221-1224.

20. Phillips, L.F., *CO_2 Transport at the Air-Sea Interface: Numerical Calculations for a Surface Renewal Model with Coupled Fluxes.* Geophys. Res. Lett., 1992. **19**(16): p. 1667-1670.
21. Robertson, J.E. and A.J. Watson, *Thermal skin effect of the surface ocean and its implications for CO_2 uptake.* Letters to Nature, 1992. **358**: p. 738-740.
22. Phillips, L.F., *Steady-sate heat and matter transfer at a non-uniform phase boundary.* Chem. Phys. Lett., 1996. **250**: p. 349-354.
23. Phillips, L.F., *Experimental demonstration of Coupling of heat and matter fluxes at a gas-water interface.* J. Geophys. Res., 1994. **99**(D9): p. 18,577-18,584.
24. Phillips, L.F., *CO_2 transfer at the air-sea interface: Numerical tests of the dual-tracer method.* Geophys. Res. Lett., 1995. **22**(19): p. 2597-2600.
25. Doney, S.C., *Comment on "Experimental demonstration of coupling of heat and matter fluxes at a gas-water interface" by Leon F. Phillips.* J. Geophys. Res., 1995. **100**(D7): p. 14,347-14,350.
26. Doney, S.C., *Irreversible thermodynamics and air-sea exchange.* J. Geophys. Res., 1995. **100**(C5): p. 8541-8553.
27. Phillips, L.F., *Reply.* J. Geophys. Res., 1995. **100**(D7): p. 14,351-14,353.
28. Doney, S.C., *Irreversible Thermodynamic Coupling between Heat and Matter Fluxes across a Gas/Liquid Interface.* J. Chem. Soc. Faraday Trans., 1994. **90**(13): p. 1865-1874.
29. Phillips, L.F., *Steady-state thermodynamics of transfer through a gas-liquid interface, treated as a limiting case of thermo-osmosis.* Chem. Phys. Lett., 1994. **228**: p. 533-538.
30. Mills, C.T. and L.F. Phillips, *Onsager heat of transport at the aniline liquid-vapour interface.* Chem. Phys. Lett., 2002. **366**: p. 279-283.
31. Phillips, L.F., *Onsager heat of transport as a consequence of a detailed balance at the gas-liquid interface.* Chem. Phys. Lett., 2004. **396**: p. 350-352.
32. Phillips, L.F., *Personal Communication*. 2007.
33. Mills, C.T., D.L. Bones, P. Casavecchia, and L.F. Phillips, *Onsager heat of transport measured at the n-heptanol liquid-vapour layer.* J. Phys. Chem., 2004. **108**: p. 2681-2685.
34. James, R.A. and L.F. Phillips, *Onsager heat of transport for water vapour at the surface of sulfuric acid.* Chem. Phys. Lett., 2005. **407(4-6)**: p. 358-361.
35. Pursell, C.J. and L.F. Phillips, *Onsager heat of transport for water vapour at the surface of water and ice: thermal accommodation coefficients for water vapour on a stainless-steel surface.* PCCP, 2006. **8**: p. 4694-4699.
36. Phillips, L.F., *Personal Communication*. 2006.
37. James, R.A., C.J. Pursell, and L.F. Phillips, *Pressure independence of the Onsager heat of transport for a gas-liquid at high pressures.* Chem. Phys. Lett., 2006. **429**: p. 153-156.
38. Loyalka, S.K., C.E. Siewert, and J. Thomas, J. R., *Temperature-jump problem with arbitrary accommodation.* Phys. Fluids, 1978. **21**(5): p. 854-855.
39. Goodman, F.O., *Thermal Accommodation Coefficients.* J. Phys. Chem., 1980. **84**: p. 1431-1445.
40. Barichello, L.B. and C.E. Siewert, *The temperature-jump problem in rarefied-gas dynamics.* Eur. J. Appl. Math., 2000. **11**: p. 353-364.
41. Biggs, G.A., *The Onsager Heat of Transport at the Liquid-Vapour Interface of p-tert-butyltoluene*. 2007, University of Canterbury.

42. Mills, C.T. and L.F. Philips, *Distillation of a cool liquid onto a warmer surface.* Chem. Phys. Lett., 2003. **372**(5-6): p. 615-619.
43. Phillips, L.F., *Surfing the Nanowaves: Progress in Understanding the Gas-Liquid Interface.* Acc. Chem. Res., 2004. **37**: p. 982-988.
44. Pao, Y., -P, *Application of Kinetic Theory to the Problem of Evaporation and Condensation.* Phys. Fluids, 1971. **14**(2): p. 306-312.
45. Fang, G. and C.A. Ward, *Temperature measured close to the interface of an evaporating liquid.* Phys. Rev. E, 1999. **64**: p. 417-428.
46. Phillips, L.F., *Surface Concentrations and Compound Formation in Aqueous Sulfuric Acid.* Aust. J. Chem, 1994. **47**: p. 91-99.
47. Chen, D.H.T. and A.R. Thompson, *Isobaric Vapour-Liquid Equilibria for the Systems Glycerol-Water and Glycerol-Water Saturated with Sodium Chloride.* J. Chem. Eng. Data, 1970. **15**(4): p. 471-474.
48. Darbari, G.S., R.P. Singh, G.S. Verma, and S. Rajagopalan, *Acoustic Absorption in Mixtures of Glycerol and Water below 1 MHz - II.* IL Nouvo Cimento, 1967. **LII B**(1): p. 1-17.
49. Singh, R.P. and G.S. Verma, *Acoustic Absorption in Mixtures of Glycerol and Water Below 1 MHz.* IL Nouvo Cimento, 1968. **LV B**(1): p. 40-50.
50. Marcus, Y., *Some thermodynamic and structural aspects of mixtures of glycerol with water.* Phys. Chem. Chem. Phys., 2000. **2**: p. 4891-4896.
51. James, R.A. and L.F. Phillips, *Onsager heat of transport for water vapour at the surface of glycerol-water mixtures.* Chem. Phys. Lett., 2006. **425**: p. 49-52.